12-2008

Hybrid Bond-Order Potential for Silicon

Suleiman Oloriegbe
Clemson University, solorie@clemson.edu

HYBRID BOND-ORDER POTENTIAL FOR SILICON

A Dissertation
Presented to
the Graduate School of
Clemson University

In Partial Fulfillment
of the Requirements for the Degree
Doctor of Philosophy
Chemistry

---

by
Suleiman Yahaya Oloriegbe
December 2008

Accepted by:
Dr. Steven J. Stuart, Committee Chair
Dr. Brian Dominy
Dr. Jason McNeill
Dr. Robert Latour

ABSTRACT

A new hybrid bond-order potential for silicon is developed. The functional form of the potential is derived from hybrid of expressions from empirical bond-order formalism and first principles approximations. The total energy is expressed as the sum of attractive, repulsive and promotion energies. By introducing a screening function derived from approximations to first principles expressions, the potential is made long-ranged by allowing covalent interactions beyond the first nearest neighbor shell of atoms in agreement with quantum mechanical descriptions of the bonding in silicon. Environment-dependent promotion energy is introduced that accurately accounts for energetic interactions due to changes in hybridization state of atoms during chemical bonding. The treatment of the bond-order has been extended beyond the tight-binding second moment approximations to include screening of the bond strength between two atoms by other atoms in their vicinity.

A database consisting of structures, cohesive energies and promotion energies of clusters of 3–8 atoms, equations of state properties for 15 phases of silicon were used to obtain optimized parameters for the potential. The resulting model is able to accurately represent silicon in a wide range of bonding environments. The potential has been validated against widely used interatomic potentials for silicon in the literature for energies and structure of small clusters, equations of state for diamond cubic and other high pressure phases of silicon.

DEDICATION

This work is dedicated to Fatimah, Amin and Laila Oloriegbe for their resilience and loving support.

ACKNOWLEDGEMENTS

All praises are due to God for the gift of life, health and endowment that makes it possible for me to carry out this work. I am highly indebted to my advisor, Dr. Steven Stuart for giving me the opportunity and encouragement to work on this exciting field of study. Many thanks for your direction, patience and understanding. Clemson University is gratefully acknowledged for providing the resources and enabling environment for this research work. Financial support for this work by the Department of Energy (DE-FG02-01ER45889), the National Science Foundation (CHE-0239448) and Department of Defence (47539-CH-MUR) is gratefully acknowledged.

Special thanks to Dr. Fatimah, Amin and Laila Oloriegbe for their love and support throughout the challenging period of this work. I would like to express my sincere appreciations to Mr. Mathew and Mrs. Felicia Ogunsile, Dr AbdulRasheed Na'Allah and his wife Dr Ramat Na'Allah for their loving support and encouragement. To my mom, thank you for your prayers and understanding. Thanks goes to the Oloriegbe Family for their patience and understanding.

I would like to acknowledge the valuable data provided to me for this research by: Dr. D. G. Pettifor and Dr. D. Nguyen-Manh (BOP4 code), Dr. Xiao Cheng Zeng (cluster energies and structures), Brian Gillespie (BOP4 bond order for silicon phases), Dr. Andres Mujica and Dr. Richard Needs (equations of state data for silicon phases), Dr. Kai Nordlund (respulsive potential data), Dr. Marie-Louise Saboungi and Dr. Louis Hennet (liquid silicon data). Lastly, my thanks goes to all members of the Stuart Research Group.

TABLE OF CONTENTS

Page

Table of Contents (Continued)

Page

LIST OF TABLES

LIST OF FIGURES

List of Figures (Continued)

Figure Page

List of Figures (Continued)

Figure Page

CHAPTER ONE

INTRODUCTION

Silicon (Si) is the main material used in integrated circuits for microelectronic applications. Integrated circuits are used in most modern electronics hardware ranging from chips in cell phones, microprocessors, household electronics, to airplanes, spacecraft and satellites. These products are shaping our world today and their development is of great technological and economic interest. Silicon is a group IV element in the periodic table and exists in nature as minerals in the form of silica (SiO_2) and silicates, which are compounds of silicon, oxygen and metals. The pure form of silicon takes the diamond cubic lattice structure at ambient conditions. The diamond cubic silicon is a semiconductor. That is, it is naturally an electrical insulator, but can be made to conduct electricity under the influence of heat or electric current. This ability is one of the reasons why silicon is the material of choice for microelectronic applications. The vast abundance of silicon in the soil as a raw material also makes it economically attractive compared to other semiconductor elements.

The continued miniaturization of feature size on silicon chips in semiconductor fabrication to less than 100 *nm* size is now helping to advance many electronic applications [1]. This advancement also comes with difficulty in controlling the quality and yield of microelectronic appliances as the size of the circuit features in these appliances approaches dimensions where quantum effects becomes relevant. Processes such as defects, ion migration, surface reconstruction, fracture and crack propagation are some of the underlying phenomena occurring during semiconductor fabrication which

can negatively affect the yield and quality of microelectronic products. Current day research and developments in semiconductor materials are now focusing on understanding these fundamental processes occurring at the atomic length scales in order to improve product quality and yield.

Computational modeling and simulation is playing an important role in semiconductor materials design and property predictions in advance of fabrication [2]. "Computer experiments" through modeling and simulation can be helpful in revealing atomistic processes useful for experimental interpretation or at least help guide experimental design for product development. These "computer experiments" can be achieved through the use of molecular dynamics (MD) simulations.

In MD, the phase space trajectory of a system (positions and velocities of all atoms at all time) is computed by solving Newton's equations of motion numerically [3,4]. The basic principle in MD is to reproduce the motion of atoms in the system as they occur in nature. The macroscopic properties of materials such as temperature, pressure, heat capacity and density can be obtained through analysis of the atomic motion of the system. MD simulations method can be classified into two major types: classical MD and ab initio MD. The most prominent ab initio molecular dynamics simulation method is the Car-Parinello molecular dynamics (CPMD).

In classical MD, potential energy and forces on the atoms are computed using an interatomic potential representing the interactions between these atoms. The forces are then used to integrate Newton's equations of motion in time. The CPMD [5] method on the other hand, does not require an interatomic potential, but rather, quantum mechanical

description of the electrons using density functional theory (DFT) and classical dynamics of the nuclei are used to perform the simulation. The basic physics of condensed matter are inherently described when the electronic degrees of freedom are treated explicitly by quantum mechanics in the CPMD method. Therefore, the Car-Parrinello MD is capable of providing accurate prediction of material properties. However, the computational expense required to solve many important problems of interest using this method can be several orders of magnitude compare to classical MD that uses an interatomic potential [2]. Consequently, only small system and short time scales are accessible when using Car-Parinello MD. Furthermore, the Car-Parrinello method is unsuitable for treating van der Waals-like forces in condensed phases. A major limitation of classical molecular dynamics is the lack of realistic and time-efficient interatomic interaction potentials. The development of such potentials is essential to the accurate prediction of materials properties and processes through molecular simulation.

There is no dearth of interatomic potentials for silicon in the literature [6-32]. Most of the available potentials have provided a wealth of knowledge in prediction of bulk properties, defects, cluster energetics and surface properties. Various potentials have strengths and shortcomings in regard to their ability to accurately predict various properties of interest. Some were developed specifically to model clusters [23,28-29], or a combination of clusters and bulk properties, liquids and equilibrium behavior [14,21-22] and a whole host of other important characteristics.

A long-standing problem of classical inteatomic potentials for silicon is transferability, or the ability to predict with reasonable accuracy the properties of silicon

in wide ranging environments. Some of the most demanding environments are encountered during chemical vapor deposition, ion implantation and etching processes. These place a stringent requirement on a potential to accurately model defects and defect migrations, surface reconstructions, cluster structures and energies, liquid structures, grain boundaries, equilibrium properties, scattering cross-sections and high-temperature and stress-strain behavior. A good candidate potential should therefore provide an understanding of these complex processes and their relationship with chemical bonding concepts such as bond formation and breaking, hybridization, bond bending, charge transfer, radical formation and π bonding. A detailed comparative [73] study of some silicon potentials in use reveals useful insight into their strengths and weaknesses. While they all provide reasonable description of equilibrium properties of cubic diamond silicon, they are non-transferable to different silicon environments. The quest to develop accurate classical potentials that are computationally efficient and provide better transferability in various silicon environments is an ongoing effort with some success [33-37]. Some of these successes can be attributed to the effort made to incorporate approximate quantum mechanical description of the covalent bonding and behaviors of silicon in its diverse polymorphs [35].

Interatomic potentials for silicon in general can be classified into three major categories. These are bond-order potentials, cluster potentials and embedded atom method (EAM) potentials. These potentials differ from one another primarily due to their functional representation but are similar in regards to their empirical nature. The potentials are empirical because they are mathematical representations determined from

experimental properties of silicon. These functions are not in any way derived from first principles, however, recent advances [36] in tight binding methods using moment approximations in the Green's functions formalism has lead to series of analytical bond order potentials (BOP). Potentials derived using the BOP theory are obtained by approximations from first principles. The potential described in this dissertation is a hybrid of BOP functions combined with other empirical expressions which we referred to as a hybrid bond-order potential (HBOP) for silicon.

The first class of empirical potential for silicon is the bond-order potentials. The bond order potential formalism was originally introduced by Abell [17]. In general, the potential energy for this class of potential can be written as:

$$E_{coh} = \sum_{i} \sum_{(j \neq i)} f_c\left(r_{ij}\right)\left[V_{ij}^{A}\left(r_{ij}\right) + b_{ij} V_{ij}^{R}\left(r_{ij}\right)\right] \tag{1.1}$$

where r_{ij} is the distance from atom i to atom j.

Here, V_{ij}^{A} and V_{ij}^{R} are the attractive and repulsive part of the potential energy and b_{ij} is the bond order for the ij bond. The function $f_c(r_{ij})$ represents a smooth cutoff function to limit the range of the potential. The main characteristic of this class of potential is the variable and configuration-dependent bond order or the strength of the bond. The coordination number of the participating atoms and the bond angles formed with their neighbors are the main factors affecting the strength of the bond. For example, when an atom has a high coordination number, the bonds formed with its neighbors are weaker than those atoms with few neighbors. Therefore, bond order decrease monotonically with increase in coordination number of atoms i and j forming the bond. Additionally, the

bond-order expression favors open structures with bond angles corresponding to those of diamond structure.

The functions V_{ij}^{A} and V_{ij}^{R} are represented as exponential functions:

$$V_{ij}^{A}\left(r_{ij}\right) = A\exp\left(-\alpha r_{ij}\right) \tag{1.2}$$

and

$$V_{ij}^{R}\left(r_{ij}\right) = B\exp\left(-\beta r_{ij}\right) \tag{1.3}$$

A, α and *B*, β are adjustable parameters corresponding to coefficients and characteristic lengths for the attractive and repulsive components of the potential respectively. The form of these functions, Eqs. 1.2 and 1.3, shows that the bonding is modeled by pairwise functions, but the full potential include the bond order (Eq. 1.1) which is a many-body function depending on the local environment of the bond. The bond-order term is further expressed in terms of atomic coordinates and angles as follow:

$$b_{ij} = f\left(\xi_{ij}\right) \tag{1.4}$$

$$\xi_{ij} = \sum_{k\neq i,j} V_3\left(r_{ij}, r_{ik}, \theta\right) \tag{1.5}$$

$$V_3\left(r_{ij}, r_{ik}, \theta\right) = \varphi\left(r_{ij}, r_{ik}\right) g\left(\theta_{jik}, \theta_{ijk}\right) \tag{1.6}$$

where $f(\xi)$ is usually $(1 + \xi)^{-1/2}$ and

$\varphi(r_{ij}, r_{ik})$ is usually represented by an exponential function of r_{ij} and r_{ik}. The functional form of the term describing the dependence of bond order on bond angle, $g(\theta_{jik}, \theta_{ijk})$ is formulated such that structures with angles corresponding to the diamond cubic phase are

stabilized. A detail comparison of different functional forms used for $g(\theta_{jik}, \theta_{ijk})$ is presented in section 2.2.

Extensions to the bond-order model have been derived for applications to different chemical interactions. For example, the reactive bond-order (REBO) potential [38,39] for hydrocarbons have additional terms in the bond order accounting for the influence of radical energetics and π-bond conjugation on the bond energies and also incorporate the effect of dihedral angle rotation about the carbon-carbon double bonds. Additional terms in the form of non-bonded interactions have been introduced in the potential energy expression (Eq. 1.1) to enable the REBO potential account for dispersive forces as intermolecular interactions in hydrocarbons [40,41] and torsional interactions in carbon-carbon single bonds [40]. A variety of bond-order potentials have been derived for silicon following the bond-order formalism [8,12,14]. The formalism has also been applied to multi-component systems involving silicon with fluorine and chlorine [42], silicon-carbon-hydrogen [43], silicon-hydrogen [44] and silicon-germanium systems [45]. All these extensions have aided in the modeling of several systems and processes of interest in semiconductor and other materials.

The second class of potential is the cluster potentials modeled by two and three-body interactions. The potential energy is generally represented by

$$E_{coh} = \sum_{i,j} V_2'(r_{ij}) + \sum_{i,j,k} V_3'(r_{ij}, r_{ik}, r_{jk}). \tag{1.7}$$

The pairwise two-body term $V'_2(r_{ij})$ is the sum over contributions from $N(N+1)/2$ atomic pairs i and j depending on the distance r_{ij} between them. Typical functional forms of the two-body terms are the Morse potential [20], the Rydberg function [16], and the widely

used Stillinger-Weber (SW) type exponential functions [9,30-31]. An example of the two-body potential used in the SW potential [9] is given by

$$V_2'(r_{ij}) = \begin{cases} A\left(Br_{ij}^{-p} - r_{ij}^{-q}\right)\exp\left[\left(r_{ij}-a\right)^{-1}\right], & r_{ij} < a \\ 0, & r_{ij} > a \end{cases} \tag{1.8}$$

where *A, B, p, q* and *a* are positive parameters. The exponential term is a cutoff function that enables the potential to smoothly go to zero at $r = a$. The above function (Eq. 1.8) can be interpreted physically as representation of steric repulsion and electrostatic interaction between the atoms.

In monoatomic solids, the three body $V'_3(r_{ij}, r_{ik}, r_{jk})$ is symmetric with respect to exchange of *i, j* and *k* atoms in the triple sum. Using the SW potential [30] as an example, the three-body potential is given by

$$V_3' = (r_i, r_j, r_k) = h(r_{ij}, r_{ik}, \theta_{jik}) + h(r_{ji}, r_{jk}, \theta_{ijk}) + h(r_{ki}, r_{kj}, \theta_{ikj}) \tag{1.9}$$

and the h function is given by the formula

$$h(r_{ij}, r_{ik}, \theta_{jik}) = \lambda \exp\left[\gamma\left(r_{ij}-a\right)^{-1} + \gamma\left(r_{ik}-a\right)^{-1}\right] \times \left(\cos\theta_{jik} + \frac{1}{3}\right) \tag{1.10}$$

where λ and γ are constant parameters. This three-body term is repulsive and by construction the sum vanishes exactly for the diamond structure (θ_{jik} = 109.47°). This function, (Eq. 1.10) vanishes when $\cos(\theta_{jik})$ = -1/3, therefore other lattices are destabilized relative to the diamond cubic lattice. The interpretation of this choice is that the potential has tendency to form sp^3 covalent bonds in silicon. Additionally, the *h* functions account for covalent effects through bond bending using the angular term and stretching of atomic bonds (r_{ij}, r_{ik}, r_{jk}). These properties enable the potential to give the

correct ground state (diamond cubic structure) of the crystal silicon at ambient conditions. A number of extensions to the cluster potentials have been derived. In an attempt to predict the correct cluster energies, four-body interactions [31] has been added to Eq. 1.7, while environmental dependence of the energy has been achieved through the use of effective coordination in the two- and three-body terms to help describe defects and disordered phases in silicon [30].

The EAM potentials are the third class of silicon potentials available in the literature. The general form of the potential energy for these potentials can be written as

$$E_{coh} = \sum_i F_i(\rho_i) + \frac{1}{2}\sum_{i \neq j} \phi(r_{ij}), \tag{1.11}$$

where $F_i(\rho_i)$ represents the embedded-atom energy of atom i, and ρ_i denotes the local electron density at atom i, which is computed as a superposition of individual atomic electron densities from other atoms that are neighbors of atom i. The term $\phi(r_{ij})$ is the pairwise interaction between atoms i and j separated by a distance r_{ij}.

This functional form works well for close-packed materials such as metals, but does not work well for covalent systems due to a lack of the angular dependent terms needed to describe covalent bonding. For use in covalent systems, modifications are usually made to the EAM functions in the form of modified embedded-atom methods (MEAM) by introducing explicit angular-dependent functions [11,55], or indirectly through screening functions in the local electron density terms [24]. An example of such screening function is described in section 2.3.3.

The current study enumerates the importance of different physical contribution to covalent bonding starting from the bond-order formalism originally introduced by Abell [46] and implemented for silicon by Tersoff [6]. This formalism has found success in hydrocarbons in the form of the REBO potential [39]. The aim is of this work is to provide a systematic development and evaluation of the influence of different physical effects and their functional representations in a silicon potential. These effects include screening, in which covalent bonding interaction between two atoms is weakened due to the presence of other neighboring atoms in their environment. Another important property considered is the promotion energy. This is the energy associated with the change of occupancy of atomic orbitals when an electron is promoted from the free atom s^2p^2 configuration to the hybrid sp^3 configuration when forming the solid. The potential is also made long-ranged to better reproduce the quantum mechanical description of bonding in silicon. It is important to note that most interatomic potentials are made short-ranged and usually limited to first nearest neighbor interaction in silicon at equilibrium densities. In contrast, the quantum mechanical description of covalent bonding between atoms extends beyond the first nearest neighbors in silicon. The short-range cutoff distances adopted are normally implemented for computational convenience or difficulty of dealing with strongly covalent bonded second-nearest and further neighbors that may result due to the nature of the potential expressions used. The key remedy for this shortcoming adopted in this study is to introduce the screening effect. This essentially circumvents the problem of strong covalent interactions when atoms are far apart from one another in condensed phases.

The goal of this research work is to develop a bond-order potential for silicon that is reasonably accurate and time-efficient for use in molecular dynamics simulations for predicting properties of silicon in crystal, bulk, liquid and surfaces.

In Chapter 2, a brief description of the various components of the potential are presented with their functional forms and justification. The development of the model using screening function, bond-order and promotion energy terms is presented. This is followed by the fitting procedure for the potential. Systematic derivation of the potential through incremental addition of functions and parameters and the improvements obtained are presented. The justifications for using long-range interaction are enumerated.

The final potential obtained is used to predict equations of state for crystalline phases, cluster energies and promotion energies in Chapter 3. The final results are compared with those of existing silicon potentials and final concluding remarks are made in Chapter 4.

CHAPTER TWO

MODEL DEVELOPMENT

2.1 Introduction

The fundamental basis of the potential described here arises from the use of coarse-grained first principles density functional theory to deduce the pertinent components of the total energy and their representation in an analytically tractable form suitable for use in classical molecular dynamics simulations. Approximate tight binding (TB) methods have been developed previously with this type of aim in mind. This formalism has been successful in many theoretical investigations [47-51]. A reduction of TB equations using moment approximations to density of states in the Green's function formalism has led to a series of analytical bond order potentials (BOP) [33,35,37]. In the moment approximations, the *n*th moment of the local density of states for a given atom *i* is determined by summing all the hopping or the bonding paths of length *n* that start and end at atom *i*. This concept provides the link between electronic structure calculations involving the diagonalization of the Hamiltonian and using an interatomic potential when evaluating the energy of atomic systems.

The second-moment approximation based on the BOP formalism was shown to reduce to the Tersoff potential [6]. However, the second-moment approximation is unable to provide a good description of the energy difference among three-dimensional structural phases, such as diamond, FCC, SC, BCC and HCP.

The fourth-moment description is more accurate and able to provide a good description of the relative stability among these polymorphs. However, the complicated

nature of the expressions in the fourth-moment expansions requires significant computational expense compared to traditional classical potentials [36]. The computational burden using these expressions grows exponentially as more distant neighbors are added to extend the range of the potential. Here, we devise a similar but computationally efficient method of obtaining the bond order, while at the same time incorporating the effect of long-range interactions between the atoms. In this study, both the bond energy and the bond order are screened as will be presented in details in section 2.3. Atoms in the second, third, fourth and fifth neighbor shells are included in covalent bonding through the use of a screening function. The screening function ensures that forces on atoms are gradually reduced as the distance between them increases, and fall smoothly to zero just after the fifth nearest neighbor shell in diamond cubic structure.

The binding energy is expressed as a sum over bonds in the form

$$E_B = \sum_i \sum_{j>i} f_c\left(r_{ij}\right)\left[V_R\left(r_{ij}\right) - S_{ij} b_{ij} b_1 V_A\left(r_{ij}\right)\right] + V_{prom} \tag{2.1}$$

The pair-additive repulsive part of the potential, V_R, and the attractive function, V_A, are given by:

$$V_R\left(r_{ij}\right) = A\left(1 + \frac{Q}{r_{ij}}\right) e^{\left(-\beta r_{ij}\right)} \tag{2.2}$$

$$V_A\left(r_{ij}\right) = e^{\left(-\alpha r_{ij}\right)} \tag{2.3}$$

where r_{ij} is the distance between atoms i and j. The potential is smoothly reduced to zero by multiplying them by the cutoff function, $f_c(r_{ij})$ [57], given by:

$$f_c\left(r_{ij}\right)=\begin{cases}1 & r_{ij}\le r_{\min}\\ a_0\left(r_{\max}-r_{ij}\right)^2+a_1 r_{ij}\left(r_{\max}-r_{ij}\right)^2+a_2 r_{ij}^2\left(r_{\max}-r_{ij}\right)^2 & r_{\min}\le r_{ij}\le r_{\max}\\ 0 & r_{ij}\le r_{\max}\end{cases} \qquad (2.4)$$

Here we use a r_{min} value of 5.5 Å and r_{max} (r_{cut}) of 5.95 Å.

The parameters a_0, a_1 and a_2 are chosen so that $f_c(r_{ij})$ and its first two derivatives are continuous at r_{min} and by construction $f_c(r_{ij})$ and its first derivative are also continuous at r_{max}. The symbols A, Q, α, β, and b_1 are adjustable parameters.

The terms b_{ij} is the bond-order for the bond connecting i and j, S_{ij} represent the screening of atoms i and j by other atoms in their vicinity, and V_{prom} is the total promotion energy of all atoms in the system. Details of the functional representations for the bond-order, screening function and the promotion energy are described in sections 2.2, 2.3 and 2.4 respectively.

The form of the repulsive and attractive terms in Eq. 2.1 - 2.3 are identical to those in the Tersoff [8] and Brenner [39] bond-order potentials for silicon and carbon respectively. These potentials are short-ranged, with only first nearest neighbor interactions in diamond solid at standard conditions. In general, potentials for covalent system are much longer ranged and this feature is essential for adequate description of surfaces, amorphous, liquid and vapor phase energetics of materials when performing 'computer experiments' such as film deposition, a procedure that is accompanied by inherent complex processes such as defect formation, chemical reactions, surface reconstruction and stress-strain behaviors.

2.2 Bond-Order

In the second-moment approximation, only the first nearest neighbor atoms contribute to the bond order. The bond-order expression described here is modeled after the second- moment approximations in the BOP theory with modifications to ensure that distant atoms up to the fifth nearest neighbor shells also contribute to the overall bond order.

The bond-order expression is given by:

$$b_{ij} = \frac{\left(b_{ij}^{\sigma} + b_{ji}^{\sigma}\right)}{2} \tag{2.5}$$

where b_{ij}^{σ} represents the bond order resulting from the neighbors of atom i, and b_{ji}^{σ} represent the bond order contribution due to neighbors of atom j.

These terms are given by;

$$b_{ij}^{\sigma} = \frac{1}{\sqrt{\left(1 + \sum_{(k \neq i,j)} S_{ik} * f_c\left(r_{ik}\right) * g\left(\theta_{jik}\right)\right)}} \tag{2.6}$$

Where the S_{ik} function represents the screening of the individual contributions to the bond order from the *k* atoms that are neighbors of *i*. The *k'* atoms are the neighbors of atoms *i* and *k* in the *ik* bond.

$$S_{ik} = \prod_{k' \neq i,k} \left(1 - f_c\left(\Delta r_{ikk'}\right) \exp\left(-\lambda\left(\Delta r_{ikk'}\right)\right)\right). \tag{2.7}$$

and $f_c(\Delta r_{ikk'})$ is the cutoff function computed using Eq. 2.4 with the argument

$\Delta r_{ikk'} = r_{ik'} + r_{kk'} - r_{ik.}$

In the second-moment approximation, the dependence of the bond-order on the angle θ_{ijk} formed by a pair of nearest neighbor atoms is

$$g(\theta_{jik}) = \left\{ \left(\frac{p_\sigma}{1+p_\sigma} \right) \left(\left(\frac{1}{p_\sigma} \right) + \cos(\theta_{jik}) \right) \right\}^2 \tag{2.8}$$

This function has a similar shape as the angular function in the Tersoff potential, but with the advantage of using only one parameter p_σ as opposed to three in the Tersoff potential [8].

The angular expression for Tersoff Potential [8] is given by:

$$g(\theta_{ijk}) = 1 + \frac{c^2}{d^2} - \left[\frac{c^2}{d^2 + (h - \cos(\theta_{ijl}))^2} \right] \tag{2.9}$$

Where θ_{ijk} is the angle between bonds *ij* and *ik* and *c*, *d* and *h* are adjustable parameters. A major drawback of using only this expression for calculating bond-order is that structural differentiation in different silicon phases is not well resolved by the Tersoff potential and other similar potentials utilizing this formalism [33]. Secondly, it is valid only for atoms within the shell of first nearest neighbors, a deficiency that is the probable caused by the first problem.

An extension of the angular function in Tersoff potentials [6-8] was implemented in REBO and the adaptive intermolecular REBO (AIREBO) potentials [38-40] for carbon by addition of ad hoc functions and parameters. While these additions help in correcting for energetics of small hydrocarbon molecules, applying them to calculations beyond this

fitting region when estimating the sp^3 fraction in amorphous carbon at high densities resulted in unsatisfactory results [52,56].

The empirical bond-order potential for semiconductors developed by Conrad and Scheerscmidt [25] uses a different variant of the second moment approximation to TB for its bond-order model. Similar to HBOP, the angular terms depend on the hopping elements (ssσ and ppσ) that makes up the p_σ parameter. Here,

$$g_\sigma\left(\theta_{jik}\right) = a + b * \cos\left(\theta_{jik}\right) + c * \cos\left(2 * \theta_{jik}\right), \tag{2.10}$$

$$a = 1 - b - c, \tag{2.11}$$

$$b = \frac{4c}{p_\sigma}, \tag{2.12}$$

$$c = \frac{p_\sigma^2}{2\left(1 + p_\sigma\right)^2}, \tag{2.13}$$

$$p_\sigma = \frac{pp\sigma}{\left|ss\sigma\right|} \tag{2.14}$$

Where *a*, *b* and *c* are parameters determined from TB Hamiltonian bond integral matrix elements $ss\sigma$ and $pp\sigma$ that depends on the atomic species. A comparison of the angular function for all three empirical potentials given by Eqs. 2.8-2.10 is shown in Figure 2.1. They have closely similar shape between angles 0 and 90 degrees, but all of them approach zero at different bond angles. For example, the Tersoff potential [8] has its angular function at a minimum of about $2.0 * 10^{-5}$ and bond angle of 126.6 degrees, the Conrad and Scheerscmidt potential [25] has its minimum value of zero at a bond angle of

101.82 degrees, while HBOP gives a minimum of zero at the tetrahedral bond angle of 109.47 degrees. A theoretical interpretation of this function is that bond order is maximum (or $g(\theta)$ is minimum) for bonds in the tetrahedral geometry ($\theta_{jik} \sim 109.47$). By careful selection of $p_\sigma = 3$ in HBOP, $g(\theta)$ becomes zero at the tetrahedral angle. In graphitic silicon with an sp^2 structure, the bond angles are at 120 *degrees* , which is close to the minimum value of $g(\theta)$ for the HBOP function.

In this study, we follow a more pragmatic approach compare to the fourth moment approximation for computing the bond-order by using the second moment expression with the range extended with a cutoff function by including atoms that are up to 5.95 Å distance apart in the covalent interaction. A mere extension of the range of the potential while utilizing Eq. 2.6 results in an unsatisfactory potential that is not transferable between the bulk phases and clusters. The reason for this poor transferability is because atoms that are at larger distances away from the *ij* bond have equal weights of contribution to the bond order as atoms in the first neighbor shell when using Eq. 2.59 in section 2.6. This should not be the case as the first nearest neighbors have greater influence on the bond order. A more severe problem is that some of these long distance neighbors are at lower angles relative to the *ij* pair in question. These lower the bond order to unphysical values, especially for short bonds, which are more likely to have fewer atoms screening them strongly from one another, but which still have a larger number of distant neighbors. We therefore remedy this deficiency by screening the bond order contribution from each *ij* bond interaction in angular part of the potential using a similar screening function as that of bond energy (Eq. 2.7).

The idea is to ensure that more distant neighbors of atoms *i* and *j* that are highly screened contribute less to the bond order, while those atoms in the first coordination shell dominate the angular contribution to the bond order as expected. The screening of the bond-order is represented in Eq. 2.6. In the bulk phase, the screened bond-order expression ensures that *k* atoms (neighbors of the *ij* bond) that are farther away from the

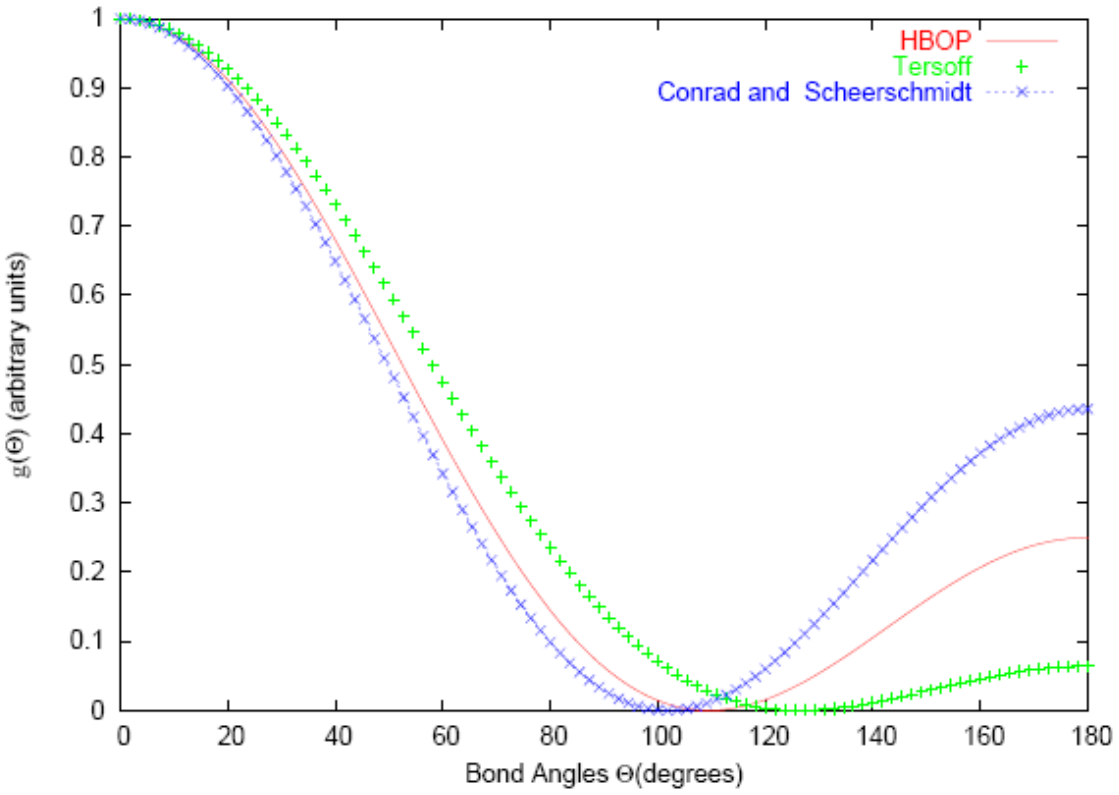

Figure 2.1 A comparative plot of g(θ) functions for bond-order potentials HBOP, Tersoff Potential [13] and the potential of Conrad and Scheerscmidt [78]. The $g(\theta)$ values for the Tersoff potential and Conrad and Scheerscmidt potential are normalized for easy comparison. The plot for Conrad and Scheerscmidt potential is $[g_{\sigma}(\theta)]^2$.

ij bond and having more intervening atoms are properly screened. This implies that, for long distant *ik* and *jk* bonds, lower numerical values of S_{ik} in Eq. 2.7 are obtained and hence a lowering of the angular contribution to the bond order in Eq. 2.6. Therefore, shorter *ik* bonds that are in the first neighbor shell of interaction have higher influence on the bond order as explained earlier.

An important feature of the fourth moment approximation in the BOP formulation is that atoms up to and including the third nearest neighbors of the *ij* bond and fifth nearest neighbor of one another are included in computing the bond order. While the current implementation avoids using those complex loops required by the BOP formalism, a computationally intensive procedure, we devise a method that incorporates up to the fifth nearest neighbors of the *ij* bond using a single expression (Eqs. 2.5-2.8) that is appropriately screened for the long distance atoms. This implementation gives a potential that is transferable between the bulk crystal phases and clusters, as demonstrated in Chapter 3.

2.3 Screening

A key feature of the current potential implementation for silicon is the inclusion of a bond screening term S_{ij} in the bond energy and bond order expressions. Screening is a quantum mechanical effect occurring between atoms in condensed phases and even clusters. The bond energy and bond order between two atoms is weakened by the presence of other atoms in their environment due to screening. The quantum mechanical

nature of the screening owes its origin to interference due to orbital overlap in covalent bonding. For example, the covalent interaction between a pair of Si atoms at a distance of 5 Å apart depends strongly on whether there is a third atom between them that screens their interaction by preventing orbital overlap. An expression describing the screening function was derived using approximations from BOP theory by inverting the nonorthogonality tight binding matrix [35]. This expression forms the starting point for our model of screening which is presented in section 2.3.4. Various other ad-hoc expressions [24,47,53] have been implemented for screening in classical potentials. A common feature of all the screening expressions is that the covalent interaction between two atoms is completely screened when another atom is directly on the line connecting them, but such screening gradually falls off as the interfering atoms get father away from the pair of atoms in question. Here, the mathematical expressions used for screening various potentials will be examined with their similarities and differences. Among these methods are the tight binding potentials for carbon [47], the embedded atom methods for silicon [24] and nickel [53], and analytical bond order potentials (BOP) [35,37]. A systematic derivation of the screening function for the current work is also presented.

2.3.1 Ames Group

Tsang, Wang, Chan and Ho [47] at Ames laboratory incorporated environmental dependence in the TB hopping integrals and the pairwise repulsive potential between two atoms i and j in carbon using a screening function. The two-center hopping integral in the minimal basis set in the TB Hamiltonian between a given pair of atoms *i* and *j* at

distance r_{ij} is given by

$$h^{\alpha\beta}\left(r_{ij}\right) = h_o^{\alpha\beta}\left(r_{ij}\right)\left(1 - S_{ij}^{\alpha\beta}\right) \tag{2.15}$$

Where α and β represent the atomic orbitals s or p and the screening function is modeled as

$$S_{ij}^{\alpha\beta} = \frac{\exp\left(\xi_{ij}\right) - \exp\left(-\xi_{ij}\right)}{\exp\left(\xi_{ij}\right) + \exp\left(\xi_{ij}\right)} \tag{2.16}$$

with

$$\xi_{ij} = \beta_1 \sum_l \exp\left[-\beta_2\left(\frac{r_{il} + r_{jl}}{r_{ij}}\right)^{\beta_3}\right] \tag{2.17}$$

where ξ_{ij} depends on the position of atoms *i* and *j* and those of their neighbors *l* and β_1, β_2 and β_3 are adjustable parameters. The function $h_o^{\alpha\beta}\left(r_{ij}\right)$ is the unscreened hopping integral which depends on the distance between atoms *i* and *j* [47]. In this formalism, the screening function $S_{ij}^{\alpha\beta}$ can be different for different hopping integrals depending on their environment. The TB hopping integrals, screening function and the pairwise repulsion are all smoothly cutoff at 5.2 Å. For calculating the screening function, all neighboring atoms *l* within a circular cutoff radius of 5.2 Å from both atoms *i* and *j* are included as shown in Figure 2.2 and Eq.2.17. This screening function was used in the TB expression to model binding energies of carbon [47] and silicon [54] in different environments such as graphite, BCC, SC, FCC and diamond. The expressions in Eqs. 2.16 and 2.17 are complicated with no theoretical basis other than having the mathematical appeal to describing the screening effect.

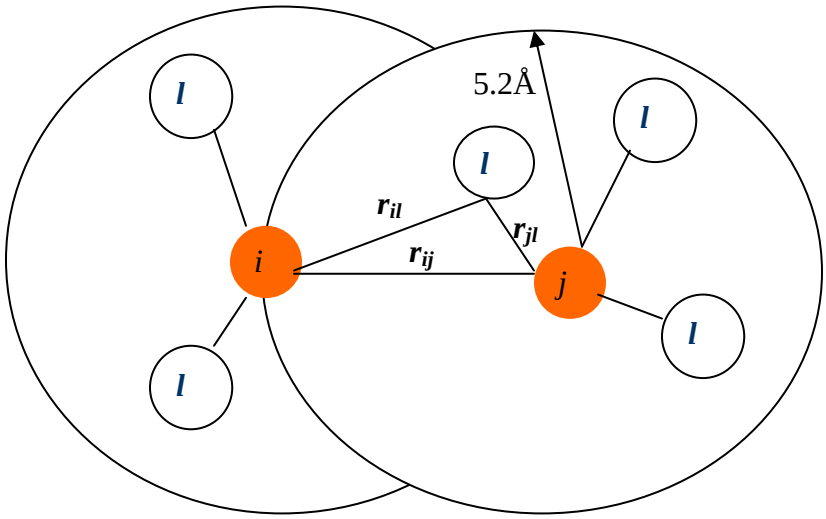

Figure 2.2. Schematic illustration of the screening of atoms *i* and *j* by atoms labeled *l* as described in the tight binding implementation for carbon by Tsang, Wang, Chan and Ho [47]. All atoms labeled *l* within the two circles with cutoff radius of 5.2 Å are included in calculating the screening functions in Eq. 2.16 and 2.17.

2.3.2 Cai Model

A modified embedded atom method (EAM) potential for silicon developed by Cai [24] incorporated screening in the embedding energy $F(\rho_i)$, where ρ_i is the local electron density at atom i obtained from linear superposition of electron densities of neighboring atoms around it. The EAM method [58-59] works well for metals and closely-packed materials because of the symmetric nature of their atomic arrangement. However, in covalent systems such as silicon, angular dependence in the bond energy makes it more difficult to model the covalent interactions using EAM-type models. Cai introduced a screening function that is able to model this angular behavior indirectly by multiplying the individual atomic electron density $f(r_{ij})$ of atom i due to atom j with the screening function S_{ijk}, where S_{ijk} is the screening function due to atom k in the vicinity of atoms i and j. Therefore, the local electron density of atom i is obtained as the sum of individual screened electron densities due to its neighbors j as

$$\rho_i = \sum_{j \neq (i)} S_{ij} f\left(r_{ij}\right) \tag{2.18}$$

where for a many-atom system, the screening of the contribution to electron density at atom i by its neighbors except for atom j is given by

$$S_{ij} = \prod_{k(\neq i,j)} S_{ijk} = \exp\left(- \sum_{k(\neq i,j)} g_{ijk} \right) \tag{2.19}$$

with

$$g_{ik} = \begin{cases} 0 & r_{ik} + r_{jk} - r_{ij} \geq 2r_{ij} \\ \dfrac{r_{ij}}{r_e}\left(\dfrac{r_{ij}}{r_{ik} + r_{jk} - r_{ij}} - \dfrac{1}{2} \right) & 0 \leq r_{ik} + r_{jk} - r_{ij} \geq 2r_{ij} \\ \infty & r_{ik} + r_{jk} - r_{ij} = 0 \end{cases} \tag{2.20}$$

The screening cutoff implementation uses a variable ellipsoidal radius of twice the distance between atoms *i* and *j* in question, or simply 2 r_{ij}. This choice is arbitrary and adopted for its mathematical convenience. The cutoff implementation for the Cai method is illustrated in Figure 2.3. The work presented in this dissertation adopts a similar strategy to that used by Cai although with crucial differences. In the current study, we also use a cutoff criteria depending on the geometry of the three atoms involved *(i, j* and *k*), with covalently bonded atoms *i* and *j* being screened by atom *k*. The cut off implementation for the HBOP also has elliptical symmetry, although with a fixed cutoff distance that does not depend on r_{ij} distant. They also differ in how this cutoff function is implemented.

In Cai's implementation, when atoms *i, k* and *j* are arranged in a straight line, with atom *k* on the line joining atoms *i* and *j*, or when angle θ_{jik} is 0 degrees, from Eq. 2.20, the screening S_{ijk} becomes 0. The physical interpretation of this scenario is that atom k completely screens the covalent interaction between atoms *i* and *j*. On the other extreme, when the three atoms are arranged in a straight line with atom k located at one end of the line, the screening becomes 1. That is, atom *k* has no effect on the covalent bonding between atoms *i* and *j* and therefore the multiplication factor S_{ij} in Eq. 2.19 will be 1. Cai demonstrated that the individual contribution to the atomic density given by S_{ijk} varies from 0 to 1 as the angle θ_{jik} (angle between the *ij* and *ik* bonds) varies from 0 to 180 degrees when using a three atom systems *(i, j* and *k*) arranged in isosceles triangle with distance $r_{ij} = r_{ik.}$ The behavior of S_{ijk} as a function of angle θ_{jik} presented in Cai's work [24], shows that the screening S_{ijk} rapidly approaches 1 as soon as the angle θ_{jik}

approaches 90 degrees for trimer of atoms. These key features help to connect the screening function indirectly with angular functions that are known to have more theoretical appeal [13, 46] for covalent systems. Even for different choices of the parameter r_e in Eq. 2.20 the screening function S_{ijk} is not too dissimilar for all angles between 90 and 180 degrees for the isosceles trimer example.

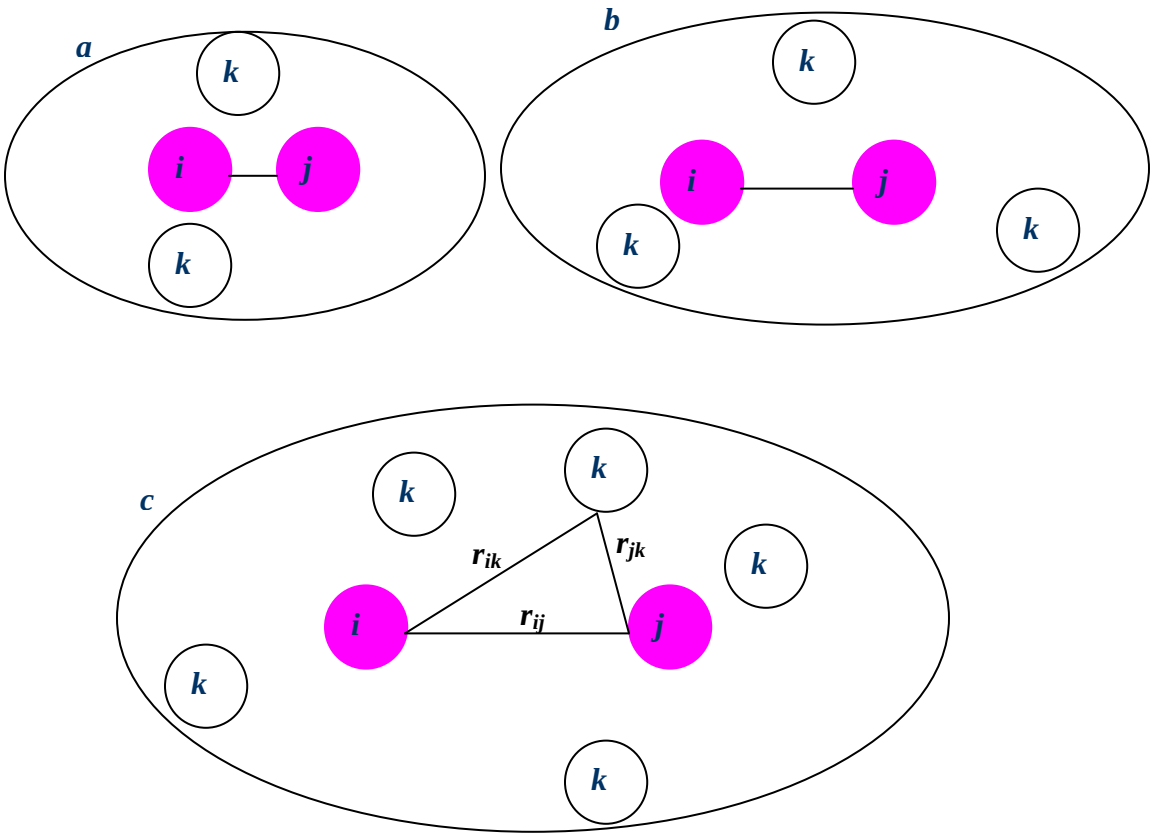

Figure 2.3 Schematic illustration of the screening of atoms i and j by atoms labeled k for silicon MEAM potential of Cai [24]. All atoms within the ellipse satisfy the condition $r_{ik} + r_{jk} - r_{ij} \geq 2\, r_{ij}$. The smallest ellipse labeled a represents the cutoff boundary for k atoms participating in screening of atoms i and j with short r_{ij} distance. The biggest ellipse labeled c with the largest r_{ij} has larger cutoff radius and more neighbors.

By physical intuition, the screening of the covalent bonding in atoms *i* and *j* as described by Cai's shows that screening decreases rapidly as atom *k* moves away from the covalent bonded atoms *i* and *j*. A drawback with this implementation is that computation of energy for an atom pair at large distant apart in the condensed phase will involve considerable computational expense due to large number of atoms necessary to compute the screening function. Even worse, this increased computational expense is needed only for the most weakly bound atoms, the ones for which screening is least useful. Because of mathematical nature of the cutoff implementation, this method will require substantial computational expense relative to most classical interatomic potentials for silicon when performing molecular dynamics simulation

An important difference between Cai's method and our implementation is that, while we maintain a similar elliptical screening cutoff, we avoid this pitfall by limiting the range at which atoms are able to participate in screening. Nonetheless, the screened MEAM potential of Cai was used to predict accurate lattice constant, cohesive energy, elastic constants and a negative Cauchy pressure of silicon in diamond cubic phase.

2.3.3 Baskes Method

One of the pioneers of the EAM method, M. I. Baskes [53] argues that the traditional implementation of the EAM models with a short radial cut off is not general because long-range psuodopotentials and electrostatic forces cannot use short range cutoffs. However, the justification that small forces on atoms at longer distances can be ignored has been widely adopted in many classical interatomic potentials for

silicon [8-10, 12-23]. The Baskes [53] implementation of screening was aimed at extending the range of the EAM potential for nickel by gradually reducing the forces on well separated atoms. In this implementation, two atoms *i* and *k* that are located at the edge of the minor axis of an ellipse are screened by atoms that are within the ellipse. This is illustrated in Figure 2.4. Atoms outside the ellipse formed this way are excluded from screening atoms *i* and *k*. In a similar manner to Cai, the atomic electron densities are multiplied by the screening function S_{ik} (screening between atoms *i* and *k* due to other atoms j in the system). Here, if atoms are unscreened S_{ik} = 0 and S_{ik} = 1 if they are completely screened.

The screening function is represented as

$$S_{ik} = \prod_{j \neq i,k} S_{ijk} \tag{2.21}$$

where S_{ijk} is computed as

$$S_{ijk} = f_c\left[\frac{C - C_{\min}}{C_{\max} - C_{\min}}\right] \tag{2.22}$$

with

$$C = \frac{2\left(X_{ik} + X_{kj}\right) - \left(X_{ik} - X_{kj}\right)^2 - 1}{1 - \left(X_{ik} - X_{kj}\right)} \tag{2.23}$$

and the equation for the ellipse in Figure 2.4 is given by

$$x^2 + \frac{1}{C} y^2 = \left(\frac{1}{2} r_{ik}\right)^2 \tag{2.24}$$

where $X_{ij} = \left(r_{ij} / r_{ik}\right)^2$ and $X_{jk} = \left(r_{jk} / r_{ik}\right)^2$ with C_{min} and C_{max} as the limiting values of C as shown in the ellipses of Figure 2.4. C_{min} and C_{max} are determined through fitting to be 0.8 and 2.8 respectively. The cutoff function f_c is represented as:

$$f_c(x) = \begin{cases} 1 & x \geq 1 \\ 1 - \left[1 - (1-x)^4\right]^2 & 0 < x < 1 \\ 0 & x \leq 0 \end{cases} \tag{2.25}$$

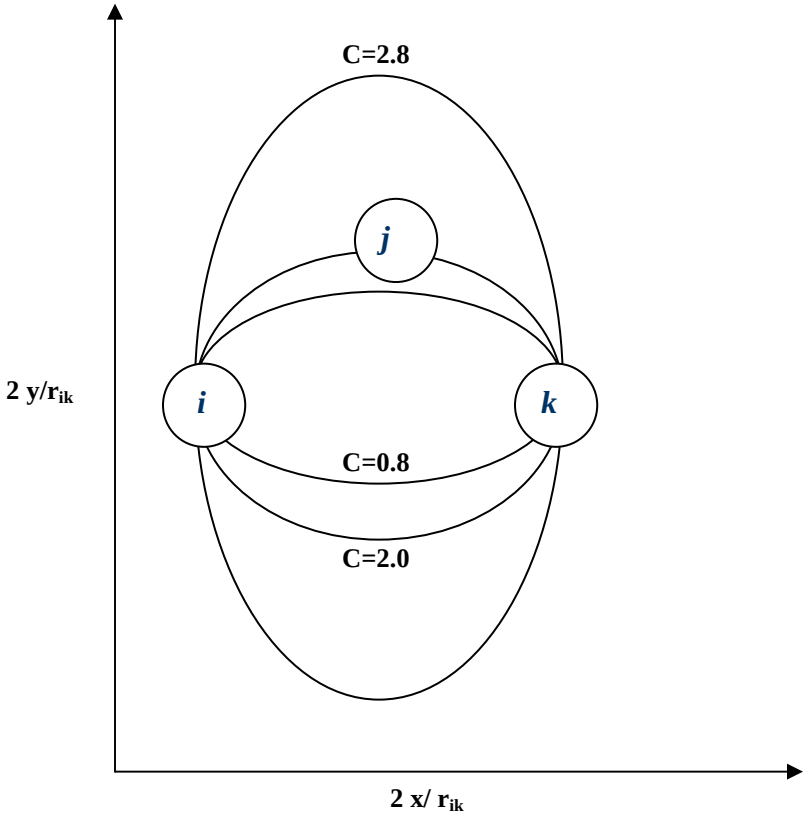

Figure 2.4 Schematic illustration of screening of atoms *i* and *k* by atom *j*. Atoms outside the ellipse bounded with C = 2.8 do not screen atoms *i* and *k*, while those inside the ellipse with C = 0.8 screen atoms *i* and *k* completely.

A unique difference between this implementation and those presented earlier is how the cutoff is applied. The cutoff ellipse depends on the distance of the bond *ik* with limiting conditions set forth by C_{min} and C_{max}. The potential expression has a radial cutoff distance of 4.0 Å for the *ik* bond in nickel. The screening expressions were used in the MEAM potential to successfully reproduce the experimental binding energies of FCC, HCP and BCC phases and vacancy formation, vacancy migration and stacking fault energies in nickel [53]. There is no provision to justify that those atoms within the small ellipse with C = 0.8 will completely screen the *ik* bond. For example, condensed phase liquid at high density may have abundant number of configurations with atoms closely packed within C = 0.8 ellipse of one and other. This type of scenario will lead to several atom pairs been completely screened by nearby atoms when using Eq. 2.21 – 2.25 and thereby resulting in zero contribution to the total energy of the system by these pairs. In practice, these atom pairs will still have some covalent interaction with each other and thereby contributing to the total energy. This may consequently lead to a wrong liquid structure and thereby render the potential unsatisfactory in this regime.

2.3.4 Analytical Bond-order Potential

All the previous expressions presented in sections 2.3.1-2.3.3 are ad hoc schemes introduced into their respective potentials to model the environmental dependent nature of covalent bonding through screening. A theoretically motivated expression for the screening function has been derived [35] from first principles and is presented in this section. Nguyen-Manh, Pettifor and Vitek [35] derived an analytical screening expression

to model the environmental dependence of the σ, π and δ bond integrals within the two-center TB approximation by using the BOP theory to invert the nonorthogonality matrix. The expression was derived by expressing the Hamiltonian matrix in terms of two-center bond integrals and Slater-Koster angular functions using the following assumptions;

(a) All sites have the same on-site energy.

(b) The screening of the *ij* bond is via the *s* orbitals on the neighboring *k* sites. The contributions from the *p* and *d* orbitals of *k* sites are neglected. The contributions from *s*, *p* and *d* orbitals of the sites *i* and *j* are considered in the screening expression.

(c) Three levels of Lanczos recursion are used to evaluate the determinant of the matrix within the BOP theory.

(d) All four-body and other higher contributions are neglected.

(e) The determinant of the off-diagonal *ik* and *jk* elements in the screened Hamiltonian matrix elements are assumed to be the same as those of the ij bond whose screening is of interest.

The final expression for the screening function is

$$S_{ll'\tau}^{ij} = \frac{\left(c_1^{ij}\right)_{ll'\tau} - \left(\overline{\mu}_2\right)_{ll'\tau} + \left(\overline{\mu}_3\right)_{ll'\tau}}{1 + O_{ll'\tau}^2\left(R_{ij}\right) - 2\left(\overline{\mu}_2\right)_{ll'\tau} + \left(\overline{\mu}_3\right)_{ll'\tau}} \tag{2.26}$$

with the *i*th atom second-moment contribution given by:

$$\left(\mu_2^i\right)_{ll'\tau} = O_{ll'\tau}^2\left(R_{ij}\right) + \sum_{k \neq i,j}\left[\left(1 + \delta_{\tau o}\right)/2\right] O_{ls\sigma}^2\left(R_{ik}\right) g_{l\tau}^2\left(\theta_{jik}\right) \tag{2.27}$$

while the *i*th third-moment contribution is

$$\left(\mu_3^i\right)_{ll'\tau} = \sum_{k\neq i,j}\left(1+\delta_{\tau\sigma}\right)O^3_{ikji}\, g_{l\tau}\left(\theta_{jik}\right)g_{l'\tau}\left(-\theta_{ijk}\right) \tag{2.28}$$

and

$$\left(c_1^{ij}\right)_{ll'\tau} = \sum_{k\neq i,j}\frac{\left[\left(1+\delta_{\tau\sigma}\right)/4\right]\left\{\begin{bmatrix}\left[\beta_{ls\sigma}\left(R_{ik}\right)O_{sl'}\left(R_{kj}\right)+O_{ls\sigma}\left(R_{ik}\right)\beta_{sl'\sigma}\left(R_{kj}\right)\right]g_{l\tau}\left(\theta_{jik}\right)g_{l'\tau}\left(-\theta_{ijk}\right)-\\ \beta_{ls\sigma}\left(R_{ik}\right)O_{sl\sigma}\left(R_{ki}\right)O_{ll'\tau}\left(R_{ij}\right)g^2_{l\tau}\left(\theta_{jik}\right)+\\ O_{ll'\tau}\left(R_{ij}\right)O_{l's\sigma}\left(R_{jk}\right)\beta_{sl'\sigma}\left(R_{kj}\right)g^2_{l'\tau}\left(\theta_{ijk}\right)\end{bmatrix}\right\}}{\beta_{ll'\tau}\left(R_{ij}\right)} \tag{2.29}$$

with

$$O^3_{ikji} = O_{ls\sigma}\left(R_{ik}\right)O_{sl'\sigma}\left(R_{kj}\right)O_{l'l\sigma}\left(R_{ji}\right) \tag{2.30}$$

θ_{jik} is the angle between bond *ij* and *ik* and R_{ab} is the *ab* bond distance. The *l*, *l'* = *s*, *p* or *d* represent orbitals and $\tau = \sigma$, π, or δ represent bond types. The average values of the second and third-moment contributions are written as

$$\left(\overline{\mu}_2\right)_{ll'\tau} = \frac{1}{2}\left[\left(\mu_2^i\right)_{ll'\tau} + \left(\mu_2^j\right)_{ll'\tau}\right] \tag{2.31}$$

and

$$\left(\overline{\mu}_3\right)_{ll'\tau} = \frac{1}{2}\left[\left(\mu_3^i\right)_{ll'\tau} + \left(\mu_3^j\right)_{ll'\tau}\right] \tag{2.32}$$

The bond integrals are expressed as:

$$\beta^{\mu\nu}_{ll'\tau}\left(R_{ij}\right) = A^{\mu\nu}_{ll'\tau}\exp\left(-\lambda^{\mu\nu}_{ll'\tau}R_{ij}\right) \tag{2.33}$$

A and λ are parameters determined by fitting to first and second nearest neighbor screened LMTO bond integrals. The overlap integrals are expressed as:

$$O^{\mu\nu}_{ll'\tau} = \exp\left(-\lambda^{\mu\nu}_{ll'\tau}R_{ij}\right) \tag{2.34}$$

The angular functions are defined as follow:

$$g_{o\sigma}(\theta) = 1 \tag{2.35}$$

$$g_{1\sigma}(\theta) = \cos(\theta) \tag{2.36}$$

$$g_{1\pi}(\theta) = \sin(\theta) \tag{2.37}$$

$$g_{2\sigma}(\theta) = (1/4)\,(1 + 3\cos(2\theta)) \tag{2.38}$$

$$g_{2\pi}(\theta) = (\sqrt{3}/2)\,\sin(2\theta) \tag{2.39}$$

$$g_{2\delta}(\theta) = (\sqrt{3}/4)\,(1 - \cos(2\theta)) \tag{2.40}$$

δ_{ij} is the kronecker delta function.

The above expressions Eq. 2.26- 2.40 were applied to compute the screened bond integrals in elemental BCC molybdenum, silicon and binary $MoSi_2$ [35]. The bond and overlap integrals as well as the screening function are cut off before the third neighbor shell. The screening function was also used to developed potentials for titanium (Ti), aluminum (Al) and alumina (TiAl) and to predict their correct elastic constants, stacking fault energies in excellent agreement with experimental and ab initio values [37]. The screened BOP expressions also reproduced the correct LMTO bond integrals in these elements (Ti and Al) and TiAl.

For the purpose of computing Eq. 2.26, the interference, second and third-moment contributions (Eqs. 2.27, 2.28 and 2.29) are first calculated and summed over all the *k* atoms that are neighbors of atoms *i* and *j* while considering at the same time, the *s*, *p* and *d* orbitals in the *ij* bond.

For application of this equation (Eq. 2.26) to silicon [35], the implication of cutting off the potential interaction before the third neighbor shell in bcc lattice is that

only atoms in the first and second nearest neighbor shells are included in the screening and therefore considered in the summations in Eqs. 2.27-2.29. The computational expense required to perform this task for use in molecular dynamics applications will be prohibitive to the extent of making it unattractive for investigating long time dynamical properties.

In the current work, a further simplifying assumption was made to reduce the complexity of the screening expression. We assume that only the *s* orbitals participate in screening of the *i* and *j* atoms. That is, we are concerned only with the $l = l' = s$ and $\tau = \sigma$ interactions. If we consider a trimer of atoms with only one *k* atom screening the *ij* bond and substituting Eq. 2.33 and 2.34 for the overlap and bond integral respectively into Eq. 2.29, for each *ij*, *ik* and *jk* bonds, the interference function simplifies to

$$c_1^{ij} = \frac{O_{ik}O_{kj}}{O_{ij}} - \frac{1}{2}O_{ik}^2 - \frac{1}{2}O_{jk}^2 \tag{2.41}$$

By writing this explicitly as

$$c_1^{ij} = e^{-\lambda\left(R_{ik}+R_{jk}-R_{ij}\right)} - \frac{1}{2}e^{-2\lambda R_{ik}} - \frac{1}{2}e^{-2\lambda R_{jk}} \tag{2.42}$$

it is apparent why Nguyen-Manh, Pettifor and Vitek [35] stated that for the $ss\sigma$ bond, the interference function is 'not too dissimilar in form' to the Ames' group [47] expression, which is given by

$$\xi_{ij} = \beta_1 \sum_l \exp\left[-\beta_2 \left(\frac{r_{il} + r_{jl}}{r_{ij}} \right)^{\beta_3} \right]$$

in Eq. 2.17. An important point to note in this comparison (Eqs. 2.41, 2.42 and 2.17) is that as R_{ik} and R_{jk} increase, the second and third terms of Eq. 2.41 decay faster than the first term. Then, Eq. 2.40 approaches the form of Eq. 2.17 and they will become identical for the case where β_3 = 1. A decrease in R_{ij} also results in a decrease in the overall function in both models. These features are essential to reproduce reasonable physical behavior for the screening function.

We made further simplification to Eq. 2.26. By substituting Eqs. 2.27, 2.28, 2.30, 2.31, 2.32, 2.33, 2.34, 2.35, 2.36 and 2.38 into Eq. 2.26 for the specific case of a single *k* atom interacting only through σ bonding, we arrived at

$$S_{ss\sigma}^{ij} = \frac{O_{ik}O_{kj} - \alpha}{1 - \alpha} \tag{2.43}$$

where, $\alpha = O_{ij}^2 + O_{ik}^2 + O_{jk}^2 - 2O_{ik}O_{kj}O_{ij}$ (2.44)

The above screening expression (Eq. 2.43) is identical to the BOP result [35] for the $ss\sigma$ bond interaction in a trimer. Using the definition of overlap integral in Eq. 2.34 to obtain a simplified expression for Eq. 2.43, the resulting equation is appealing enough for efficient use in a classical interatomic potential. We did in fact implement this, but we later discovered that in a disordered phase, some atomic configurations lead to a scenario where Eq. 2.41 is singular when α = 1. This leads to infinite forces that are not suitable for molecular dynamics simulations.

We made a second assumption in order to circumvent the singularity problem by ignoring α in Eq. 2.43. We assume that in Eq. 2.43.

$$\alpha << \frac{O_{ik}O_{kj}}{O_{ij}} \tag{2.45}$$

Therefore the screening expression reduces to

$$S_{ij} = \frac{O_{ik}O_{kj}}{O_{ij}} = e^{-\lambda\left(r_{ik}+r_{kj}-r_{ij}\right)} \tag{2.46}$$

Eq. 2.46 is simple enough for straightforward implementation in an empirical potential. The equation also posses desirable mathematical features that are essential for physical interpretation of screening in covalent bonding. Firstly, Eq. 2.46 satisfies the condition that the screening function take a value of 1 when atom *k* is located in between atoms *i* and *j* and on the line directly connecting them. Under this scenario the argument $r_{ik} + r_{kj} - r_{ij} = 0$ and Eq. 2.46 gives a screening of 1. The second feature is that the screening will be 0 if atoms *i* and *j* are not neighbors. In other words, if r_{ij} approaches infinity, then Eq. 2.46 becomes 0. For many-atoms system, we therefore compute the screening function for atoms *i* and *j* in presence of their neighbors *k* using a product of all the three-atom expression in Eq. 2.46. The S_{ij} expression is given by:

$$S_{ij} = \prod_{k\neq i,j}\left(1 - f_c\left(\Delta r_{ijk}\right)\exp\left(-\lambda\left(r_{ik}+r_{jk}-r_{ij}\right)\right)\right) \tag{2.47}$$

where $f_c\left(\Delta r_{ijk}\right)$ is given by Eq. 2.4 and $\Delta r_{ijk} = r_{ik} + r_{jk} - r_{ij}$.

Similarly, a_0, a_1 and a_2 retain their values as presented earlier in section 2.1. The inclusion of the cutoff function ensures that the screening goes smoothly to zero at elliptic radius of $\Delta r_{ijk} = 5.95\,\text{Å}$. The function S_{ij} is zero when atoms *i* and *j* are completely screened and S_{ij} is 1 when no screening exist. The implementation of this scheme can be

visualized by looking at two atoms labeled *i* and *j* whose bond energy is to be evaluated (See Figure. 2.5). Their bond energy is screened by atoms labeled *k*. Atoms that are labeled *k'* are further away and outside the ellipse, do not screen the *ij* bond. The introduction of the ellipsoidal cutoff ensures that atoms that are sufficiently far away from the pair are completely prevented from screening the bond energy.

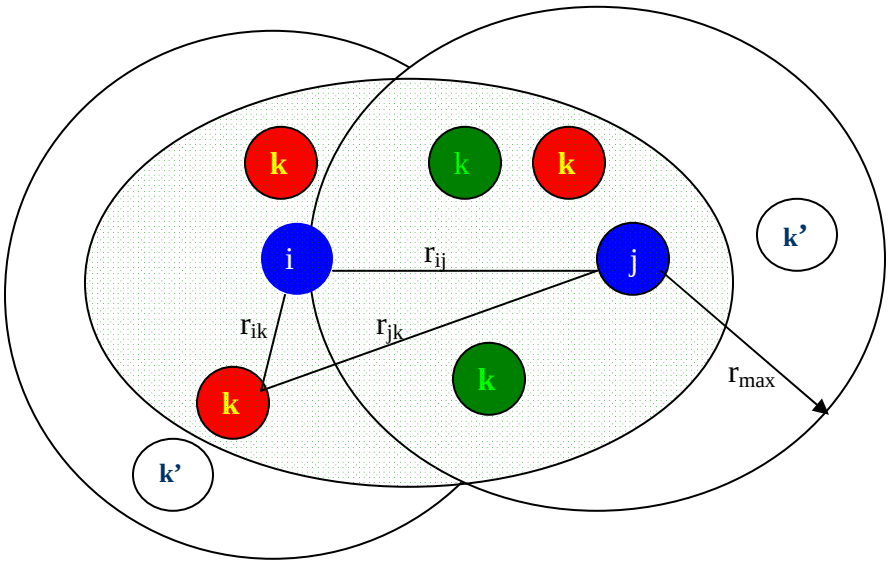

Figure 2.5. Schematic illustration of the screening of atoms *i* and *j* by atoms labeled *k* within the cut-off ellipse shown. The ellipse satisfies the cutoff condition for the potential under study. Atoms labeled *k'* within the circular bond energy cut-off radius of atoms *i* and *j*, but outside the ellipse do not screen the *i-j* interaction.

2.4 Promotion Energy

In trying to understand the chemical basis for interaction of atoms in tetrahedral solids such as silicon, several different expressions have been derived from first principles to account for various components of the total energy [49-50, 60-61]. Among these components is the energy associated with change of occupancy of the orbitals when electrons are promoted from the free atom s^2p^2 configuration to the hybrid sp^3 configuration when forming the solid. This is known as the promotion energy [49-50].

One of the pertinent features of bonding in tetrahedral silicon is the balance between promotion energy cost for sp^3 hybridization and bonding energy gained that controls the *s* and *p* orbital occupancies, a treatment that can be described with the Weaire-Thorpe model [62]. In this model, the total energy is computed as the sum of bond energy, resulting from matrix element between the overlapping hybrids of two different atoms and promotion energy, which is the on-site matrix element between different hybrids on the same atom. A good example of this is the tight-binding bond model (TBBM). Here, binding energy is defined as the difference in total energy of the condensed solid and that of the free atoms forming it. [50]. Despite its success in tight binding (TB) model, the use of promotion energy as an additive term to model interatomic potential has yet to receive proper attention, probably due to lack of progress in simplifying the first principles expression to a simpler formula that can be easily calculated .

This changed in 1990, when Petiffor et al. [33] introduced approximations to the promotion energy derived from the second-moment approximation to the local density of

states in a minimal basis using tight binding (TB) theory. The expression has been used along with a pair potential and covalent bond energies to estimate the total energy in Petiffor's analytical bond order potential BOP [34]. The BOP model including the promotion energy has been used successfully to predict energetic and other properties of crystals in some covalent [13, 34,] and multi-component systems [63] of interest. To our knowledge, no empirical potential has explicitly used promotion energy as a functional term in the potential energy despite the fact that it's importance was suggested more than a decade ago [64].

One mathematical definition of promotion energy can be obtained from the tight binding model exploiting the variational principle of density functional theory (DFT). In this formalism known as the TBBM [50], the total energy of a solid is obtained as a function of an approximate charge density by iterating the Schrödinger equation once (that is, non self-consistent solution). The binding energy of the solid is then expressed as a sum of four terms: covalent bond energy, promotion energy, electrostatic energy and exchange correlation energy.

In a more general treatment [49] using the non-orthogonal basis set the promotion energy is defined as

$$E_{prom} = \sum_{\alpha} \left(q_{\alpha} - N_{\alpha}^{freeatom} \right) H_{\alpha\alpha} \tag{2.48}$$

This expression calculates the promotion energy as the sum of on-site orbital energies $H_{\alpha\alpha}$, weighted by the difference in charge density between the hybrids q_{α} and the free atoms ($N_{\alpha}^{freeatom}$).

$$q_\alpha = \sum_\beta \sum_n f_n c_n^\alpha \left(c_n^\beta\right) * O_{\beta\alpha} \tag{2.49}$$

is use to calculate the gross charge density of orbital α in the molecule.

Here f_n is the occupation number for the one-electron wave function φ_α

and c_n^α and c_n^β are expansion coefficients, with the overlap matrix defined as

$$O_{\beta\alpha} = \langle \varphi_\beta \mid \varphi_\alpha \rangle \tag{2.50}$$

The orbital-resolved bond order here is defined as

$$\theta_{\alpha\beta} = \sum_n f_n c_n^\alpha \left(c_n^\beta\right) * O_{\beta\alpha} \tag{2.51}$$

and the summation of $\theta_{\alpha\beta}$ over all orbitals of atoms *i* and *j* yield the bond order θ_{ij} between the two atoms. This has a physically transparent meaning in chemical bonding.

In order to obtain a simplified expression suitable for use in classical molecular dynamics, Eq. 2.48 was reformulated [33] to define the promotion energy of an atom *i* as

$$E_{prom} = \sum_i \left(E_p^\alpha - E_s^\alpha\right)\left(\Delta N_p\right)_i^\alpha \delta_{\mu\alpha} \tag{2.52}$$

where $\left(E_p^\alpha - E_s^\alpha\right)$ is the splitting between *s* and *p* energy levels on species α. $\delta_{\mu\alpha}$ is a kronecker delta function for species μ and α. The splitting energy is assumed to be constant and $\left(\Delta N_p\right)_i^\alpha$ is the change in the number of *p* orbital electrons on specie α at site *i* compared to the free atom. For local charge neutrality $\left(\Delta N_p\right) + \left(\Delta N_s\right) = 0$ so that promotion energy tends to zero as the atoms move apart.

Both $\left(\Delta N_p\right)_i^\alpha$ in Eq. 2.52 and the term in the bracket of Eq. 2.48 represent the change in occupation number due to hybridization, a key to understanding the meaning of promotion energy. In both cases, the total promotion energy is obtained by multiplying the number of electrons transferred by the splitting energies between the *s* and *p* orbitals as represented by $\left(E_p^\alpha - E_s^\alpha\right)$ in Eq. 2.52.

The BOP theory approximation using a recursive Green function has been performed [63] to obtain the promotion energy as a function of measurable quantities. The final expression is given by

$$E_{prom} = \delta\left[1 - \frac{1}{\sqrt{1 + A\sum_{j\neq i}\frac{\beta_{ij}^\sigma}{\delta}}}\right] \tag{2.53}$$

Where $\delta = \left(\varepsilon_i - \varepsilon_j\right)$ is the splitting energy, A is a fitting parameter, and β_{ij}^σ is the σ bond energy between atoms *i* and *j*.

It is clear from Eq. 2.52 that the promotion energy is function of the bond energy without the inclusion of the bond order. The promotion energy is a property of an atom in covalent environment. In general, the promotion energy depends on the environment of the atom. For example, the *s*-*p* mixing increases with decreasing volume in Si, SiC and C [60]. Since this affects the promotion energy, this energy is generally expected to be dependent on the volume and the atomic environment [61]. The inclusion of the bond order should ensure a more complete and accurate definition, but such treatment will also

lead to a more complicated expression that is more expensive to evaluate in molecular dynamics simulations.

The inclusion of promotion energy in analytical bond order potentials has been shown to help in providing a consistent description [65] of second-order properties such as the bulk modulus. An extensive study of the effects of different energy contributions in the TB [66] description of surface reconstruction of Si (110), Si (100) and Si (111) has shown that lowering of the surface binding energy upon surface reconstruction is due in part to reduction in the promotion energy. The tilting of the surface atoms that occurs when a silicon surface undergoes reconstruction is attributed to the strong tendency to lower surface energy by means of re-hybridization of the surface atoms. This re-hybridization is best described by including the promotion energy of the system into the interatomic potential. In view of this importance, we have included the effect of promotion energy in the present potential. We investigated three different expressions, bearing in mind that promotion energy is a property of an atom in its environment.

The first of these expressions defines promotion energy as a function of the coordination number of the atom in question. This was motivated by the first principles Eqs. 2.48 and 2.51. We can see that a relationship exists between the promotion energy and effective bond-order of atom *i* with all its neighboring atoms or, indirectly, the coordination number.

Brenner [67] has derived the relationship between the cohesive energy and the bond order starting from the bond energy of an atom i in the second moment approximation. For a regular solid, this bond-order was shown previously to be

proportional to the inverse square root of the local coordination number by Abell [46].

Using the specific definition of coordination number as presented by Fournier et al. [64], a definition of promotion energy consistent with Eq. 2.48 as the product of splitting energy and effective bond orders between atom *i* and its neighbors is:

$$\left(V_{prom}\right)^i = \sigma\left[1-\frac{1}{\sqrt{1+dz_i}}\right] \tag{2.54}$$

where σ and *d* are parameters and *z* is the coordination number defined as [64].

$$z_i = \frac{\left(\sum_j S_{ij}b_{ij}\right)^2}{\sum_j \left(S_{ij}b_{ij}\right)^2} \tag{2.55}$$

b_{ij} and S_{ij} retain their original definitions in Eqs. 2.6 and 2.47.

The second equation considered in this study is motivated by Eq. 2.52 and is given by

$$V_{prom} = \sigma_1\left[1-\frac{1}{\sqrt{1+\sigma_2\left(\sum_{j\neq i} S_{ij} * b_1 * b_{ij} V_{ij}^A\right)^2}}\right] \tag{2.56}$$

Where σ_1 and σ_2 are fitting parameters, and S_{ij}, b_{ij}, and V_{ij}^A are functions defined by Eqs. 2.47, 2.6 and 2.3 respectively.

The idea is to include the bond-order and screening functions in the definition of promotion energy. However this equation is complicated and requires significant computational expense to perform molecular dynamics particularly in evaluating the

forces via the gradient of Eq. 2.56. We therefore simplify this expression further by eliminating dependence on the bond-order and the screening functions to reduce to

$$V_{prom} = \sigma_1 \left[1 - \frac{1}{\sqrt{1 + \sigma_2 \left(\sum_{j \neq i} b_1 * V_{ij}^A \right)^2}} \right] \tag{2.57}$$

The above equation, Eq. 2.57 is now similar to Eq. 2.53 with the exception that we have redefined the fitting parameters and allow the splitting energy to be an adjustable parameter. We performed fitting of cluster promotion energies using all the three expressions, Eqs. 2.54, 2.56 and 2.57. The results show that there is little difference in the accuracy in going from one equation to another. We therefore use Eq. 2.57 for the remainder of this work.

There are problems associated with the implementations of Eqs. 2.54 and 2.56 that make them less attractive compared to Eq. 2.57. Firstly, it was difficult to enforce the right boundary conditions (by ensuring that the promotion energy smoothly reduces to zero) for Eq. 2.54 because the promotion energy function cannot be smoothly reduced to zero using a cutoff function, primarily because the function represent the energy of an atom and not an atom pair having an explicit distant dependence. Secondly, the coordination number function Eq. 2.55 can become singular in some disordered configurations leading to infinite forces, which is problematic for performing molecular dynamics simulations. On the other hand, the complicated nature of Eq. 2.56 as mentioned earlier, make force computations significantly expensive in performing MD simulations.

2.5 The Case for a Long-Range Interaction

The current potential is completely described by Eqs. 2.1-2.8 and Eq. 2.57 along with the parameters listed in Table. 2.1. The parameters were obtained by fitting described in section 2.6.

Table 2.1. Parameters for the silicon bond order potential expressed in equations. 2.1-2.8 and 2.57.

b_1 = 44.7104248 eV	α = 6.62764953 $Å^{-1}$	σ_1 = 1.5532618 eV
β = 0.940243093 $Å^{-1}$	Q = 270.715816 Å	σ_2 = 0.193761112 eV
A = 8250.13723 eV	λ = 0.762678054 $Å^{-1}$	

The potential is made long-ranged by allowing silicon atoms up to and including the fifth-nearest neighbor shell in the diamond cubic phase to interact covalently. This is a marked difference from most short-ranged potentials that consider covalent interactions only between the first nearest neighbors. The long-range nature of the covalent interactions is in agreement with quantum mechanical descriptions of the bonding in silicon as shown Figure 2.6. In the figure the dimer potential energy curve for the Tersoff [8] and SW [9] potentials are too short-ranged compared to the quantum mechanical MCRI results for silicon. It is also essential to note that an accurate description of processes involving clusters, such as vapor deposition or ion implantation will require clusters interacting with the bulk surface at distances longer than the first-nearest neighbors. This will require long-range treatment of the covalent interactions which are essential for accurate description of these dynamical processes occurring in vapor deposition, crystal growth and etching. A short-ranged potential

will usually cut off these interactions too early as can be seen in Figure 2.6. For example, when atoms are ejected from the bulk surface during etching or when atoms or clusters of atoms approach the bulk surface from large distances during vapor depositions, they will have interactions that are long-ranged. Similarly, in condensed phases such as liquids at high densities, oscillatory and destabilizing effect can occur when atoms in the shell of second nearest neighbors are drawn into the cut-off region. This effect has been shown to result in unphysical characteristics such as disordered structures having lower energies than the native diamond cubic phase [68].

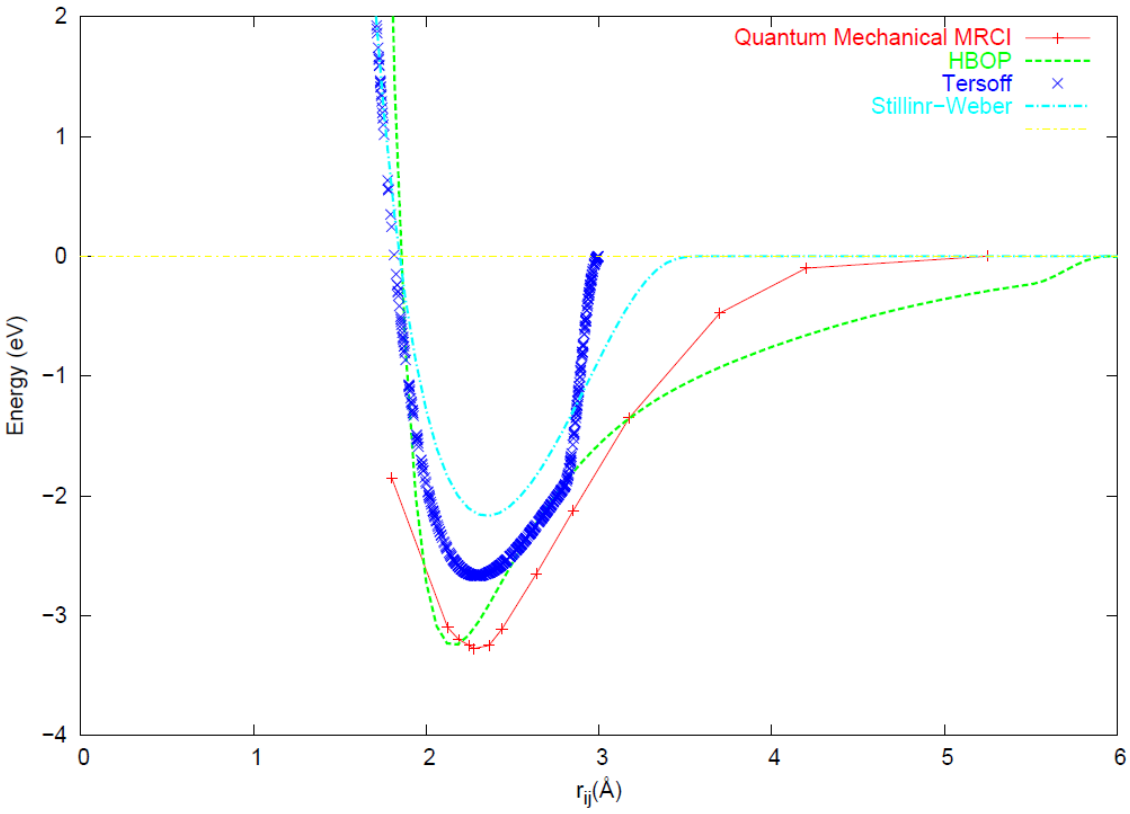

Figure 2.6 Comparative plots of two-body potential energy curves for silicon. The multirefrence configuration interaction (MRCI) data points were taken from Ref. [73].

Long-range interactions have been implemented for classical silicon potentials [20, 68-69]. However, the extended range alone does not necessarily guarantee a better potential. In the case of the potential of Pearson, Takai, Halicioglu and Tiller (PTHT) [69], the minimum energy configuration turns out to be the simple hexagonal structure instead of the traditional diamond cubic. It is not clear if this flaw can be corrected by better fitting. The problem might be due to an inherent limitation of the functional form itself.

We introduce screening functions in the binding energy expression, a theoretical procedure that has proven effective for extending the range of interatomic potentials [24,37]. The question about how far the range of the potential needs to be extended has been addressed using different arguments. In the case of the MEAM potential [11] for silicon, the potential range was set at a point where the fit to the potential becomes optimum with respect to the cutoff distance. While for a silicon tight binding potential [70] the cutoff distance was moved to the point where the clathrate structure becomes higher in energy than the diamond structure. A more compelling argument about what constitutes a "good" cutoff distance was investigated using a fit to phonon frequencies [16-19]. An illustration of the effect of cut-off distance on the error in fitting the current potential can be visualized in Figures 2.7. A rigorous fit of the potential P1 (described in section 2.6) to the equation of state properties E_0 (cohesive energy), B_0 (bulk modulus) B' (pressure derivative of bulk modulus), and V_0 (equilibrium volume) to 11 different silicon bulk phases was performed at 6 different cutoff distances of 4.75 Å, 5.0 Å, 5.25 Å, 5.50 Å, 5.75 Å and 5.95 Å. The mean absolute average error in equation of state properties

decreases with increasing cutoff distances and begins to saturate after 5.75 Å, which can be viewed as a specific parameterization of the HBOP. Note that the HBOP in general shows lower average error compare to the Tersoff potential for silicon. On the basis of the above study and in order to reproduce the correct phonon behavior, a cutoff distance of 5.95 Å is used for the current potential in all subsequent fits

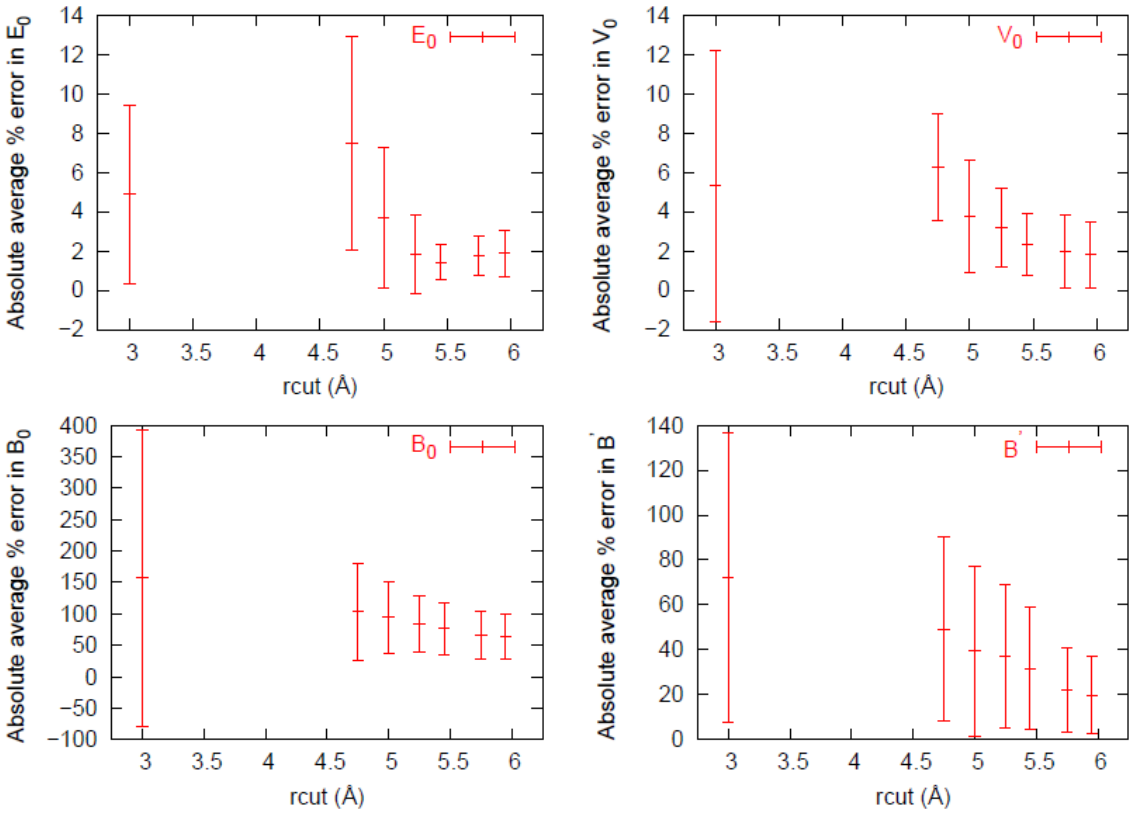

Figure 2.7 Plots of absolute average percent error in equations of state properties of 11 silicon phases namely: diamond, hexagonal diamond, *SC*, *FCC*, *BCC*, *BC8*, *R8*, *ST12*, simple hexagonal, *β-Sn* and *BCT5*. Where E_0, is the Cohesive energy, V_0 is the equilibrium volume, B_0 is bulk modulus, and $B' = dB/dP$ as a function of potential cutoff distances. The Tersoff potential is indicated at rcut distance of 3.0Å.

2.6 Fitting Procedure

Four different screened potentials were studied, starting with the simplest form and then increasing the complexity by adding new functions and parameters. The starting potential, named P1, is written as

$$E_B = \sum_i \sum_{j>i} f_c\left(r_{ij}\right)\left[V_R\left(r_{ij}\right) - S_{ij} b_{ij} b_1 V_A\left(r_{ij}\right)\right] \tag{2.58}$$

where all symbols retain their definitions as given by Eqs. 2.2-2.5 and Eqs. 2.7-2.8 except that the σ bond-order is given by

$$b_{ij}^{\sigma} = \frac{1}{\sqrt{\left(1 + \sum_{(k\neq i,j)} f_c(r_{ij}) g\left(\cos\left(\theta_{jik}\right)\right)\right)}} \tag{2.59}$$

Thus this potential include screening only in the bond energy and not in the bond order, and does not include promotion energy.

The second potential named P2 is written as

$$E_B = \sum_i \sum_{j>i} f_c\left(r_{ij}\right)\left[V_R\left(r_{ij}\right) - S_{ij} b_{ij} b_1 V_A\left(r_{ij}\right)\right] + V_{prom} \tag{2.60}$$

This is exactly Eq. 2.58 with the addition of the promotion energy V_{prom} defined in Eq. 2.57 with unscreened bond order Eq. 2.59 rather than Eq. 2.6.

The third potential, named P3, is defined by Eq. 2.58 with b_{ij} given by Eq. 2.6. P3 has screening introduced in the bond-order, but excludes the promotion energy term. The final potential named, P4, is completely described by Eqs. 2.1-2.8, 2.57 and Table 2.1. This is the most complex of the four potentials and includes both a screened bond order as well as a contribution from the promotion energy. This systematic procedure of adding

terms and parameters to the equation enable us ascertains their influence on the accuracy and the behavior of the potential with respect to their addition or omission to the potential expression.

Starting with P1, the potentials were each fitted to reproduce the Murnaghan equation of state (EOS) parameters for 15 silicon phases and cluster binding energies for clusters Si_3-Si_8 shown in Appendix 1.1. Additionally, V_{prom} in potentials P2 and P4 were fitted to cluster promotion energies [64]. The Murnaghan EOS [77] is given by

$$E_b(V) = E_0 + \left(\frac{B_0 V}{B'(B'-1)}\right)\left[B'\left(1-\frac{V_0}{V}\right)+\left(\frac{V_0}{V}\right)^{B'}-1\right] \tag{2.61}$$

Where $E_b(V)$ is the cohesive energy as a function of volume, E_0 is the equilibrium cohesive energy, V_0 is the equilibrium volume, B_0 is the bulk modulus and B' is the pressure derivative of the bulk modulus.

The fitting database consists of 15 different silicon phases at various strains ranging from 0.8 to 1.2, and the binding and promotion energies of the 17 silicon cluster structures shown in Appendix 1.1. The choice of this fitting database is aimed at exploring the wide polymorphic arrangement of crystalline silicon bulk phases including high-coordinate phases, and the opposite extreme of low coordinate clusters. The goal is that this will enable the potential to perform well in the intermediate structures like surfaces, amorphous, defects and liquids. A common practice is to fit potentials to equilibrium properties such as lattice constants, cohesive energies, phonon frequencies and elastic constants of diamond cubic silicon. Sometimes other non-equilibrium properties are included to improve transferability, however, the use of a large fitting

database does not necessarily guarantee that the potential will be transferable to some other extreme conditions away from equilibrium not represented in the fitting database.

Another problem is that the potential expressions can have inherent physical limitations that are not easily remedied by adding more functions and parameters. Having a large number of parameters and functions can be helpful [14], but the fundamental flaws may still be apparent in configurations far from equilibrium. Large number of parameters might be unhelpful in explaining these deficiencies if the physical interpretations of these parameters are unrelated to the problem.

Silicon is one of the most challenging elements for modeling and simulations primarily because of its many diverse polymorphs with the ability to exist in covalent or metallic bonding at different pressures. Silicon clusters can also take properties between these two extremes, and silicon's surface behaviors and defects are also complex. It is therefore pertinent to take all these systems into consideration when developing and performing a fit to a potential. An important procedure for probing the limits of any potential expression was demonstrated for the "glue" model potentials for aluminum [71]. The authors performed extensive tests for over 25 models on a large database from experiments and ab initio calculations. The strategy used in the study called for dividing the database into two parts, one for fitting the potentials and the others for the testing. A similar procedure has been adopted with success for aluminum and nickel potentials [72]. By following the change in the root mean square error in the properties between the fitting and testing stage, it was clear that the use of more parameters does not necessarily result in a better fit. However, by rigorous fitting to the database, it was possible to

ascertain the optimum number of parameters and even functional representations that provide an optimal fit to the available data. We employ a similar approach used in these studies [71-72] in development of the current potential. One of the crucial lessons from those studies is that a functional form with as few as four parameters was able to perform at the same level of accuracy as potentials with nine parameters. The performance of these two functional forms also happens to be the limit of the possible accuracy that can be obtained from the large database used. It is more important that the choice of the functional form used reflects the physical bonding characteristics of the system than it is to introduce elaborate numbers of non-physically motivated parameters.

The database used for EOS properties for the 15 silicon phases were obtained from references 74-76, 102-110 and 126 as displayed in Table 3.1 of Chapter 3. All binding and promotion energies for clusters were obtained from DFT work of Fournier, Sinnott, and DePristo [64]. The fitting was carried out by minimizing an objective function using a global minimization algorithm referred to as the controlled random search method [116-117, 133-136].

The objective function is defined as;

$$z = \sum_{i=1}^{L} \sum_{k=1}^{M} \left[\frac{\left(p_k^i - p_k^{i,o} \right)^2}{\left(\omega_k^i \right)^2} \right] \tag{2.62}$$

where p_k^i the numerical values of the properties k in phase *i* as computed by HBOP and $p_k^{i,o}$ are the corresponding experimental/DFT values of those properties and ω_k^i are the weights used in fitting the model to the properties and *M* is the total number of properties used and *L* is the total number of silicon phases and clusters used for the fitting.

This objective function is used to perform an optimization in a multidimensional parameter space. A preliminary selection of an initial starting point in parameter space was done by randomly generating a large (about 100,000) combination of numerical values of potential parameters (A, Q, α, β, b_1, λ, σ_1 and σ_2). In order to determine what constitute a good range of parameter values, we examined five different interatomic potentials in the literature that share similar characteristics to our potential [8, 25, 32, 131, 132]. In Table 2.2, the list of these potentials and the numerical values of their parameters are shown. It is pertinent to note that these potentials are each a sum of two exponential functions (Eq. 1.1 -1.3) with four major parameters A, α, b_1 and β as described in Chapter 1. From Table 2.2, good ranges for these parameters ware determined based on typical values among all these potentials. These ranges serve as the initial domain that was used to generate random combinations of parameters A, α, b_1 and β for the HBOP model. The initial domain for these parameters was set as follow:

$100 \leq A \leq 5000$ eV, $2.0 \leq \alpha \leq 7.0$ Å^{-1}, $10 \leq b_1 \leq 1200.0$ eV and $1.0 \leq \beta \leq 3.0$ Å^{-1} .

Table 2.2 Parameters in silicon potentials having the form defined in Eqs. 1.1 -1.3

Potential	b_1 (eV)	β (Å^{-1})	A (eV)	α (Å^{-1})
Tersoff [a)]	471.1800	1.7322	1830.8000	2.4792
Conrad and Scheerschmidt [b)]	75.0300	1.6600	1845.8640	2.6000
Khor and Sharma [c)]	230.5726	1.3415	2794.2386	3.1327
Dodson [d)]	155.0800	1.3969	1614.6	2.7793
Ackland [e)]	16.6359	1.1448	208.4428	5.6736

a) Ref. 8, [b)] Ref. 25, [c)] Ref. 32, [d)] Ref 131, [e)] Ref. 132

For the parameter *Q*, a good starting point was identified from the REBO potential, which uses an identical expression to that of HBOP. A value of about 0.3 Å was used as the final optimized value in REBO while experience during fitting of this potential (REBO) shows that Q can take values up to 10,000 Å. We therefore set $0.1 \leq Q \leq 100{,}000$ Å.

The screening function implemented in the BOP [35] has the coefficient of the overlap and hopping integrals for silicon taking values ranging from 0.60 and 0.95 $Å^{-1}$. The parameter λ is the screening coefficient in HBOP and it has the role of controlling the strength of the screening between two atoms from their neighbors. If $\lambda >> 1$ $Å^{-1}$, then the screening curve decays quickly to zero at distances less than 1 Å, resulting into a weak screening for most physically realistic configurations. On the other hand, values of $\lambda << 1$ $Å^{-1}$ can result in a screening effect that is too strong. Therefore, λ values ranging from 0.1 to 5.0 $Å^{-1}$ were chosen as an initial domain, to span a wide range of parameter values that is sufficient to capture the two extremes of weak and strong screening.

A careful look at the BOP [63] potential using promotion energy reveals that σ_1 in HBOP corresponds to the splitting energy of silicon used for computing the promotion energy in the BOP theory. The splitting energy of silicon in BOP is 7.0 eV, but a DFT study [64] and TB method [62] have both computed values close to 4.0 eV for this energy. The splitting energy is derived from theoretical calculations in the BOP promotion energy, but for the sake of flexibility, the corresponding value of σ_1 in HBOP is treated as an adjustable parameter. We compare σ_2 to the parameter *A* in Eq. 50 of reference 63. Therefore, the following initial domain were chosen for σ_1 and σ_2 : $0.5 \leq \sigma_1 \leq 15.0$ eV and $0.5 \leq \sigma_2 \leq 20.0$ eV.

Confining these parameters to the limits set above, 100,000 random parameter values were generated using a uniform distribution within the bounds for each parameter. In the next stage, these parameters were randomly combine to form a complete set {*A*, *Q*, α, β, b_1, λ, σ_1 , σ_2} of 100,000 points in the 8-dimensional parameter space. Each set of parameters completely defined the HBOP potential (Eqs. 2.1- 2.8 and 2.57). The set of parameters along with experimental/DFT properties and their respective weights were fed into a MD simulation using Clemson University condor pool to compute the objective function in Eq. 2.62. For the weights, we have chosen the following values after several adjustments to obtain the best possible fit. For diamond and hexagonal diamond phases, the following weights were used.

$$\omega_{E_0}^{diamond} = 10^{-4} eV, \omega_{E_0}^{HEXD} = 10^{-4} eV, \omega_{V_0}^{diamond} = 5.0 \times 10^{-4} \text{Å}^3, \omega_{V_0}^{HEXD} = 5 \times 10^{-4} \text{Å}^3$$

$$\omega_{B_0}^{diamond} = 10^{-4} eV / \text{Å}^3, \omega_{B_0}^{HEXD} = 5 \times 10^{-4} eV / \text{Å}^3, \omega_{B'}^{diamond} = 5 \times 10^{-4}, \omega_{B'}^{HEXD} = 10^{-3}$$

For the remaining 13 phases (β-Sn, BC8, R8, SHEX, FCC, BCC, SC, HCP, ST12, BCT5, Imma, Si_{34}, and Si_{46}), the following weights were assigned to the EOS properties;

$$\omega_{E_0}^{i} = 2.5 \times 10^{-4} eV, \omega_{V_0}^{i} = 10^{-3} \text{Å}^3, \omega_{B_0}^{i} = 7.5 \times 10^{-4} eV / \text{Å}^3, \omega_{B'}^{i} = 5 \times 10^{-3}.$$

For cluster binding energies, the weights assigned varied from 10^{-3} eV for the highest binding energy cluster Si3.1 to 2.5 x 10^{-3} eV for the lowest binding energy cluster Si8.1. An equal weight of 10^{-3} eV was assigned for all cluster promotion energies.

The Clemson University condor pool consists of hundreds of workstations with about 1500 processors running Windows, Solaris and Linux operating systems. After completing all the 100,000 objective function or chi-square (χ^2) evaluation, the numerical

values are then sorted in increasing order of their χ^2 values. At the end of the initial function evaluation, the parameter sets with lower χ^2 values were found to have λ in the vicinity of 0.7 $Å^{-1}$ to 0.9 $Å^{-1}$. This sorting procedure helps to shrink the overall parameter domain for subsequent optimization. In the next stage, 160 sets of parameters with the lowest χ^2 were used in subsequent global optimization in the CRS algorithm.

In general, the idea behind the CRS algorithm [133-136] is to start with a predetermined number of parameter sets *N* in an initial search domain *D*. All the trial points *N* must satisfy the upper and lower bounds on each variable *n* forming the domain *D*. In the current study, these *n* variables are the parameter set $\{A, Q, \alpha, \beta, b_1, \lambda, \sigma_1, \sigma_2\}$. The limits specified for these parameters earlier ($100 \leq A \leq 5000$ eV, $2.0 \leq \alpha \leq 7.0$ $Å^{-1}$, $10 \leq b_1 \leq 1200.0$ eV and $1.0 \leq \beta \leq 3.0$ $Å^{-1}$, $0.5 \leq \sigma_1 \leq 15.0$ eV and $0.5 \leq \sigma_2 \leq 20.0$ eV and $0.1 \leq \lambda \leq 5.0$ $Å^{-1}$) form the domain *D* for which these parameters will be optimized.

The objective function (Eq. 2.62) is then evaluated at each of the *N* trial points (160 for this study) and the corresponding numerical values are stored as $f(N)$ in an array *A*. The array *A* forms a set of objective function values and their corresponding parameter set that were used to determine the χ^2. The values of $f(N)$ are sorted so that the set with the lowest value is stored as point *L* with function value f_L, while those with the highest function value are stored as point *H* with function value f_H. The suggested number of trial points *N* can vary from $10(n + 1)$ to as high as $25n$ [133-134], depending on the domain size and nature of the problem in question. The larger the value of *N* used, the bigger is the size of computer memory required for storage purpose and the slower the convergent

of the optimization. For this study, $N = 20n$ (20 * 8 parameters = 160). The iteration begins by randomly selecting $n + 1$ distinct points, R_1, R_2,……..R_{n+1}, from N to form a simplex of points in n-space. The set of parameters R_{n+1} is arbitrarily taken as the pole or vertex of the simplex. The image of the pole, P is computed as the next trial point for minimization of the objective function. The trial point P is computed from R_{n+1} and the centroid G of the remaining n points R_1, R_2,……..R_n as follow:

$$\overline{P} = 2 \times \overline{G} - \overline{R}_{n+1} \tag{2.63}$$

where $\overline{P}, \overline{R}$ and $\overline{R}_{n+1}$ are position vectors in n-space of the corresponding points.

There are different variant of the CRS algorithm, differing in definition of the point P. The definition of P used for this fitting work can be found in references 116 and 117.

The procedure is illustrated diagrammatically in Figure 2.8. The point P is checked to ensure that all the parameters n making up the point satisfy the constraints or boundary conditions set for the optimization. If any of the constraint is not satisfied, (that is, one of the parameters is outside the bound) then, point P is discarded and n +1 new distinct points are randomly selected from N and used to generate a new trial point P. If those conditions are satisfied, the objective function (Eq. 2.62) is evaluated with the parameters defined by the point P as f_p. Now, f_p is compared with f_H, the highest function value in array A. If $f_p < f_H$ then point H is replaced, in A by P. The point with the second highest function in the previous set now becomes point H, with the new highest function value in array A. However, if $f_p > f_H$, then point P is discarded and then new trial points are chosen from array A to generate a new point P and the procedure is repeated.

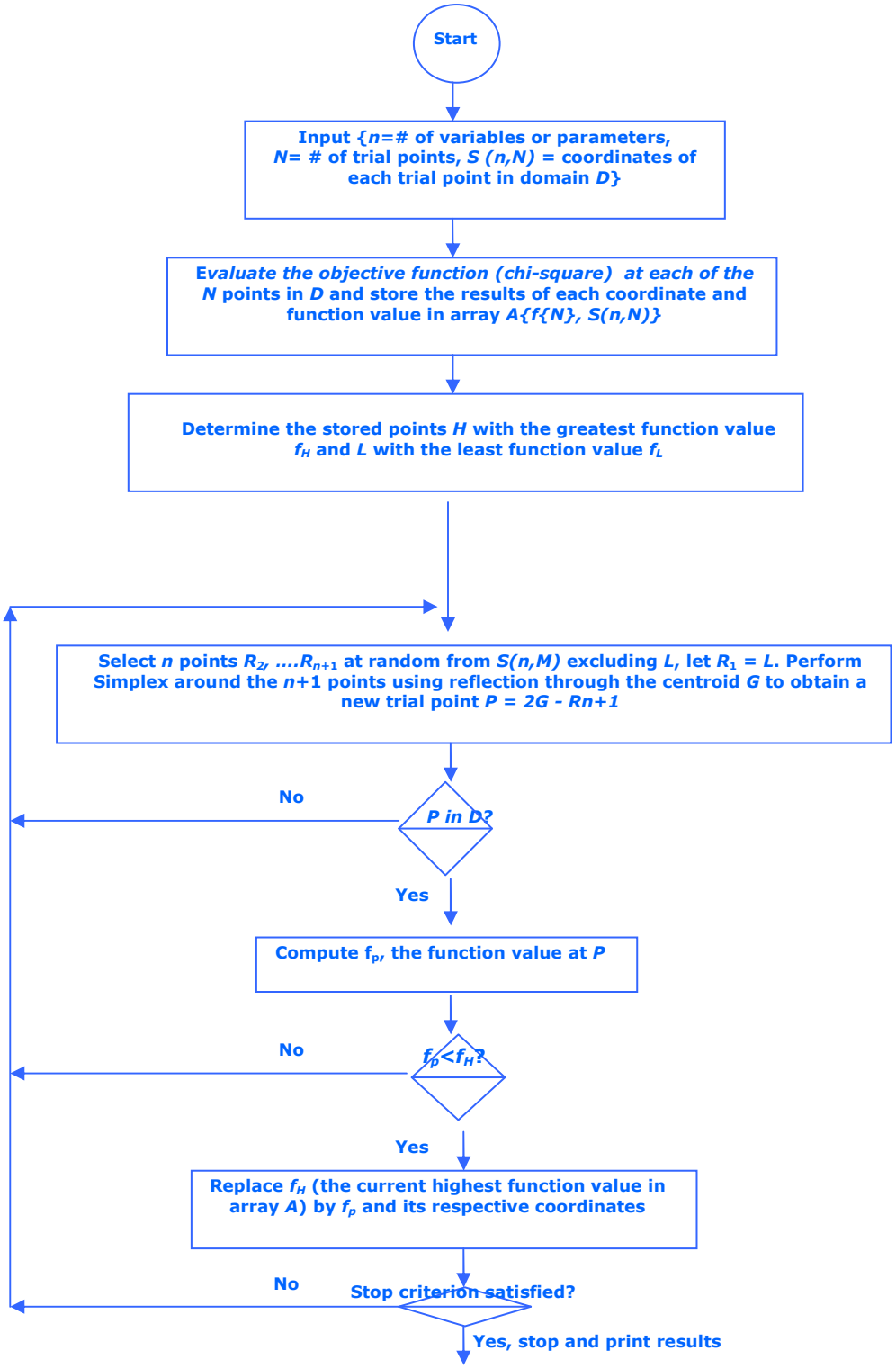

Figure 2.8 Flow diagram description of the CRS algorithm.

As the optimization proceeds, increasing number of points with lower function values are generated and replace points with higher function values in *A*. The optimization will get to a stage where all the points in *A* will cluster around minima with a function value lower than f_L. Note that the function value f_L changes as the optimization progresses. The procedure is terminated once a maximum number of iterations is achieved or when the difference between the highest function values f_H and the lowest function value f_L in array *A* falls below a define threshold.

In fitting the HBOP potential, the optimization sometimes reached a point where all the points in *A* are clustered around a boundary of one of the parameter variable *n*. When such scenario occurs, most of the new points *P* generated will falls outside the domain of the parameter *n* and a lot of wasteful computation occurs, thereby lowering the efficiency of the algorithm. It may be possible that a lower function value than f_L exists outside this boundary where the optimization is trapped. Therefore, the algorithm must be monitored at run time to determine if such condition is encountered. A simple solution that was adopted in fitting the HBOP potential is to stop the optimization and expand the domain (by increasing the range for the affected parameter) of the particular parameter that is trapped and restarting the procedure with the stored array *A* that was present at the stop time. The optimization is then continued until the termination criteria are reached or another boundary “trap” is encountered. If a boundary “trap” is encountered, the expansion of the domain is repeated as described above and the optimization is continued until the final termination is achieved. The optimization procedure used for this fitting is by no means a ‘fire and forget’ type of computation because of the possibility of

boundary “trap” that may lower the efficiency of the algorithm or possibly result in the optimization missing the “true” global minima. Therefore, the progress of the optimization must be monitored for changes in parameter and function values so as to detect this boundary “trap” as it happens.

The CRS optimization was carried out on Clemson University Palmetto cluster with Intel core 2 quad core processors running at 2.33 GHz. Evaluating the objective function (Eq. 2.62) takes about 150 seconds of CPU (Central processing Units) time, or about 24 iterations per hour. The computational requirement is inefficient for a single CPU because of the number of iterations required for convergence. The current optimization requires more than 12,000 function evaluations for convergence. It was observed that using an initial randomly generated parameters of N = 160 sets, the optimization failed to converge after 20,000 function evaluations. This is the reason why Condor was used to evaluate a large pool of initial starting points. By so doing, quality starting points were extracted for subsequent CRS optimization and this help reduce the number of function evaluations needed for convergence. To speed up the optimization, the function evaluation was reformulated through the use a parallel communication procedure (using OpenMP) which subdivides the function evaluation into 8 independent parts, with each part running on its own core within a node. The nodes consist of two Core 2 quad processors, where each processor has 4 cores. The final sum (Eq. 2.62) is then collated at the end of the run to give the $\chi 2$ value. This procedure reduces the average time to evaluate the function to about 28 seconds, a five-fold decrease in execution time.

The choice of the CRS algorithm for this problem was made because of the complex nature of the objective function. The derivative of the objective function can be discontinuous in some regions of parameter space. This makes the use of gradient methods problematic for minimization. The method also has the advantage that no gradient evaluation is required. The algorithm is also simple to implement as gradient implementation for the objective function is highly non-trivial. However when gradients are available, it can be inefficient compare to gradient and Hessian methods, as it requires more function evaluations and convergence to the minima can be slow. The final optimized parameters for potential P1, P2 and P3 are given in Appendix 2.1 -2.3, while those for P4 are shown in Table 2.1.

CHAPTER THREE

EQUATIONS OF STATE AND CLUSTER PROPERTIES

3.1 Equations of state for silicon phases

An important consideration for the development of this model is to ensure that silicon has the appropriate temperature and pressure phase diagram. This property ensures that silicon has the correct energies and structures under different conditions of temperature and pressure. In order words, we desire a transferable potential that gives the correct phase transitions and accurate structures and energies for bulk, defects, clusters, liquid and surfaces.

Silicon exists in diverse number of phases at high pressure. This “polymorphic perversity” [6-7] makes it a challenge to develop an accurate and transferable interatomic potential capable predicting properties away from the native diamond cubic phase. To our knowledge, 13 phases of silicon have been observed experimentally. Most of these crystalline phases of silicon were discovered during high pressure and heat induced phase transitions [103, 105, 109-110].

The 15 structures of silicon (all structures in Table 3.1 except the Cmca phase) at various strains used as input to fit the current potential span a wide range of the bulk structures and densities. The results of the equation of state (EOS) parameters for 16 phases (13 experimental and 3 hypothetical phases) of silicon computed using HBOP and compared with DFT/experimental values are presented in Table 3.1. The computed equilibrium energies and volume are in excellent agreement with DFT values. The absolute error in equilibrium cohesive energies and volume as computed using HBOP are

less than 5 % for most phases. The potential shows a good transferability between different silicon bulk environments. It is expected that intermediate arrangements within these structures will also be adequately described by our model.

The native diamond cubic phase (Si-I) of silicon is fourfold coordinated with each bond at a tetrahedral angle of about 109.47^{o} of each other. One of the criteria for judging the validity of an interatomic potential for silicon is to determine if the lowest energy structure is the diamond cubic phase. Among all the ordered phases presented in Table 3.1, the diamond cubic phase has the lowest cohesive energy. With the exception of the bulk modulus B_0, the other three EOS properties predicted by HBOP for diamond cubic phase are in excellent agreement with experimental values [75-76,102]. All EOS properties with double digit errors are shown in bold faces in Table 3.1. We observe that most of the least accurate results come from B_0 and B'. The prediction of these properties (B_0 and B') by various theoretical DFT methods are found to be inconsistent [74,104,106,119-121] because of the assumption of linearity of bulk modulus with pressure [i.e. $B(P) = B_0 + B'P$] in the first-order Murnaghan EOS. This assumption sometimes breaks down at high pressures, (if $P > B_0$). A second-order equation [based on $B(P) = B_0 + B'P + 1/2B''P^2$] is required to obtain more consistent values for B_0 and B' [115]. Therefore, it is not clear how well the HBOP potential performs in terms of these properties, but the cohesive energies and volumes are well reproduced by our model. The EOS properties with especially large percent error of 3 digits, are found in the hypothetical phases of silicon (SC and BCC). A number of experimental works on phase transition of silicon at high pressures have been performed [103,105,109,110,124,125].

Table 3.1. Equation of state properties for silicon crystalline phases computed using HBOP and compared alongside with DFT and experimental values. The abbreviated phases are (FCC = face-centered cubic, BCC = body-centered cubic, SC = simple cubic, HCP = hexagonal close packed, SHEX = simple hexagonal, HEXD= hexagonal diamond. The equilibrium energies, E_0 are in units of electron volts (eV), equilibrium volume, V_0, in units of ($Å^3$), the bulk modulus, B_0, in units of Pascal (Pa) and B' is dimensionless.

Phases	EOS Parameters	DFT/Experimental	HBOP	Absolute % error
Diamond	E_0	-4.6299 [a]	-4.6305	0.01
	V_0	20.0240 [b]	20.3268	1.51
	B_0	0.6109 [c]	0.7951	**30.15**
	B'	4.240 [c]	4.2573	0.41
β-Sn	E_0	-4.4077	-4.4844	1.73
	V_0	14.8859	15.2295	2.31
	B_0	0.7265	0.7435	2.35
	B'	3.8898	4.8420	**24.48**
BC8	E_0	-4.5042	-4.4047	2.21
	V_0	18.2619 [d]	18.2151	0.26
	B_0	0.5890 [e]	0.5910	0.34
	B'	5.5400 [e]	6.0525	9.25
R8	E_0	-4.5057	-4.3683	3.05
	V_0	17.4949	17.7897	1.69
	B_0	0.5478	0.6786	**23.88**
	B'	3.8980	5.6130	**44.00**
SHEX	E_0	-4.3946	-4.4825	2.00
	V_0	14.6400	14.9292	1.98
	B_0	0.7268	0.7130	1.90
	B'	3.9597	7.7785	**96.44**
FCC	E_0	-4.1580	-4.3844	5.44
	V_0	14.3372 [f]	15.0147	4.73
	B_0	0.5118 [f]	0.5843	**14.17**
	B'	4.2200 [f]	3.6715	**13.00**
HCP	E_0	-4.1855	-4.3825	4.70
	V_0	15.0180 [f]	14.8031	1.43
	B_0	0.4431 [f]	0.5407	**22.01**
	B'	3.9100 [f]	4.4598	**14.06**

Table 3.1 Continue:

ST12	E_0	-4.4945	-4.3498	3.22
	V_0	17.6500 [e]	17.9877	1.91
	B_0	0.5820 [e]	0.5650	2.93
	B'	3.4700 [e]	6.2963	**81.45**
HEXD	E_0	-4.6140	-4.5598	1.18
	V_0	19.7575	20.1322	1.90
	B_0	0.6110	0.7254	**18.72**
	B'	4.2400	4.6936	**10.70**
Cmca	E_0	-4.2625 [i]	-4.4142	3.60
	V_0	14.2404 [i]	14.6419	2.82
	B_0	0.6269 [i]	0.6491	3.54
	B'	4.4427 [i]	4.6363	4.36
Imma	E_0	-4.4089 [g]	-4.4932	1.91
	V_0	15.0250 [g]	15.0412	0.11
	B_0	0.5448 [g]	0.7609	**39.66**
	B'	4.8900 [g]	4.8822	0.16
Si_{34} Clathrate	E_0	-4.5550 [h]	-4.5597	0.10
	V_0	23.0910 [h]	21.7914	5.63
	B_0	0.5669 [h]	0.4732	**16.54**
	B'	5.2000 [h]	6.8398	**31.53**
Si_{46} Clathrate	E_0	-4.5609 [h]	-4.5456	0.33
	V_0	23.4281 [h]	21.4219	8.56
	B_0	0.5922 [h]	0.4789	**19.14**
	B'	4.0000 [h]	7.0005	**75.01**
BCT5	E_0	-4.3800	-4.5158	3.10
	V_0	16.7700	16.9109	0.84
	B_0	0.6439	0.7437	**15.59**
	B'	3.8597	5.2353	**35.64**
SC	E_0	-4.3437	-4.4189	1.73
	V_0	15.7653	15.9117	0.93
	B_0	0.6999	0.4253	**39.24**
	B'	3.3715	7.0719	**109.75**
BCC	E_0	-4.1790	-4.3227	3.44
	V_0	14.2427	14.5752	2.33
	B_0	0.6849	0.3655	**46.64**
	B'	3.2545	6.7929	**108.72**

[a] Ref 76. [b] Ref. 75. [c] Ref. 102. [d] Ref 103. [e] Ref 104,123. [f] Ref. 105
[g] Refs. 106,110. [h] Ref 107. [i] Ref 108,109,126
All data for DFT/Experimental EOS data are from reference 74 except where indicated.

Application of pressure to diamond cubic silicon in diamond anvil cell experiments results in phase transition to the β-Sn phase (Si-II) in the pressure range of 10-12 GPa [110,127,129]. Theoretical studies using DFT methods [74,119,126] have confirmed that the β-Sn structure is indeed the first phase to appear, in agreement with experimental results. Further application of pressure up to 248 GPa [105,108,115,119,124] have resulted in phase transitions to other crystalline phases with a consensus on the transition order which can be represented as follow:

Diamond (Si-I) → β-Sn (Si-II) → Imma (Si-XI) → SHEX (Si V) → Cmca (Si-VI) →HCP (Si-VII) → FCC (Si-X)

The BC8 phase (Si-III) can be obtained by decompressing the β-Sn phase to ambient pressures at room temperatures [103,124]. The HEXD (Si IV) was found when heating BC8 structure between 200-600^{o}C at ambient pressure [103,123]. When the β-Sn phase is decompressed to ambient pressure at 700^{o}C, the ST-12 (Si-IX) is formed. The silicon clathrates (Si_{34} and Si_{46}) are usually obtained as synthesized caged compounds [130]. Further studies on phase transition in silicon using HBOP will form the subject of future work.

For comparison purposes, the computed energies and lattice parameters for six silicon phases are presented in Table 3.2 for the HBOP model along with those predicted by six other interatomic potentials in the literature. Three of these potentials, namely, the Tersoff (T3) [8], Stillinger-Webber (SW) [9], and Environmental-dependent interatomic potential (EDIP) [10] are widely used interatomic potentials for silicon in various applications. In computing the root mean square error, the experimental lattice parameter

[75] and energy [76] of the cubic diamond phase along with DFT cohesive energies and lattice parameters for five other silicon phases (SC, BCC, FCC, β-Sn and BC8 structures) were taken as the correct standard in column 3 of Table 3.2. To ensure proper comparison, only the lattice parameters "*a*" were used for the non-cubic phases, β-Sn and BC8. This is to ensure consistency among all the phases considered. The root mean square errors in lattice parameter and energies for the seven interatomic potentials are presented in Figure 3.1.

The Tersoff potential [8] and second generation REBO potential for silicon (2B-Si) [12] both give root mean square values much less than 0.1 Å for the lattice parameters. This excellent agreement with experimental and DFT values can be attributed to the inclusion of these quantities in the fitting database for these potentials. The potential developed in this work gives a consistently lower root mean square error of approximately 0.1 (Å or eV) in both lattice constant and cohesive energies. It is important to mention that all of these properties were also used to fit the current potential. The less accurate results come from the high coordination number phases (FCC and BCC) where our model predicted lower energies than those of DFT values. This shortcoming can be observed visually on the equation of state plots in Figure 3.2. A plausible explanation for this problem is that bond energies involving atom pairs in highly coordinated phases are not optimally screened despite the large numbers of nearest neighbors contributing to the screening. This ultimately results in an overall lower energy for the structure than expected. It may be possible to remedy this problem by optimizing the screening coefficient λ with respect to other parameters in the potential. The EDIP model shows

Table 3.2: The cohesive energies and lattice parameters for silicon phases (*SC* = simple cubic, *BCC* = body center cubic, *FCC* = face center cubic, *β-Sn* = beta tin, *HCP* = hexagonal close packed). The energies E_0 are in units of electron volts (eV) while the lattice parameters a_0 are in Angstrom units Å.

Structure	Properties	Exp/DFT[a)]	HBOP	T3[b)]	SW[c)]	EDIP[d)]	MEAM[e)]	2B-Si[f)]	BOP4[g)]
Diamond Cubic	A_0	5.429 [h)]	5.458	5.432	5.431	5.429	5.429	5.429	5.430
	E_0	-4.63 [i)]	-4.63	-4.63	-4.63	-4.65	-4.63	-4.63	-4.63
SC	A_0	2.515	2.515	2.544	2.612	2.503	2.404	2.545	2.530
	E_0	-4.34	-4.42	-4.31	-4.34	-4.10	-4.28	-4.13	-4.21
BCC	A_0	3.088	3.160	3.084	3.245	3.243	3.187	3.076	3.010
	E_0	-4.18	-4.32	-4.20	-4.33	-3.036	-4.11	-4.02	-4.03
FCC	a_0	3.855 [j)]	4.069	3.897	4.147	4.081	4.363	3.944	3.881
	E_0	-4.16	-4.38	-3.87	-4.21	-2.79	-3.93	-3.37	-4.11
β-Sn	a_0	4.822	4.738	4.905	4.969	4.760	4.169	4.819	4.828
	E_0	-4.41	-4.48	-4.30	-4.42	-3.96	-4.32	-4.21	-4.30
BC8	a_0	6.640 [k)]	6.637	6.644	6.591	5.910	6181	6.657	6.185
	E_0	-4.50	-4.41	-4.39	-4.43	-4.40	-4.55	-4.31	-4.55
RMS Error in E_0 (eV)			0.099	0.04	0.155	0.319	0.391	0.04	0.196
RMS Error in a_0 (Å)			0.121	0.135	0.071	0.759	0.110	0.358	0.097

[a)] Ref. 74. [b)] Refs. 8,73 [c)] Refs. 9, 30, 73. [d)] Refs. 10, 12, 30. [e)] Ref. 11. [f)] Ref. 12. [g)] Refs. 12, 13. [h)] Ref 75. [i)] Ref. 76. [j)] Ref. 105. [k)] Ref. 103.

Cohesive energy and lattice constant for diamond-cubic are from experiment (Exp), while data for other phases, SC, BCC, FCC, β-Sn and BC8 are from DFT results of reference 74 expect where indicated.

unusually high root mean square deviations for both properties among the pack. The extent of this error in equilibrium structures and energies should be taken seriously when using the EDIP model for applications that may involve phase transitions and structural rearrangements. The EDIP model however predicts good results for defects and elastic properties [30].

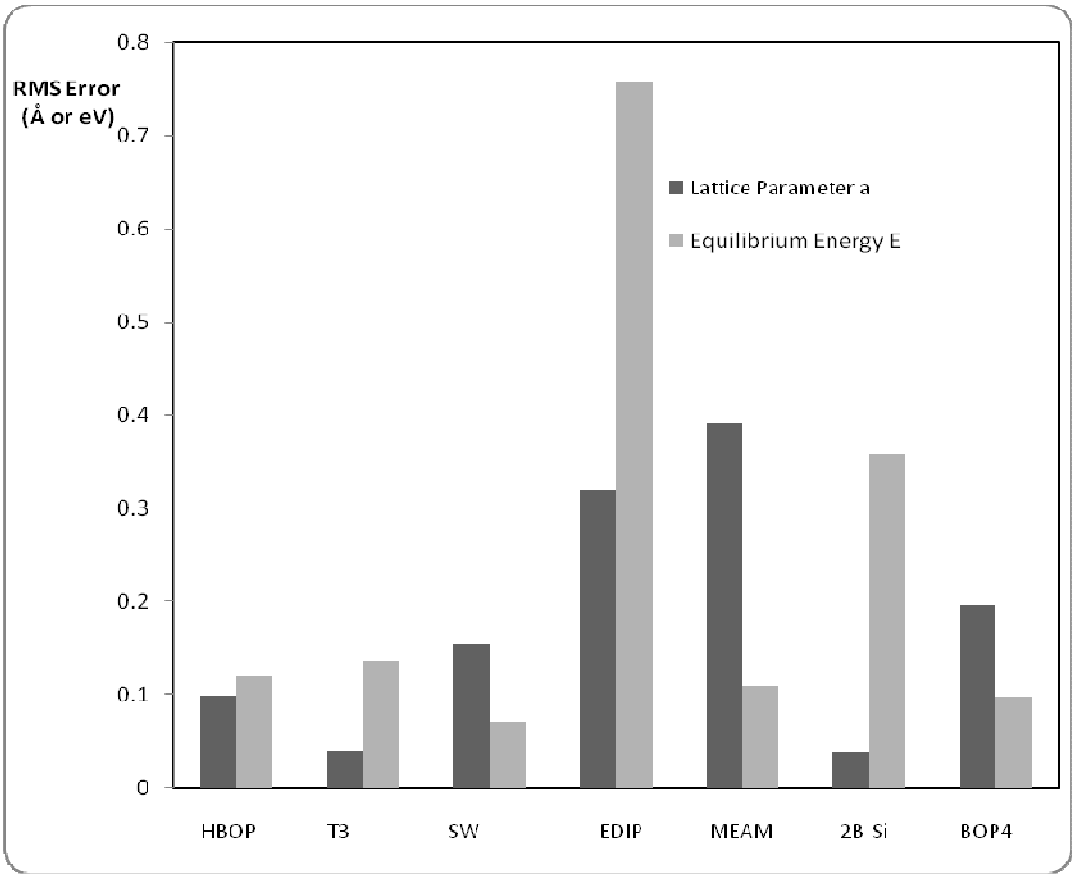

Figure 3.1: The root mean square (RMS) deviation from experiment/DFT for lattice parameters "*a*" and cohesive energies E_0 among six silicon phases (diamond, SC, BCC, FCC, β-Sn and BC8 structures) for potentials indicated in the abscissa. HBOP (current model), T3 (Tersoff Potential), SW (Stillinger-Weber Potential), EDIP (Environmental dependent interatomic potential), MEAM (Modified embedded atom method), 2B-Si (REBO for silicon), BOP4 (Bond order potential for Silicon).

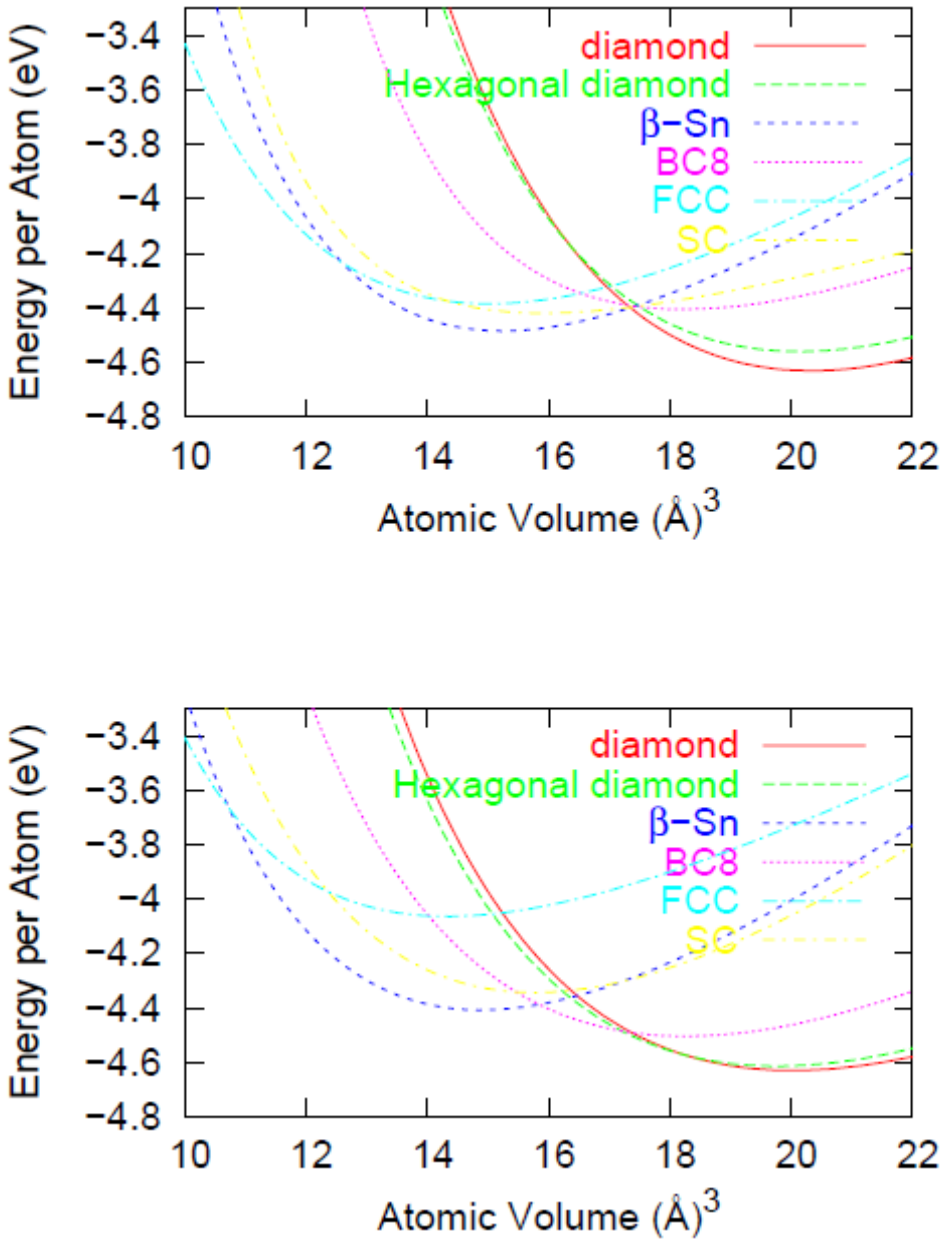

Figure 3.2: Equations of state curves for silicon phases. The bottom panel represents the DFT results of Need and Mujica [74] with the cohesive energy of the diamond structure normalized to the experimental value. The top panel is the result of the HBOP model.

3.2 Clusters

Clusters of silicon are generated in etching processes or can be deposited during crystal growth. Thus accurate prediction of energetics and structures of small silicon clusters is of paramount importance in explaining some of the phenomena encountered in silicon nanoelectronic applications. Silicon clusters of Si_n with n up to 200 have been studied extensively using experimental [78-83] and theoretical [64, 84-93] methods. These studies have provided a wealth of information about structures, energies, cluster rearrangements, polarizabilities, ion mobility, and ionization potentials of silicon clusters and the trends observed in these properties.

An important consideration that is of great interest in developing an interatomic potential is to reproduce different cluster structures with correct relative energies and to predict the correct global minimum structure among any given cluster of size n. Extensive global optimization studies [94-100] have been carried out to determine global minimum structures or to test the accuracy of several empirical potential models using clusters up to $n \leq 50$. The lesson from these studies is that no current empirical potential is able to predict all the correct global geometries even for cluster of size $n \leq 10$.

Experimental [78,101] investigations have only established global minimum structures for silicon clusters (Si_n) with $n \leq 7$ and there is disparity among the global minima for structures with $n \geq 8$ obtained using theoretical quantum mechanical methods in the literature. The differences in the level of theory between these quantum mechanical methods such as the generalized valence bond method [86], Hatree-Fork calculations [85], density functional theory, [64] couple cluster theory [87] and quantum Monte Carlo

calculations [88] are primarily due to different treatment of electron correlation with direct effect on the final energy differences among these clusters. The energies obtained by these quantum mechanical methods are usually obtained as the differences between large numerical values computed using different definitions of zero point energies. Smaller clusters with $n \leq 6$ with double and/or triple bonds, having the same number of atoms but different structural arrangements can sometimes exhibit very low energy differences in the order of 0.05 eV. The result is a flat potential energy surface in the vicinity of these structures. Such a scenario sometimes leads to wrong prediction of the global minimum structure.

The current potential is based on the fundamental principle that covalent bonding between two atoms is weakened in the presence of other neighboring atoms and their bond order is dependent on the local environment. This important physics is what is essential for differentiating between different environments, viz: bulk surfaces, clusters, liquid and amorphous structures. We focus on predicting the energy differences among small clusters of interest ($n \leq 8$) that constitute the major by-product of laser ablation, etching and crystal growth processes. We therefore fit the potentials to energies of 17 clusters of silicon (Si_n, $n \leq 8$) and equations of state for 15 bulk phases. It may not be possible to obtain a complete one to one mapping of the quantum mechanical potential energy surface with a classical potential but the goal is to provide reasonably accurate ground state energies and energy differences between small clusters in comparison with quantum mechanical results. The cohesive energies of clusters of silicon Si_3-Si_{10} clusters calculated using (HBOP) are presented and compared with DFT

Table 3.3 Cohesive energies (eV) for the most stable silicon clusters of Si_3-Si_{10} from various interatomic potentials and DFT results [64]. The abbreviations shown are interpreted as (HBOP, current model), (T3, Tersoff potential [8]), (SW, Stillinger and Weber Potential [9]), (B& A, Potential of Bouldin and Anderson [14]), (SWG, Stillinger, Weber and Gong potential [15,100]), (Li ,Johnston and Murrell potential [16-19,94]), (BH, Biswas and Herman potential [20]), (CH, Thermodynamic interatomic force field potential of Chelikowsky et al [21-23]). The root mean square error (RMS) is in units of eV.

Cluster	***DFT***	***HBOP***	***T3***	***SW***	***B&A***	***SWG***	***LJM***	***BH***	***CH***
Si_3	7.82	7.64	7.66	4.44	7.81	5.26	5.90	5.46	5.10
Si_4	12.36	11.92	13.01	8.65	13.36	8.68	10.69	9.12	10.40
Si_5	16.50	15.77	20.06	11.57	16.47	12.48	15.03	12.50	15.01
Si_6	20.72	19.62	26.07	15.15	21.33	16.64	19.50	16.20	20.70
Si_7	24.91	23.50	30.20	17.91	23.68	20.88	23.70	20.33	24.50
Si_8	28.01	27.14	35.04	22.96	27.75	25.03	28.76	25.32	29.20
Si_9	32.83	31.58	39.22	25.96	33.95	29.51	32.19	29.27	33.30
Si_{10}	37.68	36.33	43.36	29.94	37.94	33.96	37.43	33.39	37.50
RMS error		1.00	4.90	5.72	0.73	3.59	1.26	3.74	1.38

results [64] as well as those from seven interatomic potentials in the literature in Table 3.3 and Figure 3.5. The structural geometries and energies of all the clusters were taken from reference 64 as we believe DFT calculations give ground state energy values consistent with those obtained from experiments on small silicon clusters without the

need for scaling usually associated with Hartree-Fork and Mϕller-Plesset methods [14]. The binding energies computed by our model agree favorably with DFT values as presented in Figure 3.3. The trend in energy within cluster structures with the same number of atoms also follows closely with their corresponding theoretical values.

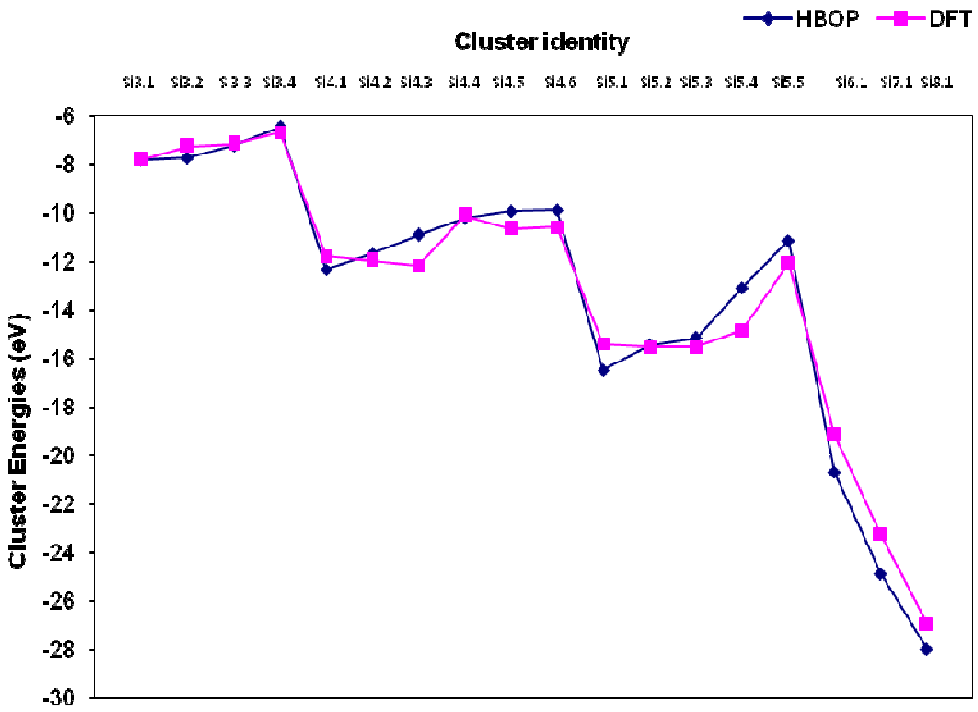

Figure 3.3: Binding energies of silicon clusters Si_n with $3 \leq n \leq 8$ for the hybrid bond-order potential (♦) and those obtained from DFT method (▪). Cluster identity corresponds to the labels in Appendix 1.1.

At the moment, we are content that our potential is able to reproduce accurate binding energies for the clusters of interest. The scatter plot shown in Figure 3.4 also confirms a good correlation (> 0.97) between our predicted cluster energies and those of DFT values. An important comparison between the root mean square errors in cohesive energies of small silicon clusters (Si_3-Si_{10}) and the DFT values [64] from Table 3.2 among eight interatomic potentials for silicon is presented in a bar chart shown in Figure 3.5.

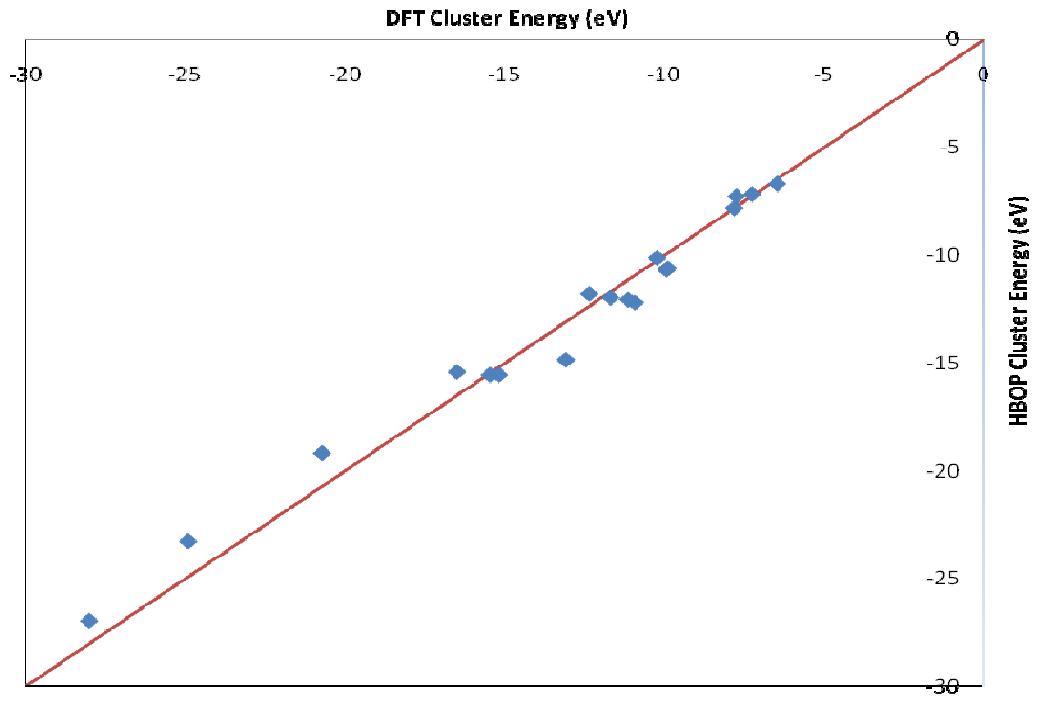

Figure 3.4: A scattered plot of silicon clusters (Si_n , $n \leq 8$) binding energies for the HBOP (vertical axis) along with their corresponding DFT values (horizontal axis). The straight line shown in the figure is the y = x plot. A point falling on the line corresponds to a perfect agreement between DFT and HBOP binding energy for the cluster in question.

The current model shows a reasonable agreement with theory in comparison with the general trend. The Tersoff [8] potential (T3) and Stillinger-Weber Potential [9] which are known to give good results for the energies and lattice parameters for bulk structures, (Table 3.1) turn out to perform poorly in terms of cluster energies (Table 3.2). This is a sign of poor transferability of these potentials from bulk to cluster properties.

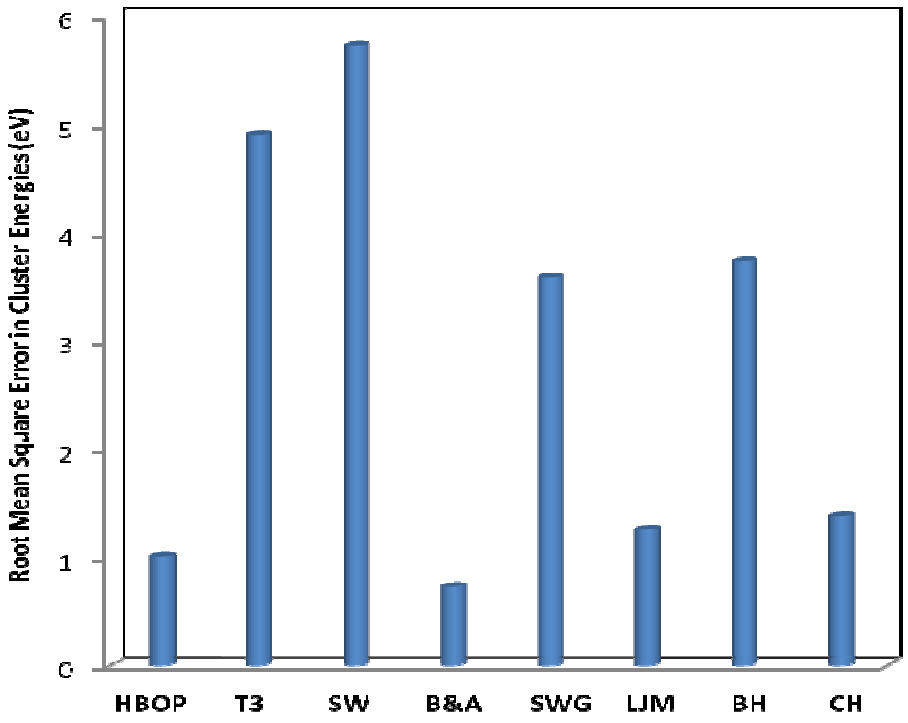

Figure 3.5: The root mean square (RMS) deviation (eV) from DFT cohesive energies of global minimum silicon clusters Si_3-Si_{10} among eight interatomic potentials described in Table 3.2 above.

In applications such as ion implantation, etching and vapor deposition where clusters are either added or removed from the bulk surface, energies of isolated clusters of silicon atoms must be correctly predicted, otherwise the outcome of such "computer experiments" will be questionable if not completely false.

In performing molecular simulations where clusters are involved, a candidate potential then needs to predict the cluster energies with reasonable accuracy. Therefore, care must be taken to access the merit of using a potential where error in cluster energies may give a completely different outcome from the experiment values.

The potential of Bouldin and Anderson (B &A) [14] shows the lowest root mean square error in this comparison of cluster energies. The B & A potential was fitted using all these cluster structures as input into complicated equations having more than 30 parameters, but the use of π-bonding expression within their formalism helps in predicting accurate energies for the lower number clusters Si_n with (n = 3-6) where others potentials are less impressive. It also important to point out that the LJM, HBOP and CH potentials were also fitted to scaled Hartree-Fork [85] and DFT [64] energies. The modified Stillinger-Weber potential or SWG [15,100], which is a refit of the original SW potential to include cluster energies in the fitting database was able to reduce the root mean square error from about 5.7 eV to approximately 3.6 eV, a substantial difference, but not convincing enough to make it accurate for cluster applications. This shows that without any modifications the two and three body expressions used for these potentials (SW and SWG) are not suitable for a transferable interatomic potential for silicon. In a similar manner the potential P1 in this study failed to simultaneously predict bulk and

cluster energies and structures as demonstrated in section 2.6. This explains why the T3 potential also failed to predict good cluster energies. The T3 and P1 potential presented in the previous chapter are analogous, except that P1 has screening incorporated in the bond energy equations. The success of the current model (HBOP) stems from the introduction of screening within the bond order expression, a feature that is absent in the Tersoff potential.

3.3 Promotion Energy

The promotion energy as defined in section 1.1 can be interpreted as energetic penalty due to under-coordination or over-coordination in clusters and bulk systems. The inclusion of this contribution to the energy provides an essential means of simultaneously modeling these two regimes within a single potential model. The expression for the promotion energy described in Eq. 1.15 was used for modeling this behavior within the current potential. Promotion energies resulting from DFT [64] calculations were obtained by multiplying the excitation energy for s^2p^2 to sp^3 with $2\text{-}ns_i$. Where $2 - ns_i$ is the number of electron promoted from the s to p orbitals. The quantity ns_i known as the *s* orbital population of atom i, was obtained using Mulliken analysis.

The results displayed in Figure 3.6 show a reasonable agreement in promotion energy for this study with those of DFT results [64]. The accuracy of the DFT results cannot be ascertained in any way as the mathematical definition of the promotion energy used in the study was formulated with simplifying assumptions. Furthermore, the use of Mulliken analysis for computing atomic charges also presents its own additional error in

the overall energy. However, the results are useful as a basis for establishing a trend among the clusters. The current potential exhibits relatively flat promotion energy values for clusters of size 3 and 5 even though the structures of these same size clusters are different from one another. A possible reason for this shortcoming may be due to neglect of π-bonding existing in some of these small clusters in HBOP model. As the size of the cluster increases, for Si_n with $n \geq 7$, the predicted promotion energies are closer to their corresponding DFT values.

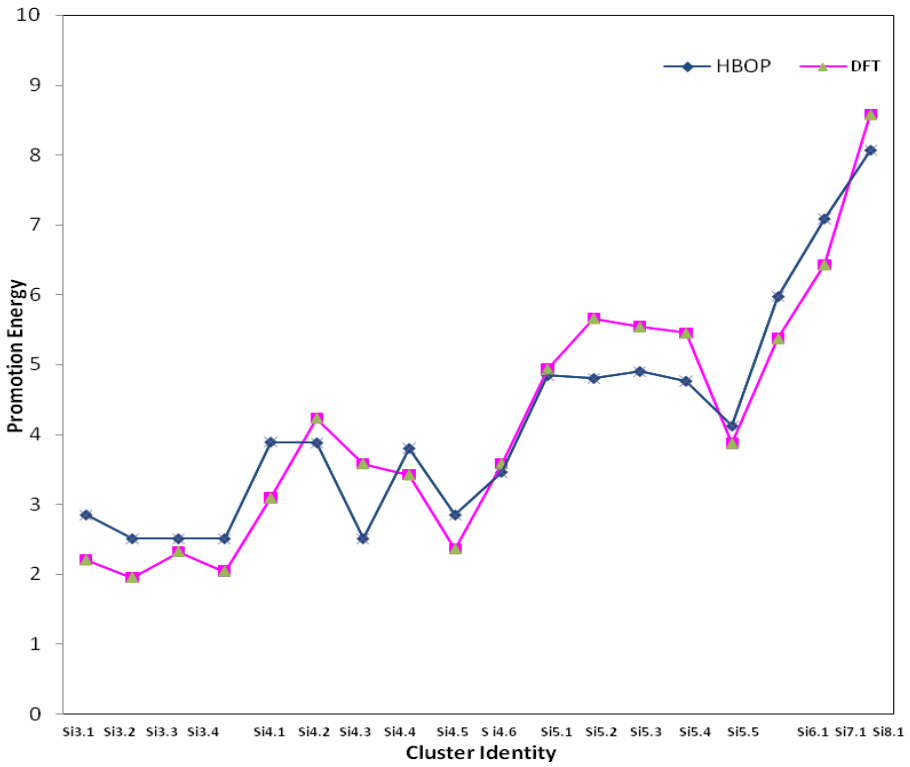

Figure 3.6: Promotion energy values for the silicon clusters in Appendix 1.1 computed using the hybrid bond order potential along with their corresponding DFT [64] values.

A correlation coefficient of 0.86 between the DFT promotion energies and those obtained by our potential (Figure 3.7) is not perfect but shows a reasonable description of the promotion energy. Further improvement in this quantity will form part of our future work.

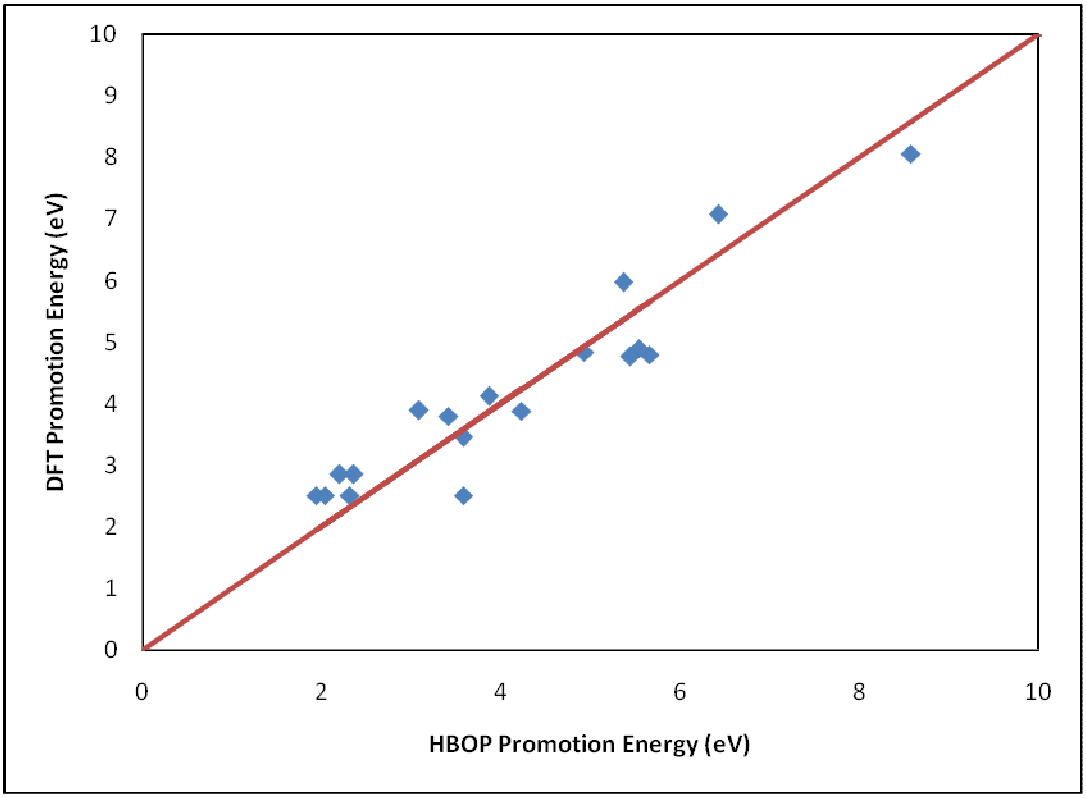

Figure 3.7: A comparative scatter plot of DFT promotion energies of clusters shown in Appendix 1.1 (vertical axis) along with their corresponding values predicted by the hybrid bond order potential (horizontal axis). The straight line shown in the figure is the y = x line. A point falling on the line corresponds to a perfect agreement between DFT and HBOP promotion energy for the cluster in question.

3.4. Average Coordination

The average coordination number of atoms in small silicon clusters helps in understanding the bonding behavior and serves as a test for the accuracy of an empirical potential [21-22]. Similar to promotion energy, the average coordination is a measure of covalent character with covalently bonded atoms having a coordination of about 4.0 in the bulk, while those displaying metallic character have values in excess of 4.0 [64]. Atoms at surfaces can have coordination numbers less than 4.0 and this is true for most small silicon Si_n clusters with $n \leq 6$. The aim of this work is not to duplicate the earlier study [64] of this property, but rather, to test the accuracy of the hybrid bond-order potential in predicting average coordination numbers in clusters.

Average coordination numbers for the clusters in study (Appendix 1.1) were computed using the bond order values and Eq. 1.16. The computations were done for two different potentials having different cut off distances at 2.8 Å and 5.95 Å. The potential with 2.8 Å was optimized by fitting the expression to equations of state properties, cluster energies and promotion energies in a similar manner as the final potential with a cut off distance of 5.95 Å. The idea is to compare a potential with the same expression but different cut-off distances. It was shown earlier in chapter two and Figure 2.2 that the current implementation requires a cut off distance of more than 5.75 Å to have an optimum potential. The calculated average coordination numbers at 2.8 Å and 5.95 Å are presented in Figure 3.8. The results obtained for the 5.95 Å cut off potential reproduces the coordination numbers better. This is not surprising as the longer-ranged potential tends to capture most of the covalent interactions among the atoms in the

cluster. The covalent interactions actually decay quite slowly as the interatomic distance increases, a characteristic that is not fully described by potentials that include only effects from first neighbor shells. The short range cut off in HBOP potential clearly does not give a good indication of the real coordination as can be seen in Figure 3.8. The coordination numbers at 2.8 Å are lower for most clusters in the group.

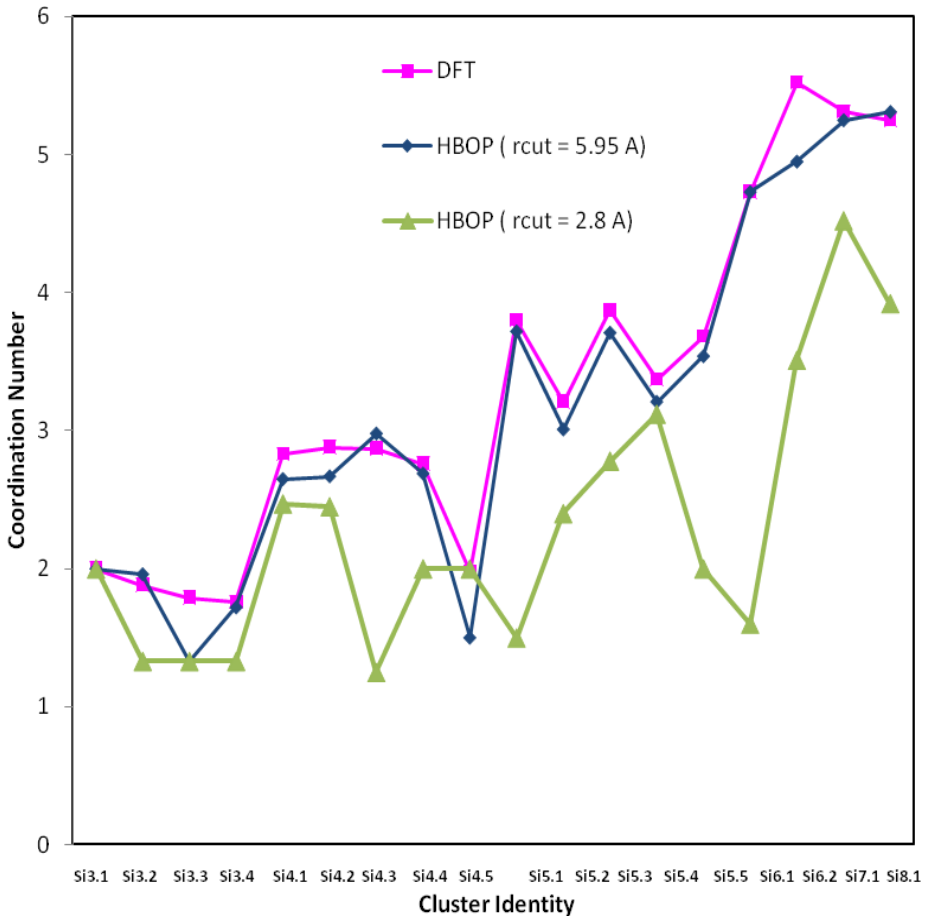

Figure 3.8: A comparison of DFT average coordination number obtained from reference 64 with those calculated by the current potential when using a cut of distances of 2.80 Å and 5.95 Å for the potential energy expression.

A scatter plot comparing average coordination numbers obtained with the DFT values (with a correlation $R^2 > 0.98$) appears in Figure 3.9. It is interesting to note that the average coordination numbers were not used to fit the potential in this study and therefore, the excellent agreement between our values and those of DFT studies is an indication of the importance of using a long range cut off distance for a realistic interatomic potential.

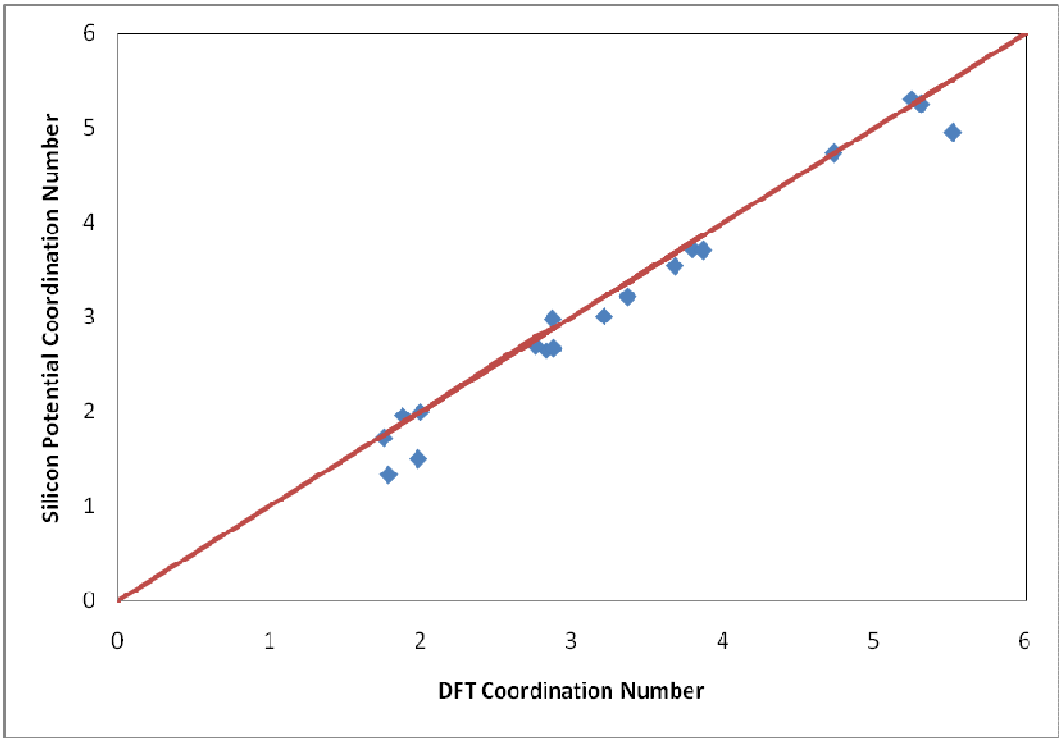

Figure 3.9: A scatter plot of cluster average coordination numbers for the hybrid bond order potential (vertical axis) along with their corresponding DFT values (horizontal axis). The straight line shown in the figure is the y = x line. A point falling on the line corresponds to a perfect agreement between DFT and silicon potential average coordination for the cluster in question.

A careful look at Figure 3.8 shows that clusters Si3.3 and Si4.5 have lower coordination numbers compared to the DFT values. These two clusters (Appendix 1.1) are linear chains. Atom number 2 in Si3.3 (Appendix 1.1) should completely screen both atoms numbers 1 and 3 from each other as can be seen from Eq. 2.3. This is expected to lead to zero sigma orbital interaction. The σ-bond order from the current potential that has atoms 1 and 3 completely screened from each other by atom 2 leading to an average coordination of (1 + 2 + 1)/3 = 1.33. However there would be some π-bond interactions from non-orthogonal overlaps of the 2pπ and 3pπ orbitals in silicon which would thus increase the average coordination number in any model, such as DFT, that allows these π-bonding interactions. The lower values of coordination numbers obtained by the hybrid potential also stem from the fact that our coordination numbers were defined only by σ-bond order alone, while DFT study [64] have π-bond interactions as is evident from their bond order values greater than unity in some individual bonds.

A similar situation happens for cluster Si4.5 with an average coordination number of (1 +2 +2 +1)/4 = 1.5. An inclusion of π-bond order in the definition of coordination number should be useful in minimizing the differences observed in the average coordination number and possibly lead to even better prediction of the promotion energies.

CHAPTER FOUR

CONCLUDING REMARKS

A new hybrid bond-order potential (HBOP) has been developed for silicon. To our knowledge, this work is the first attempt to include promotion energy in an empirical potential. Additionally, screening of bond energy between atoms is implemented using approximations to first principle equations. All other interatomic potentials [24, 53-54] including screening effect have used ad-hoc functions and equations. We believe that our scheme allows for retracing back any error to approximations made to the first principle equations. Promotion energy is a quantum mechanical property of atoms in a covalently bonded system. Quantum mechanical estimation of promotion energy requires diagonalization of Hamiltonian matrix element [25], a too complex and computationally intensive procedure that is beyond the scope of classical potentials. Petiffor et al. [36] used the second-moment approximation to the local density of states in a minimal basis in tight binding (TB) theory to derive a simplified expression for promotion energy suitable for use in molecular dynamics simulation [33-34]. The promotion energy expression used in the current work was fitted using the DFT [64] promotion energies for small silicon clusters Si_3-Si_8. The energies calculated with the HBOP (represented by potential P4 in section 2.6) agree well with those of DFT with a correlation coefficient of 0.86.

Cluster binding energies were computed for 17 different silicon structures of size Si_3-Si_{10} using HBOP, and we obtained excellent agreement with DFT [64] values. A direct comparison between cluster energies from HBOP and those of DFT gives a correlation coefficient of 0.97 for the 17 structures tested. Most of the bond-order

potentials give cluster energies that are in good agreement with the DFT values. Structures with the lowest energies for Si_3-Si_{10} clusters were compared in terms of the root-mean-square (rms) deviation from the DFT binding energies, for HBOP and seven well known potentials for silicon in the literature. The rms error obtained from bond-order potentials, namely: HBOP, the Bolding and Anderson Potential (B & A) [14] and thermodynamic interatomic force field (TIFF) potential of Chelikowsky et al [23] are generally lower than those of cluster potentials (SW, SWG and BH). The exception comes from the Tersoff potential with a much higher rms error compared with other bond order potentials. Similarly, the LJM potential has much lower rms error compared to other cluster potentials in the group. It is worth noting that cluster energies were not used in fitting the Tersoff potential used for this comparison. Nonetheless, attempts were made to perform a fitting of Tersoff potential using cluster energies with little improvement over the original potential [89,96]. This shortcoming of the Tersoff potential is similar to the failure of one of our potential named P1. The P1 potential failed to simultaneously reproduce cluster and bulk properties. At this junction, few observations can be deduced about why other bond-order potential types are successful in simultaneously predicting good bulk and cluster properties while the Tersoff potential fails in this regard. Firstly, starting from HBOP, we discovered that inclusion of promotion energy term in potential P1 (Eq. 2.58) to obtain potential P2 (Eq. 2.60) and fitting to bulk and cluster properties did not remedy this problem. We observed that cluster energies are poorly reproduced in both potentials P1 and P2 (Appendix 2.5). However, when the bond-order term in potential P1 is screened to give potential P3, upon re-fitting to cluster and bulk properties,

we immediately obtained a transferable potential with excellent cluster energies and bulk properties compared to P1 and P2 (Appendix 2.4-2.5). The primary reason for this improvement has more to do with our implementation than the functional form used. In the HBOP implementation, the covalent interaction is made long-ranged such that this interaction decays slowly to zero at 5.95 Å. Therefore atoms that are within this cutoff region are allowed to interact covalently with each other and thus have non-zero bond-order. In computing the bond order for potentials P1 and P2, all atoms within the cutoff region are considered to have equal weight contribution to the bond-order, but differing only in the angular contribution. In general, the $g(\theta_{jik})$ function in Eq. 2.8 was derived using the second moment approximation to density of states in BOP theory, and is therefore valid only for the first nearest neighbor shell of atoms. In essence, to obtain the bond-order of atoms *i* and *j*, then, all k atoms that are first nearest neighbors of atoms *i* and *j* are considered in computing the bond-order. However, potentials P1 and P2 utilized this function also for long distance neighbor atoms *k* of atoms *i* and *j* whose bond order is desired. The result is a lowering of the bond-order for closed packed structures leading to a non transferable potential. By screening the bond-order, we ensures that those *k* atom neighbors that are at larger distance from the *ij* bond have lesser contribution to the bond order compared to *k* atoms that are in the first nearest neighbor shell. This explains why potential P3 with no promotion energy term still outperform potential P2 that includes promotion energy but lacks bond-order screening (Appendix 2.1-2.5). This finding is also a testament to the fact that careful choice of functional representation of an empirical potential is more important than using large number of parameters and performing

elaborate fitting to experimental database. In this scenario, potential P3 with only 7 parameters outperform potential P2 (with 9 parameters and an additional function) when subject to the same fitting database (Appendix 2.2-2.5). The Bolding and Anderson potential with an rms error of 0.72 *eV* is impressive considering that average DFT binding energy of all the 8 clusters is about 22.6 *eV*. This excellent agreement can be attributed to the use of complicated σ and π bond-order (or interference functions as they call it) and the rigorous fitting of the potential to all the clusters tested here. The σ and π bond order were carefully formulated using large number of parameters and functions to account for physical and chemical bonding effects in silicon bulk and crystal phases. The original TIFF potential [83] was found to be less than satisfactory for predicting binding energies for clusters of Si_n for $n \leq 10$. Chelikowsky, Glassford and Phillips [6] identified that some of these clusters have under-coordinated atoms with "dangling bonds" that result in open structures and makes it difficult for a simple angular function used in their potential to simultaneously reproduce the bulk and cluster energies in silicon. This is similar to the problem with the Tersoff potential where the use of simple angular function for first neighbor shell of atoms is unable to simultaneously predict good bulk and cluster properties. The TIFF potential was later modified by introducing an additional function called "dangling-bond vector" into the potential expression to discriminate between "covalent" structures (those with average coordination number less than or equal to four) and "metallic" structures (those with average coordination number greater than four) within the system [6]. The "dangling-bond vector" introduced is ad hoc but effective

because it identifies the physical bonding effect that determines the potential energy of the system for a given atomic structure.

The cluster potentials of SW [9], and the modified form of it referred to here as SWG [15,100], as well as the Biswas and Hamman (BH) potential [20], all are unable to predict good binding energies for small clusters. The SWG form was rigorously fitted to cluster energies, but it was only able to reduce the rms error to about 3.5 eV, an error that is still about 3.5 times the magnitude of HBOP value. The BH potential with an rms error of about 3.8 eV use similar two-body function to SW, but the potential is made environment-dependent through the use of coordination number. However, this effort was still not enough to overcome the error in cluster binding energies in silicon. The Li, Johnston and Murrell (LJM) potential [94] is similar to SW, SWG and BH potentials, however, the LJM potential gives good results for bulk and cluster properties with an rms error in cluster binding energies of about 1.3 eV. The functional form of the LJM two and three-body potentials are different from other cluster potentials considered in this study. For example, the LJM two-body potential is represented as a Rydberg function while the three-body term uses a symmetry coordinates that are functions of the bond distances. The LJM potential was rigorously fitted using cluster energies of silicon Si_N with $N \leq 50$. Despite the success of the LJM potential, it failed to reproduce some closed- packed structures reported from DFT studies [64]. These structures are capped trigonal bipyramid for Si_6, pentagonal bypyramid for Si_7, and tetracapped tetrahedron for Si_8 clusters.

As a test for the HBOP potential, the average coordination number was computed for all the 17 clusters (Appendix 1.1) and to our surprise we obtain an excellent agreement with DFT results. A correlation coefficient greater than 0.98 was obtained between our potential and DFT results for cluster energies, despite the fact that average coordination number was not used in the fitting database. By comparison, we discovered that average coordination values are poorer for an optimized potential with the same functional form but a short-range cutoff distance of 2.8 Å. This discrepancy may be due to screening length that is insufficient to adequately describe the coordination at 2.8 Å cutoff distance compared to 5.95 Å distance used in HBOP.

Equations of state were computed for 16 different silicon phases, namely; diamond, face-centered cubic (FCC), body-centered cubic (BCC), simple cubic (SC), hexagonal closed packed (HCP), hexagonal diamond, simple hexagonal, β-Sn, BC8, R8, ST12, Cmca, Imma, BCT5, and Si_{34} and Si_{46} clathrates. The binding energies and lattice parameters (or equilibrium volume) obtained for all the phases are in good agreement with experimental and DFT results. The rms errors in cohesive energies and lattice parameters in six of the 15 phases obtained for HBOP are better than those for most of the potentials compared. We found that the pressure derivative of bulk modulus have larger error compared to the cohesive energies and equilibrium volume. This property is second order derivative with respect to energy and even quantum mechanical DFT methods are not able to give consistent values when calculating the equations of state properties.

In summary, a new bond-order potential has been developed based on hybrid of theoretically motivated functions and physically realistic empirical expressions. A screening function derived from approximations to first principle expressions is included to account for long range covalent interaction between atoms in silicon. Additionally, the potential also accounts for the promotion energy of atoms in the system, the first time such interaction is included in an empirical potential. The final potential is transferable between various bulk phases and clusters. We believe that intermediate structures, such as liquids and surfaces will be adequately described by the model. Overall, good results that compare favorably with experimental and DFT equations of states and cluster energies were obtained with the HBOP model.

APPENDIX

Appendix 1.1

Si3.1

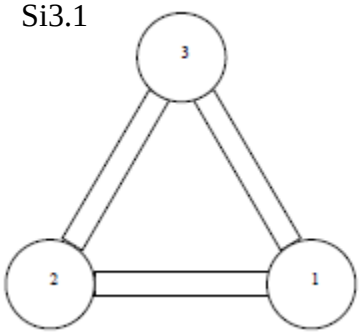

Si3.2

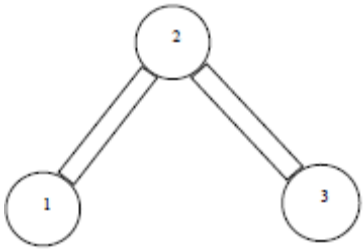

Si3.3

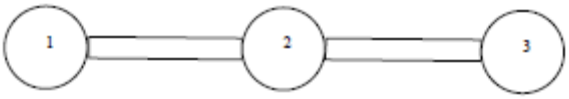

Si3.4

Si4.1/2

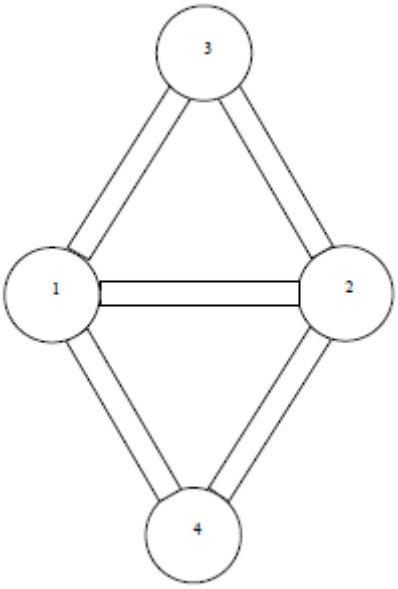

Si4.3

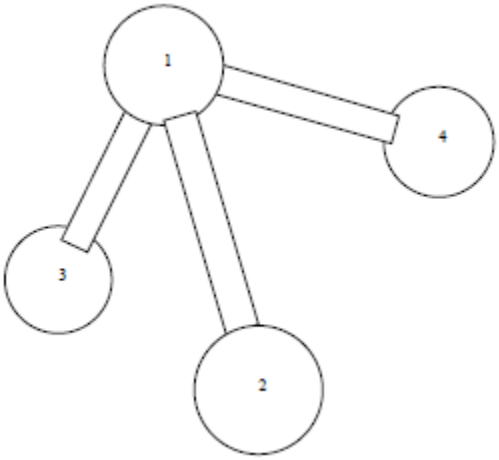

Si4.5

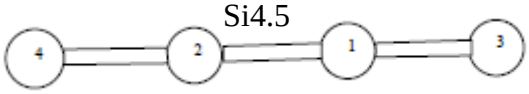

Si5.1

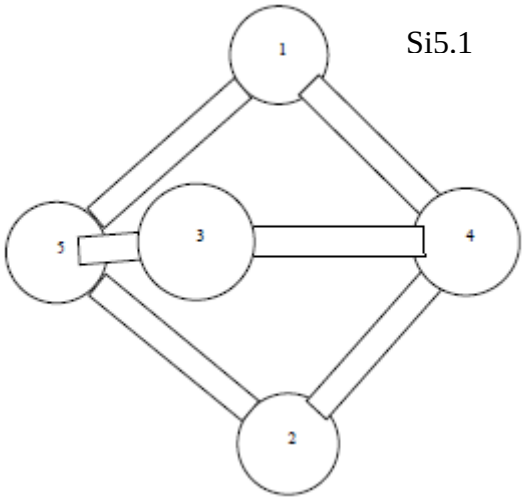

Si4.4

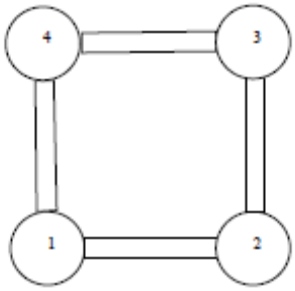

Si5.2

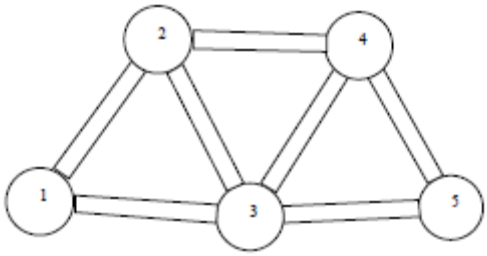

Si5.3

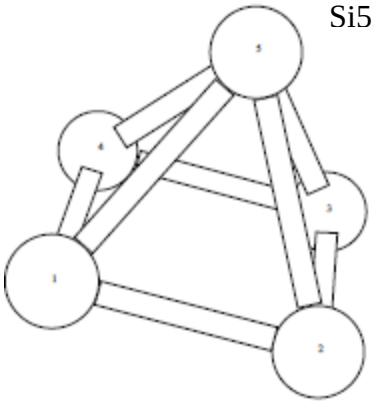

Si6.1

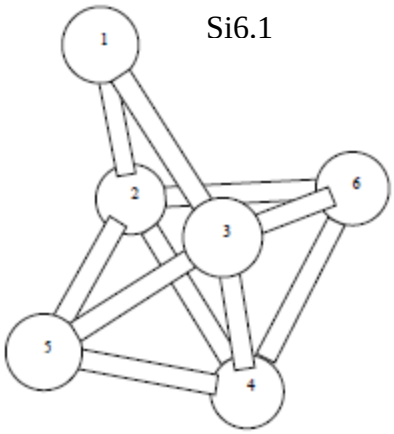

Si6.2

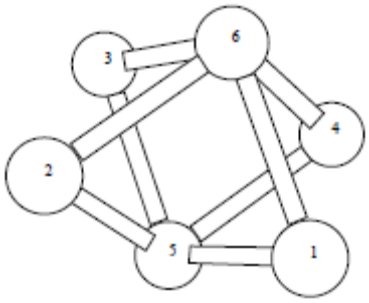

Si6.3

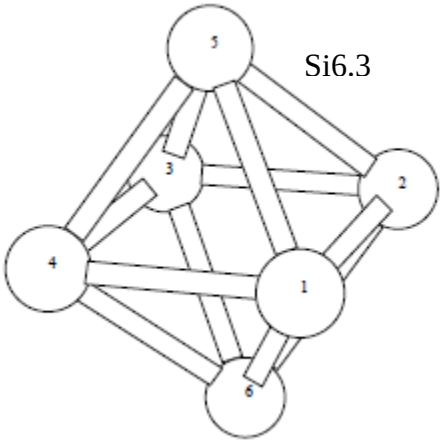

Si7.1

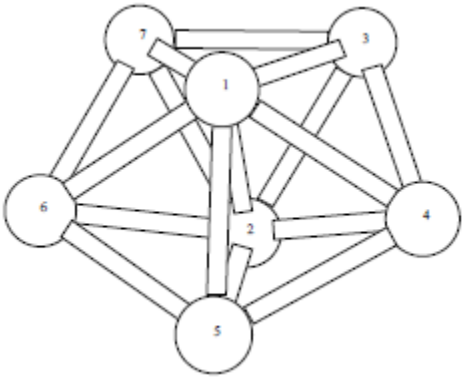

Si8.1

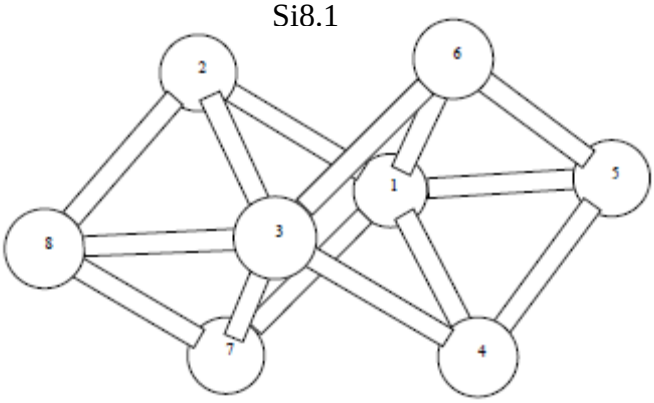

Appendix 2.1

Parameters for potential P1

b_1 = 26.2961767 eV
β = 0.873523073 $Å^{-1}$
A = 4466.88719 eV
α = 6.00848751 $Å^{-1}$
Q = 91.4655993 Å
λ = 1.32226923 $Å^{-1}$

Equations of state properties for potential P1

Phase	EOS Properties			
	E_0 (eV)	V_0 ($Å^3$)	B_0 (Pa)	B'
Diamond	-4.141 5	18.3892	0.5664	6.0972
HEXD	-4.1540	19.0009	0.5507	5.2052
Si_{46}	-4.1534	23.4710	0.3919	4.3274
Si_{34}	-4.1483	23.8855	0.3906	4.2372
R8	-4.6637	17.6449	0.7478	3.6673
BC8	-4.5807	17.9841	0.6563	4.2268
ST12	-4.5922	18.0722	0.6835	3.6332
Imma	-4.9329	17.7857	0.1806	4.7024
β-Sn	-4.9199	17.3627	0.2803	3.6844
SHEX	-4.9427	16.5329	0.5117	1.9356
BCT5	-4.6196	16.7020	0.5873	4.4028
SC	-4.9282	15.8514	0.6476	3.5665
Cmca	-5.3231	13.0074	1.6215	2.5256
HCP	-4.8503	13.7579	0.2993	5.9185
BCC	-4.8010	14.6914	0.1807	5.9272
FCC	-4.8896	13.6340	0.4001	5.3231

Appendix 2.2

Parameters for potential P2

b_1 = 48.5209607 eV
β = 1.00381802 $Å^{-1}$
A = 4661.59945 eV
α = 6.2050596 $Å^{-1}$
Q = 141.051925 Å
λ = 1.16950394 $Å^{-1}$
σ_1 = 1.55362842 eV
σ_2 = 0.551940787 eV

Equations of state properties for potential P2

Phase	EOS Properties			
	E_0 (eV)	V_0(Å^3)	B_0 (Pa)	B'
Diamond	**-3.5673**	**18.5424**	**0.5739**	**6.3501**
HEXD	**-3.6002**	**19.2053**	**0.5695**	**5.334**
Si_{46}	**-3.7683**	**23.6284**	**0.4281**	**4.3712**
Si_{34}	**-3.7680**	**24.0329**	**0.4283**	**4.2775**
R8	**-4.1207**	**17.8113**	**0.8217**	**3.6820**
BC8	**-4.0375**	**18.1628**	**0.7048**	**4.2873**
ST12	**-4.0574**	**18.2730**	**0.7478**	**3.6343**
Imma	**-4.3999**	**19.6669**	**0.1326**	**4.6258**
β-Sn	**-4.3735**	**18.2725**	**0.2819**	**3.4918**
SHEX	**-4.3806**	**16.9989**	**0.5661**	**1.9133**
BCT5	**-4.0466**	**16.7907**	**0.5803**	**5.5348**
SC	**-4.3541**	**16.1038**	**0.6954**	**3.5733**
Cmca	**-4.2212**	**15.0567**	**0.3367**	**4.8373**
HCP	**-4.2099**	**15.1364**	**0.2140**	**5.5344**
BCC	**-4.1969**	**17.3801**	**0.0968**	**5.3056**
FCC	**-4.2438**	**14.5747**	**0.3317**	**5.1235**

Appendix 2.3

Parameters for potential P3

b_1 = 28.6357093 eV
β = 0.86111338 $Å^{-1}$
A = 28371.5588 eV
α = 7.16998122 $Å^{-1}$
Q = 195.514969 Å
λ = 0.761229862 $Å^{-1}$

Equations of state properties for potential P3

Phase	EOS Properties			
	E_0 (eV)	V_0 ($Å^3$)	B_0 (Pa)	B'
Diamond	-4.5712	20.2955	0.6858	4.5536
HEXD	-4.5145	20.1161	0.6274	4.9947
Si_{46}	-4.4759	21.6151	0.4267	6.9594
Si_{34}	-4.4964	21.4069	0.4497	7.8892
R8	-4.3850	17.8571	0.5818	5.7695
BC8	-4.4121	18.2620	0.5211	6.1237
ST12	-4.3689	18.0628	0.4953	6.3475
Imma	-4.5024	15.0312	0.6082	5.0750
β-Sn	-4.5006	15.1871	0.6405	4.8945
SHEX	-4.4957	15.0014	0.5886	7.1861
BCT5	-4.5023	16.9085	0.6202	5.4475
SC	-4.4427	15.8448	0.3760	6.9991
Cmca	-4.4478	14.7962	0.4463	4.9842
HCP	-4.4261	14.7590	0.4490	4.3243
BCC	-4.3806	14.4880	0.3225	6.5794
FCC	-4.4258	14.9792	0.4740	3.6053

Appendix 2.4

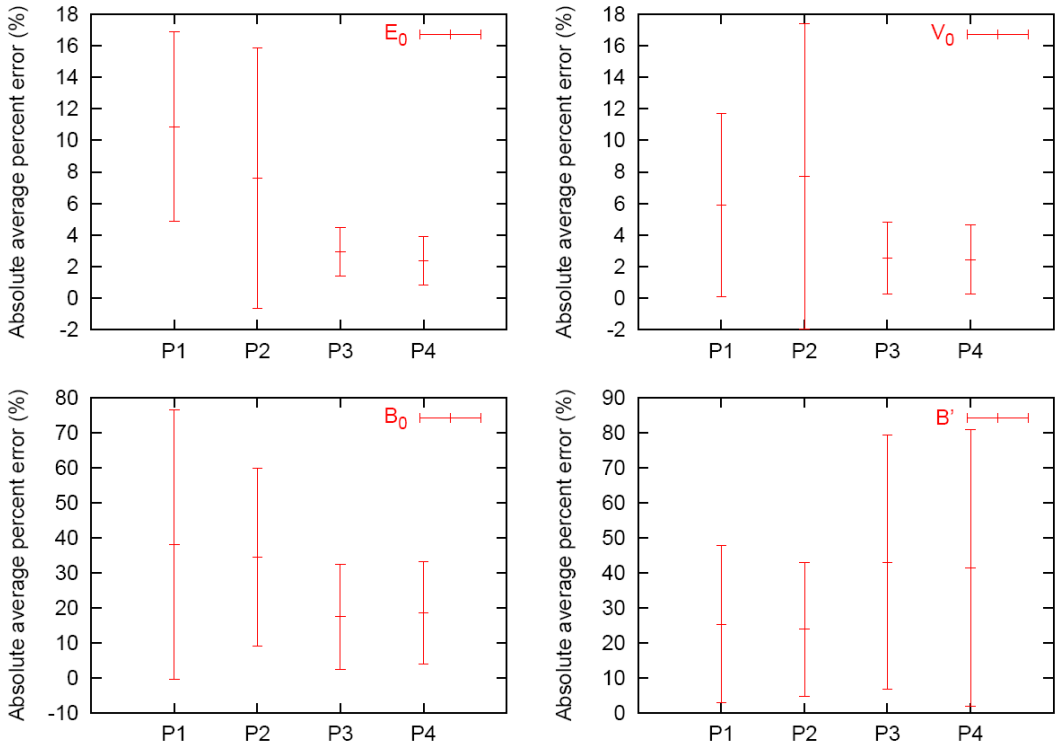

Plots of absolute average percent error in equations of state properties (E_0, V_0, B_0 and B') for potentials P1, P2, P3 and P4.

Appendix 2.5

Cluster cohesive energies for Potentials P1 – P4

Cluster	DFT Cohesive Energy (eV)	P1 Energy (eV)	P2 Energy (eV)	P3 Energy (eV)	P4 Energy (eV)
Si3.1	-7.8200	-8.0834	-7.7326	-8.0653	-7.6409
Si3.2	-7.7500	-7.4123	-6.9502	-7.5324	-7.0187
Si3.3	-7.2600	-5.5616	-4.6929	-7.1760	-6.5754
Si3.4	-6.4700	-6.1624	-5.4370	-7.0993	-6.4920
Si4.1	-12.3600	-11.6873	-11.1172	-12.0440	-11.8235
Si4.2	-11.6900	-11.7487	-11.2507	-12.1338	-11.9173
Si4.3	-11.6400	-9.5187	-8.1760	-9.3707	-8.7654
Si4.4	-10.9300	-11.6946	-11.5264	-11.8301	-11.6294
Si4.5	-9.9000	-7.5578	-6.2937	-10.4116	-9.8440
Si5.1	-16.5000	-16.6728	-15.9229	-15.7608	-15.4728
Si5.2	-15.4700	-14.9915	-14.0438	-15.8916	-15.7722
Si5.3	-15.1800	-16.8365	-16.0732	-15.8936	-15.6278
Si6.1	-20.7200	-21.4287	-20.4639	-19.5310	-19.1420
Si6.2	-20.6900	-21.3653	-19.3692	-19.0964	-19.0491
Si6.3	-19.9900	-21.7211	-19.8692	-19.6523	-19.6172
Si7.1	-24.9100	-25.6799	-23.9703	-23.8421	-23.5015
Si8.1	-28.0100	-28.6900	-26.0533	-27.4729	-27.1414

BIBLIOGRAPHY

[1] Hwaiyu, G., editor. *Semiconductor manufacturing handbook*, McGraw Hill Handbook. New York, 2005.

[2] Thompson, T. B., editor. *Chemical industry of the future: Technology roadmap for computational chemistry*, University of Maryland, March 16-17, 1998.

[3] Allen, M. P. and Tildesley, D. J. *Computer Simulation of Liquids*, Oxford University Press, New York, 1989.

[4] Smit, B. and Frenkel D. *Understanding Molecular Simulation*, Academic Press London, 2001.

[5] Car, R. and Parrinello, M., Unified approach for molecular dynamics and density-functional theory, *Phys. Rev. Lett*., **55**:2471-2474 (1985).

[6] Tersoff, J., New empirical model for the structural properties of silicon., *Phys. Rev. Lett.*, **56**:632-635 (1986).

[7] Tersoff, J., New empirical approach for the structure and energy of covalent systems., *Phys. Rev. B.*, **38**:9902-9905 (1988).

[8] Tersoff, J., Empirical interatomic potential for silicon with improved elastic properties., *Phys. Rev. B.*, **37**:6991-7000 (1988).

[9] Stillinger, F. H. and Weber, T. A., Computer Simulation of local order in condensed phase silicon, *Phys. Rev. B.*, **31**:5262-5271 (1985).

[10] Bazant, M. Z., Kaxiras, E., and Justo, J. F., Environmental-dependent interatomic potential for bulk silicon, *Phys. Rev. B.*, **56**:8542-8552 (1997).

[11] Lenosky, T. J., Sadigh, B., Alonso, E., Bulatov, V. V., Diaz de la Rubia, T., Kim, J., Voter, A. F., and Kres, J. D., Highly optimized empirical potential model for silicon, *Modelling Simul. Mater. Sci. Eng*., **8**:825-841 (2000).

[12] Schall, J. D., Gao, G., and Harrison, J. A., Elastic constants of silicon materials calculated as a function of temperature using a parameterization of the second-generation reactive empirical bond-order potential, *Phys. Rev. B.*, **77**:115209 (2008).

[13] Gillespie, B. A., Zhow, X. W., Murdick, D. A., Wadley, H. N. G., Drautz, R, and Pettifor, D. G., Bond-order potential for silicon. *Phys. Rev. B.*, **75**:155207 (2007).

[14] Bolding, B. C. and Anderson, H. C., Interatomic potential for silicon clusters, crystals, and surfaces, *Phys. Rev. B.*, **41**:10568-10584 (1990).

[15] Gong, X. G., Empirical-potential studies on the structural properties of small silicon clusters, *Phys. Rev. B.*, **47**:2329-2332 (1993).

[16] Murrell, J. N. and Mottram, R.E., Potential Energy functions for atomic solids, *Mol. Phys*. **69**:571-585 (1990).

[17] Murrell, J. N. and Rodriguez-Ruiz, J. A., Potential Energy functions for atomic solids II Potential functions for diamond-like structures, *Mol. Phys*. **71**:823-834 (1990).

[18] Al-Derzi, A. R., Johnston, R. L., Murrell, J. N. and Rodriguez-Ruiz, J. A., Potential Energy functions for atomic solids III. Fitting phonon frequencies and elastic constants of diamond structures, *Mol. Phys.* **73**:265-282 (1991).

[19] Eggen, B. R., Johnston, R. L., Murrell, J. N., Li, S., and Murrell, J. N., Potential Energy functions for atomic solids IV. Reproducing the properties of more than one solid phase ., *Mol. Phys*. **76**:619-633 (1992).

[20] Biswas, R. and Hamann, R., Interatomic potentials for silicon structural energies, *Phys. Rev. Lett*., **55**:2001-2004 (1985).

[21] Chelikowsky, J. R., Phillips, J. C., Kamal, M., and Strauss, M., Surface and thermodynamics interatomic force fields for silicon clusters and bulk phases, *Phys. Rev. Lett*., **62**: 292-295 (1989).

[22] Chelikowsky, J. R. and Phillips, J. C., Surface and thermodynamics interatomic force fields for silicon clusters and bulk phases, *Phys. Rev. B.*, **41**: 5735-5745 (1990).

[23] Chelikowsky, J. R., Glassford, K. M., and Phillips, J. C., Interatomic force fields for silicon microclusters, *Phys. Rev. B.*, **44**: 1538-1545 (1991).

[24] Cai, J., New simple analytical many-body potential for covalent materials, *Phys. Stat. Sol. (b)*, **212**:9-18 (1999).

[25] Conrad, D. and Scheerschmidt, K., Empirical bond-order potential for semiconductors, *Phys. Rev. B.*, **58**: 4538-4542 (1998).

[26] Ackland, G. J., Interpretation of cluster structures in terms of covalent bonding, *Phys. Rev. B.*, **44**: 3900-3908 (1991).

[27] Erhart, P. and Albe, K., Analytical potential for atomistic simulations of silicon, carbon and silicon carbide, *Phys. Rev. B.*, **71**: 035211 (2005).

[28] Mistriotis, A. D., Flytzanis, N., and Farantos, S. C., Potential model for silicon clusters, *Phys. Rev. B.*, **39**: 1212-1218 (1989).

[29] Calsson, A. E., Fedders, A. P., and Myles, C. W., Generalized embedded-atom format for semiconductors. *Phys. Rev. B.*, **41**: 1247-1250 (1990).

[30] Justo, J. F., Bazant, M. Z., Kaxiras, E., Bulatov, V. V., and Yip, S., Interatomic potential for silicon defects and disordered phases, *Phys. Rev. B.*, **58**: 2539-2550 (1998).

[31] Mistriotis, A. D., Froudakis, G. E., Vendras, P., and Flytzanis, N., Model potential for silicon clusters and surfaces, *Phys. Rev. B.*, **47**: 10648-10653 (1993).

[32] Khor, K. E. and Das Sarma, S., Proposed universal interatomic potential for elemental tetrahedrally bonded semiconductors, *Phys. Rev. B.*, **38**: 3318-3322 (1988).

[33] Pettifor, D. G. and Oleinik, I. I., Analytic bond-order potentials beyond Tersoff-Brenner. I. Theory, *Phys. Rev. B.*, **59**: 8487-8499 (1999).

[34] Oleinik, I. I. and Pettifor, D. G., Analytic bond-order potentials beyond Tersoff-Brenner. II. Application to the hydrocarbons, *Phys. Rev. B.*, **59**: 8500-8507 (1999).

[35] Nguyen-Mahn, D., Pettifor, D. G., and Vitek, V., Analytic environmental-dependent tight-binding bond integrals : Application to $MoSi_2$, *Phys. Rev. Lett.*, **85**:4136-4139 (2000).

[36] Horsfield, A. P., Bratkovsky, M. F., Fearn, M., Pettifor, D. G,. and Aoki, M, Bond-order potentials: Theory and implementation, *Phys. Rev. B.*, **53**: 12694-12712 (1996).

[37] Nguyen-Mahn, D., Pettifor, D. G., Cockayne, D. J. H., Mrovec, M., Znam, S., and Vitek, V, Environmental dependent bond-order potentials: New developments and applications, *Bull. Mater. Sci.*, **26**:43-51 (2003).

[38] Brenner, W. D., Empirical potential for hydrocarbons for use in simulating the chemical vapor deposition of diamond films, *Phys. Rev. B.*, **42**: 9458-9471 (1990).

[39] Brenner, W. D., Shenderova, O. A., Harrison, J. A., Stuart, S. J., Ni, B., and Sinnott, S. B., A second-generation reactive empirical bond order (REBO) potential energy expression for hydrocarbons, *J. Phys. Condens. Matter*, **14**:783-802 (2002).

[40] Stuart, S. J., Tutein, A. B., and Harrison, J. A., A reactive potential for hydrocarbons with intermolecular interactions, *J. Chem. Phys*., **112**:6472-6486 (2000).

[41] Che, J., Cagin, T., and William, A. G III., Generalized extended empirical bond-order dependent force fields including nonbond interactions, *Theo. Chem. Acct*, **102**:346-354 (1999).

[42] Humbird, D. and Graves, D. B., Improved interatomic potentials of silicon-fluorine and silicon-chlorine, *J. Chem. Phys*., **120**:2405-2412 (2004).

[43] Dyson, A. J. and Smith, P. V., Extension of the Brenner empirical interatomic potential to C-Si-H systems, *Surf. Sci*., **355**:140-150 (1996).

[44] Murty, R. M. V. and Atwater, H. A., Empirical interatomic potential for Si-H interactions, *Phys. Rev. B*., **51**: 4889-4893 (1995).

[45] Tersoff, J., Modelling solid-state chemistry: interatomic potentials for multicomponent systems, *Phys. Rev. B.*, **39**:5566-5568 (1989).

[46] Abell, G. C., Empirical chemical pseudopotential theory of molecular and metallic bonding, *Phys. Rev. B.*, **31**:6184-6196 (1985).

[47] Tang, M. S., Wang, C. Z., Chan, C. T., and Ho, K.M., Environmental-dependent tight-binding potential model, *Phys. Rev. B.*, **53**:979-982 (1996).

[48] Kwon, I., Biswas, R., Wang, C. Z., Ho, K. M., and Soukoulis, C. M., Transferable tight-binding models for silicon, *Phys. Rev. B.*, **49**:7242-7250 (1994).

[49] Börnsen, N., Meyer, B., Grotheer, O., and Fähnle, M., E_{cov} – a new tool for the analysis of electronic structure data in a chemical language, *J. Phys. Condens. Mater*. **11**:L287-L293 (1999).

[50] Sutton, A.P., Finnis, M. W., Pettifor, D. G., and Ohta, Y., The tight-binding bond model, *J. Phys. C. Solid State Phys*., **21**:35-66 (1988).

[51] Laref, A., Bouhafs, B., Certier, M., Bouarissa, N., and Aourag, H., Transferable non-orthogonal tight-binding model for silicon, *Phys. Stat. Sol. (b)* **208**:413-426 (1998).

[52] Stuart, S. J., Knippenberg, M. T., Kum, O. and Predrag, S. K., Simulation of amorphous carbon with a bond-order potential, *Phys. Scr. T*. **124**:58-64 (2006).

[53] Baskes, M. I., Determination of embedded atom method parameters for nickel, *Mater. Chem. Phys*. **50**:152-158 (1997).

[54] Lee, G., Wang, C. Z., Lu, Z. Y., and Ho, K. M., Ad-dimer diffusion between trough and dimmer row on Si (100), *Phys. Rev. Lett*., **81**:5872-5875 (1998).

[55] Baskes, M. I., Application of the embedded-atom method to covalent materials: A semiempirical potential for silicon, *Phys. Rev. Lett*., **59**:2666-2669 (1987).

[56] Marks, N. A., Cooper, N. C., McKenzie, D. R., McCulloch, D. G., Bath, P., and Russo, S. P., Comparison of density-functional, tight-binding, and empirical methods for the simulation of amorphous carbon, *Phys. Rev. B.*, **65**: 075411 (2002).

[57] Porta, M. and Castán, T., Development of a tight-binding potential for bcc Zr: Application to the study of vibrational properties, *Phys. Rev. B.*, **63**:134104 (2001).

[58] Daw, M. S. and Baskes, M. I., *Embedded*-atom method: Derivation and application to impurities, surfaces and other defects in metal, *Phys. Rev. B.*, **29**:6443-6453 (1984).

[59] Li, Y., Siegel, D. J., Adams, J. B., and Liu, X., Embedded-atom-method tantalum potential developed by force-matching method, *Phys. Rev. B.*, **67**:125101 (2003).

[60] Kohyama, M., Kose, S., Kinoshita, M., and Yamamoto, R., The self-consistent tight-binding method: application to silicon and silicon carbide, *J. Phys.: Condens. Mater* **2**:7791-7808 (1990).

[61] Paxton, A. T., Sutton, A. P., and Nex, C. M. M., Structural stability of silicon in tight-binding models, *J. Phys. C. Solid State Phys*., **20**:L263-L269 (1987).

[62] Adrian, P. S., *Electronic structure of materials*, oxford science publications, New York, 1993.

[63] Pettifor, D. G., Finnis, M. W., Nguyen-Mahn, D., Murdick, D. A., Zhou, X. W., and Wadley, H. N. G., Analytical bond-order potentials for multicomponent systems, *Mat. Sci. Eng*. **A365**:2-13 (2004).

[64] Fournier, R., Sinnott, S. B., and DePristo, A. E., Density functional study of the bonding in small silicon clusters, *J. Chem. Phys*., **97**:4149-4161 (1992).

[65] Kreuch, G. and Hafner, J., Quantum many-body potentials in a tight-binding-bond approximation: Application to the phase stability of carbon and silicon, *Phys. Rev. B*., **55**: 13503-13520 (1997).

[66] Wilson, J. H., Todd, J. D., and Sutton, A. P., Modelling of silicon surfaces: a comparative study, *J. Phys.: Condens. Mater* **2**:10258:10288 (1990).

[67] Brenner, D. W., The art and science of analytic potential, *Phys. Stat. Sol. (b)* **217**:23-40 (2000).

[68] Thijsse, B . J., Silicon potential under (ion) attack: towards a new MEAM model, *Nucl. Instr. Meth. Phys. Res.* B **228**:198-211 (2005).

[69] Rearson, E., Takai, T., Halicioglu, T., and Tiller, W. A., Computer modeling of Si and SiC surfaces and surface processes relevant to crystal growth from the vapor, *J. Cryst. Growth*, **70**:33-40 (1984).

[70] Lenosky, T. J., Kres, J. D., Kwon, I., and Voter, A. F., Highly optimized tight-binding model for silicon, *Phys. Rev. B*., **55**: 1528-1544 (1997).

[71] Robertson, I. J., Heine, V., and Payne, M. C., Cohesion in aluminum systems: A first principles assessment of 'glue" schemes, *Phys. Rev. Lett*., **70**:1944-1947 (1993).

[72] Mishin, Y., Farkas, D., Mehl, M. J., and Papaconstantopoulos, D. A., Interatomic potential for monoatomic metals from experimental data and ab initio calculations, *Phys. Rev. B*., **59**: 3393-3407 (1999).

[73] Balamane, H., Halicioglu, T., and Tiller, W. A., Comparative study of silicon empirical interatomic potentials, *Phys. Rev. B*., **46**: 2250-2279 (1992).

[74] Needs, R. J. and Mujica, A., First-principles pseudopotential study of the structural phases of silicon, *Phys. Rev. B*., **51**: 9652-9660 (1995).

[75] Okada, Y. and Tokumaru, Y., Precise determination of lattice parameters and thermal expansion coefficient of silicon between 300 and 1500 K, *J. Appl.. Phys*., **56**:314-320 (1984).

[76] Farid, B., and Godby, R. W., Cohesive energies of crystals, *Phys. Rev. B*., **43**: 14248-14250 (1991).

[77] Tyuterev, V. G., and Vast, N., Murnaghan's equation of state for the electronic ground state energy, *Comp. Mater. Sci*., **38**, 350-353 (2006).

[78] Honea, E. C., Ogura, A., Murray, C. A., Raghavachari, K., Sprenger, M. F., and Brown, W. L., Raman spectra of size selected silicon clusters and comparison with calculated structures, *Nature*, **366**, 42 (1993).

[79] Zhang, Q. L., Liu, Y., Curl, R. F., Tittel, F. K., and Smalley, R. E., Photodissociation of semiconductor positive cluster ions, *J. Chem. Phys*., **88**,1670-1677 (1988).

[80] Schäfer, R., Schlecht, S., Woenckhaus, J., and Becker, J.A., Polarizabilities of isolated semiconductor clusters, *Phys. Rev. Lett*., **76**:471-474 (1996).

[81] Bai, J., Cui, L., Wang, J., Yoo, S., LI, X., Jellinek, J., Koehler, C., Frauenheim, T., Wang, L., and Xeng, X. C., Structural evolution of anionic silicon clusters Si_N ($20 \leq N \leq 45$) , J. *Phys. Chem. A*., **118**:908-912 (2006).

[82] Jarrold, M. F. and Constant, V. A., Silicon cluster ions: evidence for a structural transition. *Phys. Rev. Lett*., **67**:2994-2997 (1991).

[83] Fuke, K., Tsukamoto, K., Misaizu, F., and Sanekata, M., Near threshold photoionization of silicon clusters in the 248-146 nm region: Ionization potentials for Si_n, *J. Chem. Phys*., **99**:7807-7812 (1993).

[84] Raghavachari, K., Theoretical study of small silicon clusters: Cyclic ground state structure of Si_3, *J. Chem. Phys*., **83**:3520-3525 (1985).

[85] Raghavachari, K., Theoretical study of small silicon clusters: Equilibrium geometries and electronic structures of Si_n (n = 2-7, 10), *J. Chem. Phys*., **84**:5672-5686 (1986).

[86] Patterson, C. H. and Messmer, R. P., Bonding and structures in silicon clusters: A valence-bond interpretation, *Phys. Rev. B*., **42**: 7530-7555 (1990).

[87] Zhu, X. and Zeng, X. C., Structures and stabilities of small silicon clusters: Ab initio molecular orbital calculations of Si_7-Si_{11}, *J. Chem. Phys*., **118**:3558-3570 (2003).

[88] Grossman, J. C. and Mitáš, L., Quantum Monte Carlo determination of electronic and structural properties of Si_n clusters ($n \leq 20$), *Phys. Rev. Lett*., **74**:1323-1326 (1995).

[89] Mahtout, S. and Belkhir, M. A., Structure and relative stability of Si_n *ACTA PHYSICA POLONICA A*, **109**, 685, (2006).

[90] Belkhir, M. A., Mahtout, S., Belabbas , I., and Samah, M., Structure and electronic property of medium-sized silicon clusters, *Physica E*, **31**:86-92 (2006).

[91] Zhu, X. L., Zeng, X. C., Lei, Y. A., and Pan, B., Structures and stabilities of small silicon clusters II: Ab initio molecular orbital calculations of Si_2-Si_{20}, *J. Chem. Phys*., **120**:8985-8995 (2004).

[92] Yoo, S., Shao, N., Koehler, C., Fraunhaum, T., and Zeng, X. C., Structures and stabilities of small silicon clusters. V: Low-lying endohedral fullerenelike clusters Si_{31}-Si_{40}, and Si_{45}, *J. Chem. Phys*., **124**:164311-(2006).

[93] Yoo, S. and Zeng, X. C., Structures and stabilities of small silicon clusters. IV: Motif-based low-lying clusters Si_{21}-Si_{30}, *J. Chem. Phys*., **124**:054304 (2006).

[94] Wales, D. J. and Waterworth, M. C., Structures and rearrangements of model silicon clusters, *J. Chem. Soc. Faraday Trans*., **88**:3409-3417 (1992).

[95] Hartke, B., Global geometry optimization of clusters guided by N-dependent model potentials, *Chem. Phys. Lett*., **258**:144-148 (1996).

[96] Ali, M. M., Storey, C., and Torn, A., Application of stochastic global optimization algorithms to practical problems, *J. Optz. Theor. Appl*., **95**:545-563 (1997).

[97] Tekin, A. and Hartke, B., Global geometry optimization of small silicon clusters with empirical potentials and at the DFT level, *Phys. Chem. Chem. Phys*., **6**:503-509 (2004).

[98] Iwamatsu, M., Global geometry optimization of silicon clusters using the space-fixed genetic algorithm, *J. Chem. Phys*., **112**:10976-10983 (2000).

[99] Hartke, B., Global geometry optimization of small silicon clusters at the level of density functional theory, *Theor. Chem. Acc*., **99**:241-247 (1998).

[100] Yoo, S. and Zeng, X., Global geometry optimization of silicon clusters described by three empirical potentials, *J. Chem. Phys*., **119**:1442-1450 (2003).

[101] Arnold, C. C. and Neumark, D. M., Study of Si_4 and Si_4^- using threshold photodetachment (ZEKE) spectroscopy, *J. Chem. Phys*., **99**:3353-3362 (1993).

[102] Mc Skimin, H. J., J. Appl. Phys., **24**:988 (1953).

[103] Wentorf, R. H. and Kasper, J. S., Two new forms of silicon, *Science*, **139**:338-339 (1963).

[104] Crain, J., Clark, S. J., Ackland, G. J., Payne, M. C., Milman, V., Hatton, P. D., and Reid, B. J., Theoretical study of high-density phases of covalent semiconductors. I. Ab initio treatment, *Phys. Rev. B.*, **49**:5329-5340 (1994).

[105] Ducklos, S. J., Vohra, Y. K., and Ruoff, A. L., Experimental study of the crystal stability and equation of state of Si to 248 GPa, *Phys. Rev. B.*, **41**:12021-12028 (1990).

[106] Gaál-Nagy, K., Pavone, P ., and Strauch, D., Ab inito study of β-tin→ Imma→ sh phase transitions in silicon and germanium, *Phys. Rev. B.*, **69**:134112 (2004).

[107] Adams, G. B. and O'Keeffe, M., Wide-band-gap Si in open fourfold-coordinated clathrate structures, *Phys. Rev. B.*, **49**:8048-8053 (1994).

[108] Christensen, N. E., Novikov, D. L. and Methfessel, M., The intermediate high-pressure phase of silicon, *Sol. State Comm.*, **110**:615 (1999).

[109] Hanfland, M., Schwarz, U., Syassen, K., and Takemura, K., Crystal structure of high-pressure phase Silicon VI, *Phys. Rev. Lett.*, **82**:1197-1200 (1999).

[110] McMahon, M. I. and Nelmes, R. J., New high-pressure phase of silicon, *Phys. Rev. B.*, **47**: 8337-8340 (1993).

[111] Liu, A. Y., Chang, K. J., and Cohen, M. L., Theory of electronic, vibrational, and superconducting properties of fcc silicon, *Phys. Rev. B.*, **37**: 6344-6348 (1988).

[112] Wittig, J., Z. Phys. **195**, 215 (1966).

[113] Chang, K. J., Dacorogna, M. M., Cohen, M. L., Mignot, J.M., Chouteau, G., and Martinez, G., Superconductivity in high-pressure metallic phases of Si, *Phys. Rev. Lett.*, **54**:2375-2378 (1985).

[114] Dacorogna, M. M., Chang, K. J., and Cohen, M. L., Pressure increase in electron-phonon interaction in superconducting hexagonal silicon, *Phys. Rev. B.*, **32**:1853-1855 (1985).

[115] Biswas, R., Martin, R. M., Needs, R. J., and Nielsen, O. H., Stability and electronic properties of complex structures of silicon and carbon under pressure: Density functional calculations, *Phys. Rev. B.*, **35**:9559-9568 (1987).

[116] Papageorgiou, D. G., Demetropoulos, I. N., and Lagaris, I. E., Merlin-3.0. A multidimensional optimization environment, *Comp. Phys. Comm.*, **109**:227-249 (1998).

[117] Papageorgiou, D. G., Demetropoulos, I. N., and Lagaris, I. E., The merlin control language for strategic optimization, *Comp. Phys. Comm.*, **109**:250-275 (1998).

[118] Bernstein, N., Mehl, M. J., Papaconstantopolous, D. A., Papanicolaou, N. I., Bazant, M. A., and Kaxiras, E., Energetic vibrational, and electronic properties of silicon using nonorthogonal tight-binding model, *Phys. Rev. B.*, **62**:4477-4487 (2000).

[119] Zandiehnadem, F., and Ching, W. Y., Total energy, lattice dynamics and structural phase transitions in silicon by the orthogonalized linear combination of atomic orbitals method, *Phys. Rev. B.*, **41**:12162-12179 (1990).

[120] Needs, R. J. and Martin, R. M., Transition from β-tin to simple hexagonal silicon under pressure, *Phys. Rev. B.*, **30**:5390-5392 (1984).

[121] Neethiulagaranjan, A. and Vijayakumar, V., Equation of state primitive-hexagonal silicon and the effect of pressure on electronic properties of three high-pressure phases of silicon, *Phys. Rev. B.*, **47**:487-489 (1993).

[122] Yin, M. T. and Cohen, M. L., Theory of static structural properties, crystal stability , and phase transformation: Application to Si and Ge, *Phys. Rev. B.*, **26**:5668-5687 (1982).

[123] Zhao, Y., Buehler, F., Sites, J. R., and Spain, I. L., New metastable phases of silicon, *Solid State Comm.*, **59**:679-682 (1986).

[124] Hu, J. Z. and Spain, I. L., Phases of silicon at high pressure, *Solid State Comm.*, **51**:263-266 (1984).

[125] Duclos, S. J., Vohra, Y. K., and Ruoff, A. L., hcp-to-fcc transition in silicon at 78 GPa and studies to 100 GPa, *Phys. Rev. Lett.*, **58**:775-777 (1987).

[126] Mujica, A., Radescu, S., MuÑoz, A., and Needs, R. J., Comparative study of novel structures in silicon and Germanium, *Phys. Stat. Sol. (b)* **223**:379-384 (2001).

[127] Bundy, F.P., Phase diagrams of silicon and germanium to 200 kbar, 1000^{o}C., *J. Chem. Phys.*, **41**:3809-3814 (1964).

[128] Welber, B., Kim, C. K., Cardona M., and Rodriguez, S., Dependence of the indirect energy gap of silicon on hydrostatic pressure, *Solid State Comm.*, **17**: 1021-1024 (1975).

[129] Gupta, M. C. and Ruoff, A. L., *Static* compression of silicon in the [100] and in the [111] directions, *J. Appl. Phys*., **51**:1072-1075 (1980).

[130] San Miguel, A. , Melinon, P., Blase, X., Tournous, F., Connetable, D., Reny, E., Yamanaka, S., Itie, J. P., Cros, C., and Pouchard, M., A new class of low compressibility materials: clathrates of silicon and related materials, *High Pressure Research,* **22**:539-544 (2002).

[131] Dodson, B. W., *Development* of a many-body Tersoff-type potential for silicon, *Phys. Rev. B.*, **35**:2795-2798 (1987).

[132] Ackland, G., Semiempirical model of covalent bonding in silicon, *Phys. Rev. B.*, **40**:10351-10355 (1989).

[133] Price, W. L., A controlled random search procedure for global optimization, *The Computer Journal*, **29**:367-370 (1976).

[134] Price, W. L., Global optimization by controlled random search, *J. Optz. Theor. Appl*., **40**:333-347 (1983).

[135] Price, W. L., Global optimization algorithms for a CAD workstation, *J. Optz. Theor. Appl.*, **55**:133-146 (1987).

[136] Ali, M. M., Törn, Viitanen, S., A numerical comparison of some controlled random search algorithms, *J. Global Optimization*, **11**:377-385 (1997).